Optimisation approach of a hybrid multi-axle heavy-duty military vehicle

van den Belt, E.W.R.

Award date:
2021

Optimisation approach of a hybrid multi-axle heavy-duty military vehicle

Master's Thesis

E.W.R. van den Belt

1273876

Master:	Automotive Technology
Department:	Department of Mechanical Engineering
Research Group:	Control Systems Technology
Supervisors:	dr. ir. T. Hofman dr. ir. S. Wilkins
External advisor:	ir. E. van den Tillaart (TNO)
Report ID:	CST 2021.025

Eindhoven, Saturday 29th May, 2021

Declaration concerning the TU/e Code of Scientific Conduct for the Master's thesis

I have read the TU/e Code of Scientific Conduct[i].

I hereby declare that my Master's thesis has been carried out in accordance with the rules of the TU/e Code of Scientific Conduct

Date

20-05-2021

Name

E.W.R. van den Belt

ID-number

1273876

Signature

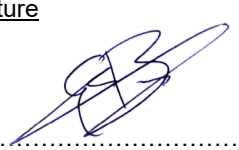

Submit the signed declaration to the student administration of your department.

[i] See: https://www.tue.nl/en/our-university/about-the-university/organization/integrity/scientific-integrity/
The Netherlands Code of Conduct for Scientific Integrity, endorsed by 6 umbrella organizations, including the VSNU, can be found here also. More information about scientific integrity is published on the websites of TU/e and VSNU

February 21, 2020

Contents

List of Figures

List of Tables

Preface

Permission

Preliminary research was conducted before the start of the graduation project regarding the subject matter. The results of this research were summarised in the Internship report "Design analysis study of military (hybrid) electric vehicles" (2020) [4]. Chapter 1 and 2 of this report contain reprinted content from this work as indicated with footnotes where applicable. I performed the literature research, compiled the data and wrote the report.

Disclaimer

Reference herein to any specific commercial company, product, process, or service by trade name, trademark, manufacturer, or otherwise, does not necessarily constitute or imply its endorsement, recommendation, or favouring by the NLD Government, the Ministry of Defence (MOD) or TNO. The opinions of the author expressed herein do not necessarily state or reflect those of the NLD Government, the MOD or TNO, and shall not be used for advertising or product endorsement purposes.

Executive summary

The current Hybrid Electric Vehicle (HEV) powertrain design research is mostly limited to topologies using a single-axle power transfer. An 8x8 vehicle presents a uniquely large design space, which is considerably larger than those commonly addressed in the literature. A multi-axle topology opens up new possibilities regarding asymmetric topologies over multi-axle propulsion. Besides the topology opportunities, the military application of the vehicle changes the optimisation criteria. While most studies only optimise over one criterion, mainly Total Cost of Ownership (TCO), the focus of the criteria could change to more functional requirements such as performance, energy usage and resilience. This study aims to extend the currently available optimisation methods to accommodate multi-axle military vehicles and develop an *Optimisation approach of a hybrid multi-axle heavy-duty military vehicle.*

This optimisation approach is achieved by a four-step method: vehicle use profile identification, topology generation, vehicle modelling and control, and topology selection and optimisation. The use profile contains the basis for creating a drive cycle and describes the vehicle's performance, mission capabilities, and additional vehicle constraints. These requirements are combined with the reference vehicles properties and converted into topology constraints.

The generation of topologies is a multi-step process to which a heuristic filter design constructed by constraints and graph theory for modelling is applied. The expense of computing individual topologies increases exponentially, and therefore a limited set of topologies is generated.

The vehicle model describes the characteristic specifications of vehicle components, and the vehicle's TCO calculation which covers both Capital Expenses and Operational Expenses except for maintenance, base vehicle costs and resale values. The control is related to energy and power management. Power management is divided into torque split between axles, torque split between power sources and transmission gearshift control. The energy management is performed by a thermostat based charge controller. All controllers are rule-based (RB) to reduce the computational resources required for the optimisation process.

The optimisation framework uses a multi-layer nested approach to overcome the various challenges of each stage of the optimisation process. This nested approach is considered to be the most computationally efficient, wherein large sections of the design space with low merit potential can be quickly disregarded. Different algorithms were selected which were considered most suitable to the nature of the problem in each layer. The outer layer is a Genetic Algorithm (GA) optimisation layer to select the topologies using discrete variables. The middle layer uses exhaustive search iterating over different numbers of gears within the transmissions and Particle Swarm Optimisation (PSO) for continuous component sizing. The inner layer consists of RB energy and power management controllers. The optimisation is repeated for multiple objectives; these are: average energy consumption per km $[kWh/km]$, average energy consumption per tonne cargo per km $[kWh/t/km]$, average costs per km $[€/km]$, average costs per tonne cargo per km $[€/t/km]$ and the minimal average fuel consumption per km $[L/km]$.

In general, all optimisation objectives show similar trends except optimisation for minimal average fuel consumption per km $[L/km]$. This study shows that fewer components, fewer MGs, and thus less complex topologies, generally produce better results when optimised for minimal energy consumption or costs, per km or tonne cargo per km. Optimisation towards minimal average costs per tonne cargo per km is the most comprehensive as it integrates energy, component and development costs with the cargo capability of the vehicle. When optimising for this objective, series topologies outperform parallel topologies, although oversizing of the ICEs influence this outcome. These significantly oversized ICEs appear to be the result of sub-optimal gearshift control. The best performing topology, independent of the optimisation objective, is a dual-motor central-drive series topology followed by a triple-motor partial central-drive series topology with one separately driven axle.

Abbreviations

Abbreviation	Definition
AECV	All-Electric Combat Vehicles
AHED	Advanced Hybrid Electric Drive
AMT	Automated Manual Transmission
APU	Auxiliary Power Unit
AX	Axle
BAE	British Aerospace
BEV	Battery Electric Vehicle
BSH	BAE Systems Hägglunds
CAPEX	Capital Expenses
CO	Convex Optimisation
COG	Centre of gravity
COTS	Commercial of the shelve
CS	Combat Support
CSS	Combat Service Support
CVT	Continuous Variable Transmissions
DARPA	Defence Advanced Research Projects Agency
DIF	Differential
DP	Dynamic Programming
EDA	European Defence Agency
EM	Electric motor
EMS	Energy Management Strategies
FCS	Future Combat Systems
FCS	Future Combat Systems
FRES	Future Rapid Effect System
GA	Genetic Algorithm
GBM	Generator Battery Motor
GCV	Ground Combat Vehicle
HED	Hybrid Electric Drive
HEV	Hybrid Electric Vehicle
ICCT	International Council on Clean Transportation
ICE	Internal Combustion Engine
KMW	Krauss-Maffei Wegmann
LFP	Lithium iron Phosphate
MG	Motor-Generator
MHDV	Medium and Heavy-Duty Vehicles
MOD	Ministry of Defence
NCA	Nickel Cobalt Aluminium oxide
NMC	Nickel Manganese Cobalt oxide
OEM	Original Equipment Manufacturer
OES	Operational Energy Strategy
OPEX	Operational Expenses
PSD	Power Split Device
PSO	Particle Swarm Optimisation
RB	Rule-Based
RTD	Renault Trucks Defense
SA	Simulated Annealing
SLD	System Level Design
SOC	State of Charge
SQP	Sequential Quadratic Programming
TCO	Total Cost of Ownership
TNO	The Netherlands Organisation for Applied Scientific Research
TR	Transmission
TtR	Through-the-Road
TU/e	Eindhoven University of Technology

Chapter 1 Introduction

In February 2016, the Dutch Ministry of Defence (MOD) published their Operational Energy Strategy (OES). As a part of this strategy, the vehicle fleet should contribute to the reduction of energy usage, as described in Defensie (2015) [5]: "Developing energy-efficient and technological concepts for weapon systems and operational platforms in cooperation with industry and knowledge institutes, such as alternative propulsion of vehicles and ships". An important note is captured in the subtitle of the OES report, "Operational Energy Strategy: as effective as necessary, as sustainable as possible". This note captures the unique position of the MOD, the obligation to fulfil its constitutional tasks and at the same time operate as sustainable as possible. In this case, the first part of the statement will always precede the latter. In September 2019, the MOD published the letter 'Defence Energy and Environment Strategy 2019-2022' [6]. The letter describes the following targets: [1]

- "in 2050 the dependency on fossil fuels should be reduced by 70% compared to 2010."
- "in 2050 military bases should be self-sufficient regarding energy usage."

To help achieve these targets, energy efficiency should be increased and fuel usage minimised. Implementation of Hybrid Electric Vehicle (HEV) technology can contribute to this goal.

NATO Secretary-General Jens Stoltenberg addressed climate change and its security implications while reflecting upon NATO 2030 [7] [8] during a speech in February 2021. He identified climate change as a crisis multiplier and therefore crucial for both environmental concerns and security reasons. As the Secretary-General said: "NATO should do its part to look into how we can reduce emissions from military operations; therefore, we do have to look into how we can reduce those emissions." Reducing emissions during military operations will also increase military effectiveness, resulting in less dependence on fossil fuels and reduced load on military supply lines.

1.1 Context

Military HEV technology is still under development and has been since 1943, according to Khalil (2009) [9]. The absence of HEV technology on the battlefield is mainly caused by the unique challenges associated with military application. These challenges consist of off-road mobility [10], reliability demands under extreme conditions and the absence of applicable duty cycles [11].[1]

The U.S. Army had two large modernisation programs for combat vehicles which included HEV technology, the Army's Future Combat Systems (FCS) program and the Ground Combat Vehicle (GCV) program. The FCS program was cancelled in 2009 due to rising costs, and the GCV program lasted until 2014 [12]. The U.S. Defence Advanced Research Projects Agency (DARPA) has been investigating sustainable solutions for energy usage since at least 2001 [13], from biofuels produced by algae, hybrid powertrains, flywheels and Lithium-ion technology to hydrogen fuel-cell technology [14].[1]

Sustainability goals and operational opportunities inspired a growing international interest in the military application of HEV technology. Such international cooperation has taken shape by the initiation of the HybridT project conducted by the European Defence Agency [15]. The HybridT project investigates the possibilities, limitations and knowledge gaps for applying HEV technology for current and future military mobility demands.

The military Original Equipment Manufacturers (OEMs) have also been conducting studies and developing HEV prototypes for the past decades. BAE Systems Hagglunds, for example, initiated their SEP program in 1990 and developed multiple tracked and wheeled variants equipped with hybrid powertrains [16] [17] until 2010. Further developments regarding research and developments of military HEVs have not been published by BAE systems Hagglunds since, although they considered upgrading the CV90 tracked infantry vehicle with a hybrid powertrain in 2013 [18]. BAE Hagglunds used their military HEV knowledge to develop a Hybrid Electric Drive (HED) system for the civilian market [19].

The evolving technology inspired more OEMs to renew or start HEV projects. Examples are the Electer VAB presented in 2014 [20], as seen in Figure 1.1, or the Scarabée in 2018, a 6x6 and 4x4 armoured vehicle

[1] Paragraph reprinted with permission from "Design analysis study of military (hybrid) electric vehicles" 2020 by EWR van den Belt [4]

respectively [21]. Both vehicles are developed by Arquus, formally known as Renault Trucks Defense (RTD), Acmat and Panhard, and is part of the Volvo group [22]. Arquus's aim in these development projects is to reduce fuel consumption by 40 [%] compared to the same vehicle with its conventional Internal Combustion Engine (ICE) powertrain.

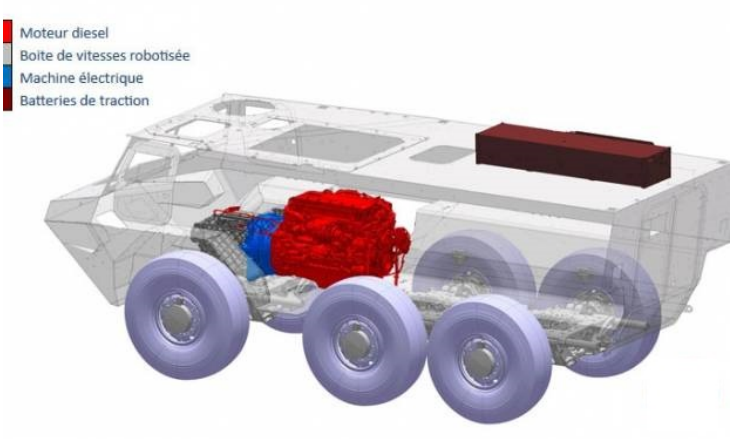

Figure 1.1: Arquus Electer VAB [1]

Other recent developments in the military HEV field are the presentation of the "AKREP II" 4x4 armoured vehicle by the Turkish Otoka. The current prototype is a Battery Electric Vehicle (BEV), powered by two 180 [kW] motors, each connected to a separate axle and has a range of approximately 200 [km] [23]. In 2020 the British Ministry of Defence (MOD) awarded NP Aerospace a contract to develop hybrid prototypes of the Foxhound and the Jackal 2, both 4x4, armoured vehicles. The development will be executed in cooperation with General Dynamics UK, Supacat and Magtec [24].

All described military vehicles in recent studies are relatively light, most invested vehicles are < 15 [$tonne$]. No heavier wheeled vehicles are currently presented or offered with HEV technology. These categories of vehicles are the heavy armoured tracked or wheeled variants and are currently all powered by a conventional ICE based powertrain. A large number of armies have a variant of an 8x8 armoured vehicle platform in their inventory. Examples of such vehicles are the Israelian EITAN, the Russian VPK7289 BUMERANG, the General Dynamics PIRANHA [25] or the Canadian LAV III [26]. The variant in use by the Dutch Army is the KMW BOXER [27]. The KMW BOXER is currently in use by Germany, Netherlands, Lithuania, Slovenia, Australia and Great Britain with a total of more than 1400 vehicles operational [28]. This research will focus on multi-axle HEV topology optimisation, with a use case presented on an 8x8 drivetrain.

1.2 Objective

The current Hybrid Electric Vehicle (HEV) powertrain design research is mostly limited to topologies using a single axle power transfer. In most cases, studies only optimise over one criterion, mainly Total Cost of Ownership (TCO). A multi-axle topology opens up new possibilities regarding asymmetric topologies over multi-axle propulsion. Besides the topology opportunities, the military application of the vehicle changes the optimisation criteria. The focus of the criteria could change from TCO to more functional requirements such as performance, energy usage and resilience. The objective of this study is to extend the currently available optimisation methods to accommodate multi-axle military vehicles. Multiple sub-objectives have to be fulfilled to achieve the main objective:

- Develop a method for multi-axle topology generation and selection.
- Create a multi-objective optimisation framework tailored to military-specific objectives.

1.3 Problem definition and research question

"Optimisation approach of a hybrid multi-axle heavy-duty military vehicle."

This research aims to develop a method to design a hybrid powertrain, optimised for the subject vehicle, given the performance requirements. The following optimisation criteria are used: energy usage, costs, mass and gravimetric cargo capacity. Additionally, the results are reflected upon concerning the resilience and complexity of the powertrain. The selected subject vehicle is an arbitrary military 46 [*tonne*] 8x8 vehicle serving in Combat Support (CS) and Combat Service Support (CSS) operations.
Multiple supporting research questions have to be answered to achieve the research goal. These questions are listed below and reflected upon in the conclusion, Chapter 7:

1. 'How should the system level multi-objective function be defined to adequately represent the optimisation criteria applicable to military usage using weighing factors?'
    - 'How to convert user requirements, such as resilience, into topology constraints to limit the feasible topology set?'
    - 'What level of fidelity models are suitable, set against operational requirements to provide realistic results?'

2. 'How to integrate the topology, technology/sizing and control optimisation within the optimisation framework?'
    - 'How to assess and select a representative subset of topologies from the feasible set?'
    - 'How to generate different topology models for simulation purposes without manually constructing separate models for each topology?'
    - 'How to control the torque split and shift strategy of the powertrain and investigate which control optimisation algorithm would be applicable?'
    - 'Which are the suitable algorithms to construct the optimisation framework, and compute within reasonable time and computational resources?'

1.4 Report structure

This report presents an approach to optimise the topology of a multi-axle heavy-duty military vehicle. The chapters chronologically describe the steps executed in this approach. After each chapter, the intermediate results are discussed and summarised. Figure 1.2 presents a flow-chart describing the inputs, the processes and the outputs of all steps of the approach. Before the optimisation approach is described, Chapter 2 offers an overview of the conducted literature research for the project. Recent state-of-the-art technology reviews providing background information are listed, and relevant findings are summarised by subject.

The first step of the approach is presented in Chapter 3. This step consists of investigating the usage of an arbitrary 8x8 heavy armoured vehicle and using it as a basis to construct a drive cycle. Furthermore, the requirements and constraints are listed and converted to the minimum required capabilities of the powertrain.

Chapter 4 explains the topology generation process. This process is a structured method to generate possible combinations of components, connecting them and applying a heuristic filter design in the form of constraints at each step to limit the results to a set of feasible topology. These topologies are first generated as logical connection matrices and consecutively converted to models for the optimisation process.

The aspects of vehicle modelling and control are addressed in Chapter 5. An overview is provided of the component models, including mass and cost calculations for both individual components and the overall vehicle. In addition to this, the energy and power management is explained, consisting of torque split control between axles and power sources and thermostat charge control.

The final step of the approach is the topology selection and optimisation process in Chapter 6. First, the framework describing the optimisation layers is discussed, followed by the optimisation objectives. An

extensive analysis of the results concludes this chapter. The report is concluded by a reflection upon the research questions, conclusions and recommendations for future work can be found in Chapter 7.

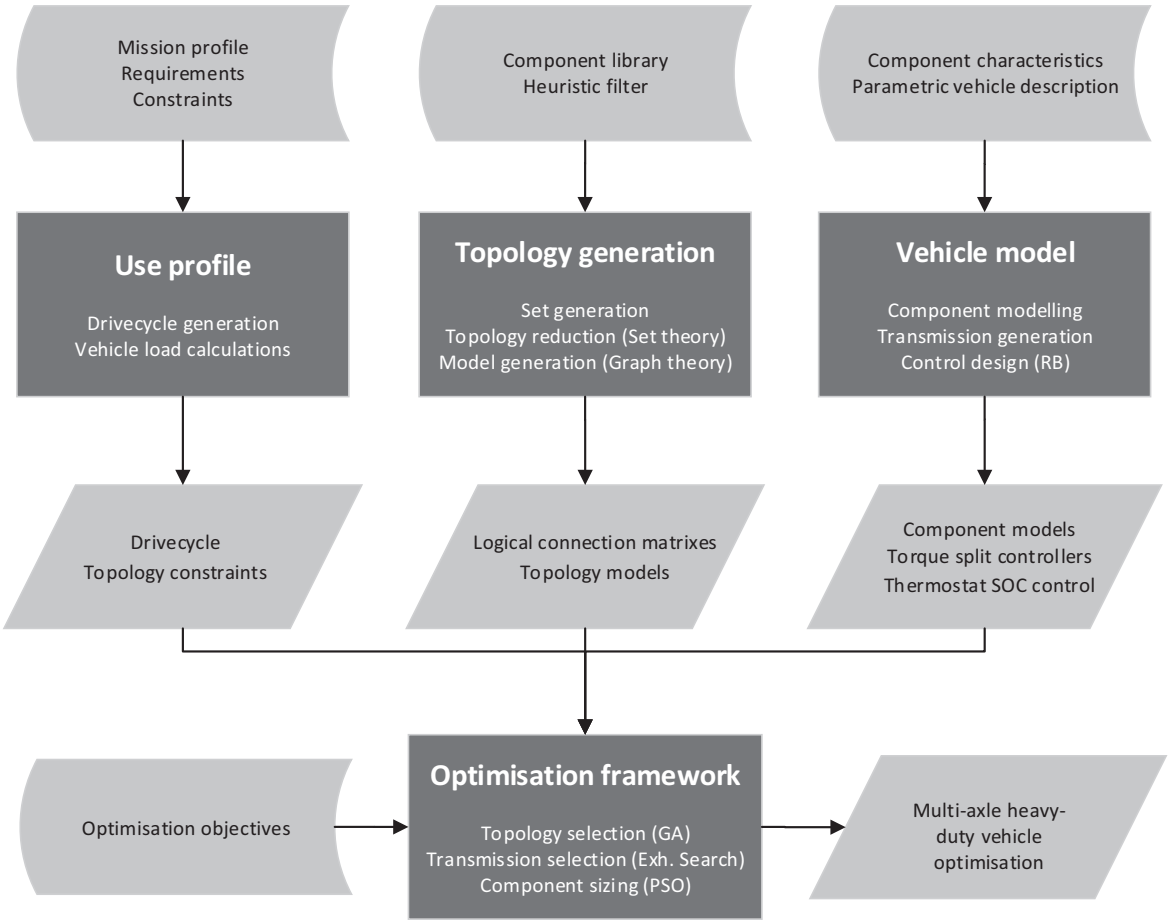

Figure 1.2: Graphical representation of the optimisation approach

Chapter 2 Literature review

Recently multiple state-of-the-art technology reviews were performed regarding heavy-duty (HD) hybridisation and electrification of trucks. These provide an insight into the current state and a starting point for the available technology. Besides these reviews, more research is ongoing on a variance of HEV topics. For the study at hand, a large part of TNO and the Ministry of Defence (MOD) libraries are available for research purposes; however, confidential information is excluded from the main report. The literature review summarises the findings relevant to the research at hand summarised by subject.

2.1 International defence studies and projects[1]

Various national and international studies have assessed the application and feasibility of vehicle hybridisation. These studies aimed to reduce emissions, increase capabilities or reduce logistical footprints of vehicles. This section provides an overview of selected studies.

2.1.1 National studies

Program V520 The program V520 'Technologies for land-based platforms in a future force' by TNO from 2005-2008 included work packages regarding firepower, active protection, mobility and energy management. The goal of this program was to gain insight into the future of land-based vehicles and weapon systems in a future force. Part of this program was the TNO-DV 2006 A449' Development of energy supply for military vehicles'[29] research conducted from 2005-2006. This research focused on energy storage and generation for military application and investigated the use of supercapacitors, li-ion batteries and auxiliary power units (APU).

Program V921 From 2009-2012 the V921 program was executed and researched the possibilities for 'Energy supply during silent watch'[30]. The investigated options for energy supplies were a Stirling engine, camouflaged solar cells, Li-ion batteries and an integrated starter generator. Additional research was conducted regarding the applicability of hydrogen fuel-cells as an APU, although it was negatively advised to use in the short term due to safety and lifecycle concerns[31].

2.1.2 International studies

NATO AVT-047, All-Electric Vehicle Study The goal of the AVT-047[32] panel is to update preceding studies and assess the feasibility of All-Electric Combat Vehicles (AECV) regarding mobility, survivability, lethality, power requirements and energy storage. This study was conducted in 1999-2003 and included two use cases; a scout vehicle, 17 [*tonne*] wheeled platform, and a direct fire vehicle, 35 [*tonne*] tracked platform. The general conclusion was that "further developing electric vehicle drives will be of advantage" [32].

NATO AVT-106 Hybrid Vehicle Rating Standards The NATO AVT-106[33] panel from 2007-2009 was a follow up on the AVT-047 panel. At this time, the technology for (hybrid) electric propulsion had reached a more mature level, and several NATO countries had invested in independent research and development of demonstrator vehicles. The goal of this panel was to compare and standardise norms for military electric vehicles and establish rating criteria.

NATO AVT-166 Evaluation Criteria for Military Hybrid Electric Vehicles From 2009-2012 the NATO AVT-166[34] followed up on the NATO AVT-106 panel findings regarding evaluation and assessment methods for military hybrid electric vehicle technology. Further research was conducted into electric power generation, energy storage, reduced logistical footprint, fuel economy and thermal management of power electronics. The report further elaborates on evaluation criteria and standards for the assessment of Hybrid Electric Vehicles (HEVs).

2.1.3 International projects

VT-E (2003-2006) Build by Krauss-Maffei Wegmann (KMW) and Magnet Motor as a proof of concept. Intended to be a hybridisation of the Fennek vehicle and ended as a completely new vehicle with a newly designed hull due to physical space limitations of the original vehicle weighing 12.7 [*tonne*]. The VT-E has a diesel-electric generator powering four electric motors (EM) mounted directly to the wheels and utilised water-cooling for the generator and electronics combined with oil-cooled EMs.

[1] Section 2.1 reprinted with permission from "Design analysis study of military (hybrid) electric vehicles" 2020 by EWR van den Belt[4]

QinetiQ E-X Drive (2007) The QinetiQ E-X Drive is an electric propulsion system developed for tracked vehicles in the weight class of 45-50 [*tonne*]. The drive system combines four electric motors for high redundancy with a multi-gear transmission and a brake system [35] [36].

AHED (2005-2007) Advanced Hybrid Electric Drive (AHED) is an 8x8 wheeled demonstrator constructed by General Dynamics. The AHED is developed for the Future Rapid Effect System (FRES) program of the British Defence Force. The vehicle combines a hybrid power generator with independent wheel-mounted electric hub drives, which significantly improve its manoeuvrability in off-road conditions. The wheel hub drives are interchangeable and therefore reduce the logistical footprint of the vehicle [37] [38].

SEP (1990-2010) SEP is an development project from BAE Systems Hägglunds (BSH) in cooperation with FMV [17] [16]. Within the project, a range of different wheeled and tracked vehicles were developed, all modular, equipped with hybrid powertrains, and within a 17 [*tonne*] weight range; the modular nature offered the possibility to reconfigure the vehicle to operate in 24 different roles. The first developed vehicles used five-cylinder 2.3l Volkswagen diesel engines and later models six-cylinder 3.2l Steyr M16 diesel engines.

FCS (2003-2009) and GCV (2009-2014) program The United States Army's Future Combat Systems (FCS) [39] was an extensive program intended to develop new manned and unmanned vehicles, including HEV technology. The FCS program was cancelled in 2009 due to rising costs. Even though this program was cancelled, the developed technology was incorporated in the succeeding Ground Combat Vehicle (GCV) program, which ended in 2014 [12].

2.2 HEV technology assessment

The 'Technical feasibility study for a universal vehicle platform' by van der Koogh [40] provides an insight into the military requirements and technology in 1985. As the technology advanced, the vehicle mobility requirements remained identical. The study analyses a high mobility vehicle platform with hybrid propulsion capabilities. It includes non-era-specific information such as an overview of rolling resistance coefficients and vehicle adhesion coefficients of different surfaces.

The report' Military vehicle optimisation and control' by Rizzo [11] provides an extensive survey regarding the status of military HEV application at that time. Verbruggen et al. [41] conducted a review of current and planned full electric trucks and compared their specifications and capabilities. These trucks' claimed, and calculated energy consumption varied slightly and resulted in a calculated average of 1.72 [kWh/km] for a full-electric, conventionally shaped, 40 [*tonne*] truck.

Smith et al. [42] conducted a thorough assessment of the state of commercial HEV technology for medium and heavy-duty vehicles (MHDV). The study covers an inventory and assessment of topologies, component technologies, performance and cost drivers, and the identification of research and development gaps. The first generations of MHDV topologies were mainly composed by integrating the best available Commercial-off-the-shelve (COTS) components instead of pursuing an optimal combination. MHDVs would benefit from more standardisation in order to facilitate standard and scalable components; currently, the availability of scalable heavy-duty components is minimal according to Smith et al. [42]. The research by Smith et al. also noted the need for high fidelity optimisation and control methods and tools to develop powertrains from an energy-efficient perspective for a wide range of operations.

Verbruggen et al. [43] assessed eight series Hybrid Electric Vehicle (HEV) topologies varying in central or distributed drive systems. Different transmission options are considered for each investigated topology, and the component sizes and Energy Management Strategies (EMS) are optimised. The topologies use a maximum of two driven wheels which are symmetrically loaded on one axle. The performance requirements are incorporated into the component constraints as part of the optimisation framework. The implications of design decisions are analysed, and optimal solutions given the limited set of investigated topologies are presented.

2.3 Drive cycle generation

Although most standard drive cycles are speed and time-dependent, other and additional metrics could be used to characterise them. In addition to speed and time, Han et al. (2012) [44] used gradient information to define the cycle. Whereas Sebeck et al. (2017) [45] added stops per mile, characteristic acceleration, aerodynamic speed and kinetic intensity to define the drive cycle. Using gradient information is especially

useful considering the possible operating theatres of military vehicles [46]. Furthermore, the number of stops is relevant to distinguish patrol or convoy operations.[1]

Sebeck et al. (2017) [45] compared drive cycles from military test circuits (Automotive Directorate, (TEDT-AT-AD) and Aberdeen Test Center, U.S. Army (2012) [47]) and commercial standard drive cycles to identify characterising elements. The elements they derived from these drive cycles were the number of "stops per mile", the "characteristic acceleration" to compute the energy used to accelerate depending on mass [48], the "aerodynamic speed" to define drag and the "kinetic intensity". The kinetic intensity describes the intensity of the cycle in a single value, based on the intensity and frequency of events, to indicate the engine load.[1]

Han et al. (2012) [44] created a methodology to combine so-called "microtrips" from real-world driving situations to a new drive-cycle. These microtrips were created by dividing real-world test data into short sections, then arranging them based on parameters that affect fuel consumption as speed and gradient. Microtrips from several different drive-cycles were combined and rearranged to form a new cycle. The similarity of the newly created drive-cycle compared to a real-world situation was assessed using the root mean square error. Han et al. (2012) [44] confirmed the methodology to be reproducible and that the characteristics of a new combined drive cycle are a good approximation of a real-world military drive cycle.[1]

A novel method is presented by Silvas [49] to synthesise drive cycles based on measured driving data using multi-dimensional Markov chains. This method includes gradient information in contradiction to current methods, which are primarily based on velocity and acceleration.

2.4 Topology generation

In contrast to current common practice, where topologies are generated manually by expert knowledge, Silvas [49] proposed a novel method to generate HEV topologies. All feasible topologies are generated based on a predefined component library. Further selection to reduce the topology set may include; efficiency analyses, performance analyses, complexity or expert knowledge-based rule-based filtering.

Van Harselaar et al. [50] developed a method to model arbitrary HEV topologies using a generalised transmission model. This transmission model provides insight into all elements' current torque and speeds within a powertrain over the drive cycle. The model allows for automated comparison of topologies and thereby solving System Level Design (SLD) problems. The studied design space uses a limited set of components and is based on a lumped single-axle vehicle model.

In 2018 Rangaranjar [51] performed a powertrain optimisation for a battery-electric HD vehicle and concluded the research with a thesis. In this thesis, all feasible topologies are generated for the chosen component library, and a rule-set is used to reduce the feasible set further. A representative subset is manually selected from this feasible set to assess the influence of topology and technology choices on the Total Costs of Ownership (TCO). The investigated topologies vary in centralised or distributed drivetrains, transmission types, including continuous variable transmissions (CVTs), and the number of electric machines.

Verbruggen [43] opted for constraint programming to generate topologies. By applying functional and application-specific constraints, the total set of topologies based on a component library could be reduced to a subset of feasible topologies. Each of the feasible topologies is paired with multiple transmission types and gears; these combinations are then considered unique powertrain configurations for further analyses. Using eight different topologies and four transmission options, 56 unique configurations were generated.

2.5 Components

A fair amount of research has been performed on individual components of a powertrain. A selection of applicable research is discussed in this section.

2.5.1 Transmission

Bartlett [52] investigated tradeoffs in transmissions design and proved that more gear stages could be more efficient in multistage gearset compared to fewer stages. He investigated 3-stage and 4-stage gearsets and analysed the influence of optimal selection of stage ratios on efficiency, acceleration and transmission

mass. Optimising the number of gear stages, even above the number minimal required, could reduce the rotational inertia of the combined gear stages, thereby maximising acceleration.

In 2020, Li et al.[53] proposed an optimisation method for two-speed transmissions. This method is based on the genetic algorithm and incorporates both economic and dynamic driving behaviour of the vehicle. In the fitness function, a split factor dictates the influence of either economic or dynamic behaviour on the optimised result.

2.5.2 Energy management

Tran et al.[54] assesses various HEV powertrain topologies and compares different energy management strategies (EMSs). The influence of modelling approaches, different operation modes for each topology and classifications of EMSs is the core of this review. These classifications cover different rule-based, on- and offline optimisation-based, and learning-based EMSs. All classifications are thoroughly surveyed, compared, and their advantages and limitations discussed.

2.5.3 Batteries

An alternative to overcome long charge durations is battery swapping, as proposed by Moultak[55]. This approach would influence not only the vehicle design but also the logistics around the vehicle. In the case of vehicle fleets, battery-pack management should be applied. Battery swapping allows for short 'refuel' stops and makes a vehicle competitive with a conventional powertrain.

In 2017, a survey by Bloomberg New Energy Finance[56] showed a reduction of 24 [%] since 2016 and 79 [%] since 2010 in battery pack prices. These numbers are averaged over batteries for light mobility, electric busses and stationary storage.

Different battery chemistries have different properties, which could be beneficial depending on the required vehicle specifications. Battery chemistry affects the volumetric and gravimetric power and energy rating, as well as other characteristics such as inherent safety, life span and costs[57]. Life span can be divided into calendar life, thus ageing over time, and cycle life, being the number of allowable full charge and discharges. Calender life is negatively affected by unfavourable temperatures and being static over prolonged periods.

Lithium iron phosphate (LFP) is safer and has a longer life span compared to lithium nickel cobalt aluminium oxide (NCA). On the other hand, NCA benefits from a higher energy density compared to LFP. Lithium nickel manganese cobalt oxide (NMC) provides a cost-efficient replacement for cobalt-based batteries; however, their lifecycle is shorter than LFP batteries[56] [57]. The superior safety of LFP is due to their chemical and thermal stability. They remain relatively stable when overcharged or short-circuited, they can handle high temperatures and the cells are less sensitive to thermal runaway[58] [59].

2.6 Optimisation methodology

The work of Silvas[49] focuses on the integrated optimal design of HEV vehicles and is partially dedicated to optimisation strategies for system-level design. Multiple bi-level optimisation strategies, such as nested or sequential approach, are compared using both gradient-based and derivative-free algorithms. Investigated optimisation methods include gradient-based Convex Optimisation (CO) and Sequential Quadratic Programming (SQP), and derivative-free algorithms such as Genetic Algorithm (GA), Particle Swarm Optimization (PSO), Pattern Search and Dynamic Programming (DP). Additionally, Rule-Based (RB) control provides sub-optimal solutions when deployed in the inner loop of an optimisation framework.

Rangarajan[51] build a powertrain design optimisation framework for a BEV truck, combining component sizing, transmission variations and single and double axle drive topologies. Rangarajan started the optimisation with a coarse exhaustive search to narrow the search space. A bi-level optimisation framework, based on Particle Swarm Optimization (PSO) and Dynamic Programming (DP), is then applied to the search space to determine the component sizing and control of the investigated topologies.

Tran et al.[54] assessed a multitude of powertrain configurations and energy management strategies. Additionally, a quantitative classification of energy management strategies and an overview of optimisation algorithms is presented and indexed based on application. Qualitative analysis is presented on the advantages and disadvantages of different optimisation strategies on the application within energy management.

2.7 Summary

The national and international projects provided an insight into general requirements for military HEVs; whereas technology advanced over the years, capability requirements stayed the same. While the investigated studies considered only single-track vehicle models, this research aims to develop an approach for a multi-axle vehicle.

The research into drive cycle development shows the value of adding terrain characteristics to the cycle data to improve the representation of mixed on and off-road usage [46]. The idea of microtrips [44] for combining short representative sections into a larger cycle is a helpful method to generate a new drive-cycle if recorded real-world test data is available. Due to the absence of this data, the microtrip method is not applicable, and a manual approach is implemented.

The rule-set filtering method by [51] is integrated in the topology generation process to reduce the number of feasible topologies from a larger set. The investigated transmission generation methods are too computationally involved to be integrated into the large scale optimisation at hand.

Choosing the best battery chemistry for an application is complex; a wide range of gravimetric and volumetric power end energy ratings are available. Due to the favourable characteristics concerning safety, the LFP chemistry is chosen as a basis for the model.

Multiple sources evaluated different optimisation strategies and presented advantages and disadvantages of applied methods. Although the implementation of optimisation methods over all layers of the framework would provide the optimal results, the computational burden would become too high for practical implementation on the scale involved. Therefore partial rule-based control is implemented.

Chapter 3 Vehicle use profile

As a basis for the optimality study, a vehicle description is defined, including its performance requirements and intended use. This description will act as a basis for a mission profile describing a representative use case. This mission profile is then converted from its descriptive form into a drive cycle for simulation purposes. Subsequently, the use profile is converted into topology constraints by calculating the minimum powertrain requirements to fulfil its capability requirements.

3.1 General use profile

8x8 Armoured vehicles exist in many variants; for example, the Boxer build by Krauss-Maffei Wegmann (KMW) is a Multirole Armoured Vehicle (MRAV) that can serve as a command post, ambulance, engineer and cargo transport [27]. For this optimisation process, an arbitrary general-purpose 8x8 armoured vehicle is modelled. Combat missions with such an armoured vehicle can be divided into separate sections of movement. These movements would start with an entry movement from a staging area to a holding area in the area of operation over secondary roads or light terrain. From this holding area, a silent movement is performed towards the front line to execute an operation. This movement is performed over a wide variety of terrain, from secondary roads to heavy terrain. After the action, the vehicle returns to a holding area for recuperation, followed by another action or return to the staging area. The latter option is simulated in the drive cycle. All movements can be performed in hybrid mode, except for the silent movement between the holding area and the action, which is electric-only. Figure 3.1 illustrates a schematic representation of such a drive cycle.

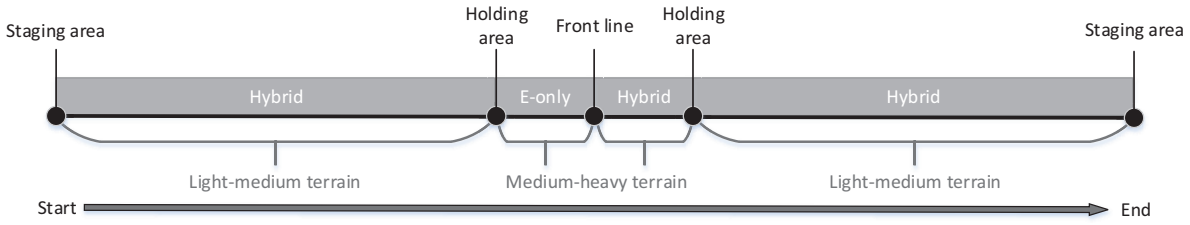

Figure 3.1: Schematic representation of the drive cycle

3.2 Requirements and constraints

The requirements and constraints can be separated into three categories, performance requirements, mission capabilities and vehicle constraints [60] [27].

Performance requirements

- The gradeability requirement is a stationary 0 $[km/h]$ hill start on a 60 $[\%]$ incline in forward and reverse direction, without restrictions on speed, time or distance. Assumed is to use peak torque capabilities of the power sources and assume the duration of the climb will fit in the peak torque time limitations.
- Top speed of 103 $[km/h]$ over flat good road conditions.
- Top speed of 32 $[km/h]$ on a 10 $[\%]$ incline on good road conditions.
- No acceleration requirements available.

Mission capabilities

- The minimum range per tank/charge is 600 $[km]$ on mixed road conditions.
- No information available regarding silent operating capability (duration) or minimum electric-only range; these criteria are therefore not included as a requirement. Nevertheless, the electric-only range is presented as a result of the optimisation.
- The auxiliary load during movement is a lumped approximation of a constant 2.5 $[kW]$ load.

Vehicle constraints

- All four axles must be driven axles.
- Electric-only operation must be possible in terrain; therefore, all axles should be at least electrically driven and through-the-road (TtR) [54] parallel hybrid topologies are excluded.
- Reduced capabilities accepted during electric-only operation, for example the need to engage ICE for maximum torque or power.
- The vehicle has to comply with Dutch road regulations.
- Vehicle dimensions of the KMW Boxer are used as reference dimensions; these dimensions are presented in Section 3.4.

3.3 Drive cycle generation

Commercially available civilian drive cycles are not representative of using a heavy military armoured vehicle; thus, a new drive cycle is synthesised. The new drive cycle simulates multiple road conditions en duplicates a mission as described in Section 3.1. This mission is constructed by a large hybrid drive and a small electric-only distance.

The drive cycle consists of a speed, acceleration, incline and rolling resistance coefficient vector. The speed vector is adapted to the road conditions, and both the top speed and a hill-start test is incorporated. The friction and adhesion coefficients for the various road conditions are based on [40]. After synthesising, the drive cycle is filtered not to exceed the maximum power required as available, based on the performance requirements described in Section 3.2. These calculated values are listed in Table 3.2. A detailed representation of the drive cycle is included in Appendix A.

3.4 Physical properties of reference vehicle

The KMW Boxer MRAV is used as a reference for vehicle measurements [27] [2] (Figure 3.2). Given the vehicle should comply with the Dutch road regulations, the maximum axle load limits the weight. The maximum axle load is 11.5 $[tonne]$ per driven axle, assuming the axles are spaced more than 1.8 $[m]$ apart [61] [62], this results in a maximum theoretical weight of 46 $[tonne]$ for a four-axle vehicle.

The tires on the reference vehicle are either 415/80 R27 or 415/80 R685 [63], and a central tire inflation system and run-flat inserts are fitted. This results in an unloaded tire radius $R_{tire,unloaded}$ as calculated in Equation 3.1. The loaded tire radius is conservatively assumed to be 98$[\%]$ of the unloaded radius on road conditions, the influence of tire deflation in terrain not included in the simulations. Lowering the tire pressure in terrain increases the contact surface, therefore increases the torque transfer capabilities and reduces the tire radius. On the other hand, it will increase the rolling resistance and, as a result, decrease the overall efficiency.

$$\begin{aligned} R_{tire,unloaded} &= 0.415 \cdot 0.8 + \frac{685}{2} \\ &= 0.675\,[m] \\ R_{tire} &= R_{tire,unloaded} \cdot 0.98 \\ &= 0.661\,[m] \end{aligned} \tag{3.1}$$

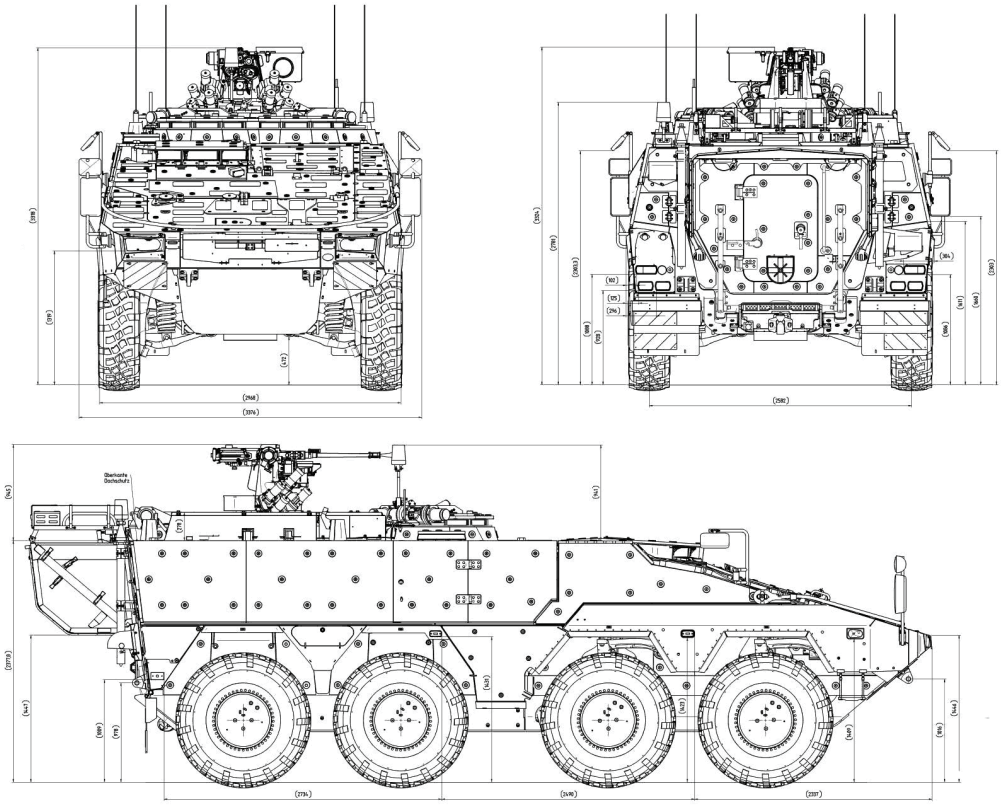

Figure 3.2: Blueprint of KMW Boxer armoured vehicle [2]

3.5 Convert requirements into topology constraints

Before constructing topologies, the performance requirements as described in Section 3.2 are used to perform a basic calculation based on a single track vehicle model to determine the minimum required torque and power at the wheels. The values might impose constraints on the topology generation, given the currently available component performance limitations.

$$
\begin{aligned}
F_{wheel} &= F_{roll} + F_{air} + F_{slope} + F_{acc} \\
P_{wheel} &= F_{wheel} \cdot v_{veh} \\
F_{roll} &= cos(arctan(\frac{\alpha}{100})) \cdot m_v \cdot g \cdot f_{roll} \\
F_{air} &= 0.5 \cdot \rho_{air} \cdot C_w \cdot A_f \cdot v_{veh}^2 \\
F_{slope} &= sin(arctan(\frac{\alpha}{100})) \cdot m_v \cdot g \\
\omega_{wheel} &= \frac{v_{veh}}{3.6 \cdot 2 \cdot \pi \cdot R_{tire}} \cdot 60
\end{aligned}
\tag{3.2}
$$

Table 3.1: Vehicle parameters

Symbol	Description	Value	Unit
m_v	vehicle mass	46000	$[kg]$
A_f	frontal area	7	$[m^2]$
ρ_{air}	air density at $20°C$	1.2041	$[kg/m^3]$
C_w	drag coefficient	0.7	[-]
R_{tire}	tire radius	0.6614	$[m]$
g	gravitational constant	9.81	$[m/s^2]$

The hill-start requirements dictate the minimal torque requirements of the vehicle. The minimum amount of power is dictated by travelling at high speeds off-road or on an inclining surface. The wheel speed to achieve the required top speed of the vehicle combined with the maximum rotational speed of a motor determines the transmission ratio between the wheels and the power source. The combined power sources in the powertrain have to be able to provide the torque and power calculated in Equation 3.2, the base calculations.

The results of these base calculations are the minimum specifications to achieve the requirements as specified in Section 3.2. The base calculations are performed assuming the requirements have to be met, without any margin for under-performance. Equation 3.2 is used to determine the required minimum torque, power and speed at the vehicles' wheels. Table 3.1 presents the vehicle simulation parameters used within Equation 3.2. Depending on the assessed requirement, the gradient α $[\%/100]$, vehicle speed v_{veh} $[m/s]$, rolling friction coefficient f_{roll} [-] and the wheel speed ω_{wheel} $[rad/s]$ are varied. The resulting powertrain requirements are listed in Table 3.2. The minimum combined torque $T_{wheel,min}$ at the wheels is required during the 60 $[\%]$ incline static hill-start, the minimum power $P_{min,vehicle}$ is required for the 32 $[km/h]$ movement on a 10 $[\%]$ incline requirement and the minimum required wheel speed $\omega_{tire,min}$ is achieved at top speed.

Table 3.2: Total vehicle power, torque and speed requirements at the wheels

Symbol	Value	Unit
$P_{min,vehicle}$	800.3	$[kW]$
$T_{wheel,min}$	179	$[kNm]$
$\omega_{tire,min}$	43.26	$[rad/s]$

3.6 Summary

The general use profile is determined as a basis for the creating of a drive cycle. The drive cycle consists of four sections, two long movements towards and from the operating theatre and two short sections: electric-only propulsion is mandatory in the first short section. A top speed test and a static hill start are included within the drive cycle to validate the performance requirements.

The requirements describe the performance of the vehicle, mission capabilities and additional vehicle constraints. Examples of performance requirements are top-speed, gradeability and minimum speed at an incline. Mission capabilities describe the range, and the vehicle constraints include compliance to Dutch road regulations and minimum propulsion requirements for the axles.

The requirements are combined with the reference vehicle properties and converted into topology constraints. These topology constraints contain the minimum wheel torque from stand-still, minimum wheel speed to achieve top speed, and minimum combined power from the power sources mechanically connected to the axles.

Chapter 4 Topology generation

The next step in the optimisation approach is the generation of topologies. First, a set of topologies is generated covering all possible combinations of components and connections between them. Secondly, this topology set is refined after a selection process to a set of feasible topologies. Finally, these feasible topologies are converted to simplified models to be used for simulations in the optimisation process. The methods to perform this generation, selection and conversion process are elaborated upon in this section.

4.1 Component combinations

The basis for all topologies are the components in the library. First the components are assessed by their functional classes describing the functionality of a component. Table 4.1 presents an overview of these classes. Since every component from the library can be used once in a topology, multiple instances of certain component classes are created in the library. These components are allowed to be present in plural form within a powertrain. The physical representation of a component could be an assembly of multiple subsystems fulfilling the task of the single component. An example of such a component is a fourfold differential, which in practise could be multiple linked twofold differentials.

Table 4.1: Component classes

Component class	Component	Description
Fuel ⇒ Mechanical	ICE	Internal combustion engine
Electric ⇒ Mechanical	MG	Motor-Generator
Mechanical transfer	PSD	Power split device
Mechanical conversion	TR	Transmission
Mechanical conversion	DIF	Differential
Mechanical transfer	AX	Axle
Mechanical ⇒ Electric ⇒ Mechanical	GBM	Generator-Battery-Motor

The library describes a component by its name, description and the number of edges. These edges are mechanical in and output ports of components. All edges must engage a connection to another component for the powertrain to function. The ICE represents a diesel engine that can be used for propulsion, or electric power generation when connected to a generator. The MGs are electric machines that can operate as both a motor and generator using all four quadrant of operation. The transmissions TR are discrete gearboxes with a variable number of gears and ratios. An axle AX is the final part connected to transfer power to the wheels and all four axles are always present.

Table 4.2: Component library

Component	Edges	Component	Edges
ICE	1	$TR1$	2
$MG1$	1	$TR2$	2
$MG2$	1	$TR3$	2
$MG3$	1	$TR4$	2
$MG4$	1	$TR5$	2
$PSD1$	3	$AX1$	1
$PSD2$	3	$AX2$	1
$PSD3$	3	$AX3$	1
$PSD4$	3	$AX4$	1
$DIF2\_a$	3	GBM	2
$DIF2\_b$	3		
$DIF3$	4		
$DIF4$	5		

The PSD is a transmission to split the required power over two power sources, and thus, has two inputs and one output edge. A PSD can be a fixed gearset or a planetary gearset. The GBM simulates the presence of a Generator-Battery-Motor combination without a mechanical connection between these

components. Additionally, the generator in the GBM is always connected to the ICE. The differentials DIF are indicated with an additional digit representing the number of outputs. The twofold differential appears twice in the library, denoted by the subscript $_a$ and subscript $_b$.

The topology generation process starts with the creation of components combination sets O_c by means of an exhaustive repetition of each component within the library in Table 4.2 being either present or not. Therefore, the number of possible component combinations (O_c) is directly dependent on the number n of components within the library:

$$|O_c| = 2^n \tag{4.1}$$

The number of all possible component combinations O_c^f, given the component library in Table 4.2 is $8.4 \cdot 10^6$.

Each component combination (O_c) is an n length array containing logical operators representing the presence of a component. The topology reduction is an integral part of the generation process to eliminate unnecessary calculations as early as possible. The reduction process is based on set theory [64]. Conditions set CC^f reduces the total set of possible component combinations to a reduced subset of feasible combinations (O_c^f) as visualised in Figure 4.1.

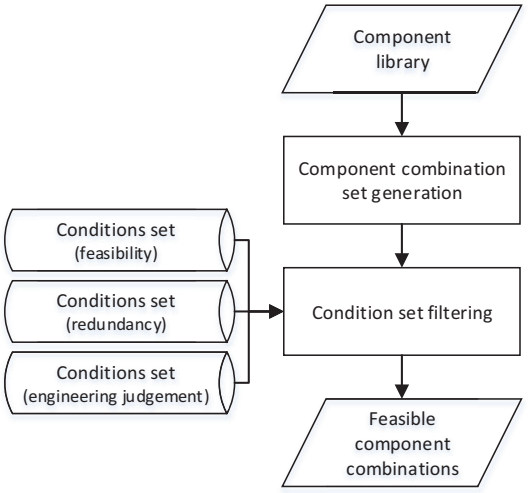

Figure 4.1: Flowchart component set generation

The first part of the conditions set CC^f is intended to exclude infeasible component combinations, conditions CC_1^f to CC_{14}^f. All components within a category are interchangeable, e.g. all MGs or all TRs, because their sizing and characteristics are not determined yet. To reduce the number of possible topologies, similar component combinations are excluded in the second part of the set using conditions $CC_1^f 5$ to CC_{22}^f. Based on engineering judgement, a set of final conditions is applied in CC_{23}^f to CC_{25}^f

$$\begin{aligned} &\text{Find all } O_c^f \subset O_c \\ &\text{s.t. } CC_1^f, ..., CC_{20}^f \subseteq CC^f \end{aligned} \tag{4.2}$$

The conditions set (CC^f) to reduce the set of combinations to the feasible set is defined as:

Conditions to exclude infeasible component combinations
CC_1^f Number of PSDs $\leq$ number of power sources -1
CC_2^f MG1 is always present to fulfil electric-drive requirement
CC_3^f If GBM is present, ICE must be present

CC_4^f If $<$ two power sources and a total of four axles, then a fourfold differential is present
CC_5^f Number of transmissions $\leq$ number of power sources
CC_6^f Number of transmissions $\geq$ number of power sources - number of PSD
CC_7^f If the fourfold differential is present, the total number of differential = 1
CC_8^f If the threefold differential is present, the total number of differential = 1
CC_9^f Number of power sources minus the number of PSD should be equal to the poweroutlets
CC_{10}^f If ICE is present, then either PSD1 or GBM must be present

Conditions to reduce the number of topologies based on redundancy
CC_{12}^f If TR(i) is present, MG(i) is present, $i \in \{1, 2, 3, 4\}$
CC_{13}^f If TR5 is present, the ICE or GBM are present
CC_{14}^f If two MG's are present, tean MG1 and MG2
CC_{15}^f If three MG's are present, then MG1, MG2 and MG3
CC_{16}^f If one twofold differential is present, then DIF2v_1
CC_{17}^f If one PSD is present, then PSD1 or PSD2
CC_{18}^f If two PSD's are present, then PSD1 and PSD2
CC_{19}^f If three PSD's are present, then PSD1, PSD2 and PSD3

Conditions to reduce the number of topologies based on engineering judgement
CC_{20}^f If a fourfold differential is present, then $\leq$ three power sources are present

The number of component combinations O_c^f is reduced from $8.4 \cdot 10^6$ to 523 by applying conditions set CC^f. The number of possible combinations for each number of components present in the component set is plotted in Figure 4.2 as 'Total'.

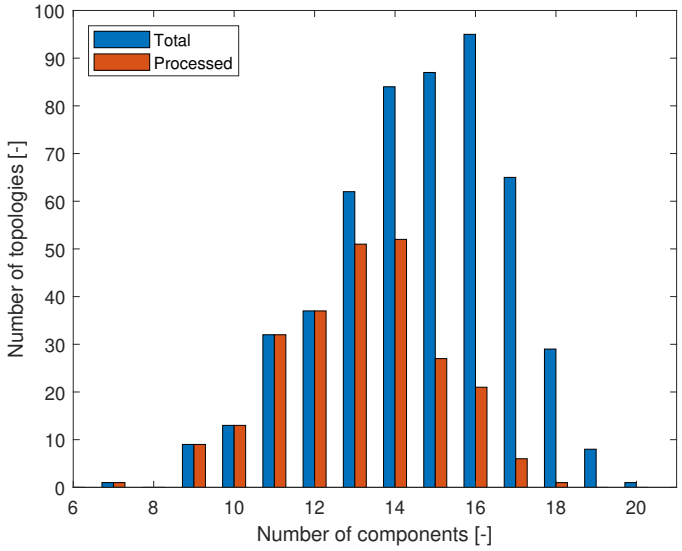

Figure 4.2: Number of processed topologies

4.2 Component edge connections

Each individual component can be connected to other components; depending on the type of component, it can engage in single or multiple connections. These components and connections can be represented as nodes and edges using graph theory [65]. A graph G describing an arbitrary powertrain is defined as:

$$G = (N, E) \tag{4.3}$$

Where N is a set of nodes and E is a set of edges. The number ${}^nC_r$ of possible edge combinations E_c for a node is described by [66]:

$$ {}^{n}C_r = \frac{n!}{r!\,(n-r)!} \tag{4.4} $$

n is the number of possibilities, in this case, the number of nodes
r is the number of objects to connect to, in this case, the number of edges ($r \in \{1, ..., n\}$)

$$ \begin{gathered} \text{Find all } E_c^f \subset E_c \\ \text{s.t. } CE_1^f, ..., CE_{32}^f \subseteq CE^f \end{gathered} \tag{4.5} $$

The conditions set (CE^f) to reduce the set of combinations E_c to the feasible set is defined as:

Conditions to exclude infeasible component combinations
CE_1^f Component is never connected to itself
CE_2^f A power source is not connected to another power source
CE_3^f A power source is not directly connected to an axle
CE_4^f A power source is not directly connected to a differential
CE_5^f The ICE cannot be connected directly to a differential
CE_6^f PSD is connected to $\leq$ one differential
CE_7^f PSD is connected to $\leq$ one axle
CE_8^f PSD is connected to $\leq$ two power sources
CE_9^f PSD is connected to $\leq$ two transmissions
CE_{10}^f GBM is always connected to ICE or PSD
CE_{11}^f GBM is never connected to a MG
CE_{12}^f GBM is never connected to an axle
CE_{13}^f GBM is never connected to a differential
CE_{14}^f TR is never connected to both a differential and an axle
CE_{15}^f TR is never connected to other transmissions
CE_{16}^f TR is never connected to two axles
CE_{17}^f TR is never connected to two differentials
CE_{18}^f TR is never connected to both ICE and GBM
CE_{19}^f TR is never connected to both ICE and an axle
CE_{20}^f An axle is never directly connected to a power source
CE_{21}^f An axle is never connected to another axle
CE_{22}^f A differential is never directly connected to a power source
CE_{23}^f A differential is never connected to another differential

Conditions to reduce the number of topologies based on redundancy
CE_{24}^f If MG(i) is connected to a transmission, then to TR(i)
CE_{25}^f If MG(i) is connected to a PSD, then to PSD(i) or PSD(i-1)
CE_{26}^f If GBM is connected to a PSD, then to PSD1
CE_{27}^f If GBM is connected to a transmission, then to TR5
CE_{28}^f If ICE is connected to a transmission, then TR5
CE_{29}^f PSD1 can be connected to : ICE - MG1 - MG2 - GBM - TR1 - TR2 - TR5 - PSD2 - any axle - any differential
CE_{30}^f PSD2 can be connected to : MG2 - MG3 - TR2 - TR3 - PSD1 - PSD3 - any axle - any differential
CE_{31}^f PSD3 can be connected to : MG3 - MG4 - TR3 - TR4 - PSD2 - PSD4 - any axle - any differential
CE_{32}^f PSD4 can be connected to : MG4 - TR4 - PSD3 - any axle - any differential

The possible edge combinations are reduced from $7.7 \cdot 10^{57}$ to $3.1 \cdot 10^{27}$ feasible edge combination E_c^f by applying condition set CE^f. Not all edge combinations are considered during the generation of a topology. Only the edge combinations E_c^f of components present in the component set O_c^f used during that particular iteration are considered in the topology generation; therefore, the actual number of considered edge combinations per topology is always lower.

4.3 Topology generation

A topology is a set of components logically connected to transfer energy between a power source and the vehicle's wheels. In the previous sections, two feasible subsets O_c^f and E_c^f are created describing all feasible component combinations and all feasible possibilities to interconnects these components. To create feasible topologies, the two feasible subsets O_c^f and E_c^f are combined, resulting in topology connection matrixes T_c of n x n size containing all connections between components. The T_c rows and columns represent the library components; the cells contain logical operators indicating which components are connected. A final conditions set CT^f is applied within the topology generation process to reduce the set of component-edge combinations T_c to a feasible set of topologies T_c^f.

$$\begin{aligned} &\text{Find all } T_c^f \subset T_c \\ &\text{s.t. } CT_1^f, ..., CT_5^f \subseteq CT \end{aligned} \tag{4.6}$$

The following conditions are applied:

CT_1^f The topology matrix must be symmetric
CT_2^f If a GBM is connected to a PSD, also an MG should be connected to the PSD
CT_3^f Two connected PSDs cannot be connected to three MGs
CT_4^f Two connected PSDs cannot be connected to two MGs and a GBM
CT_5^f A TR must be present between power source and axle

Generating topology connection matrixes is computationally intensive. To reduce the physical computation time, only edge combinations containing components present in the specific component set used in the topology at hand are considered. This is realised by automatically producing a script for each component set individually, only including the required code for the components involved. Additionally, these scripts are converted to C-code and processed in parallel to reduce the computation time.

Due to the high physical computational time required, not all components sets O_c^f are used to generate topologies. The computation time per component combination is limited to four days to keep the total required computational time within practical limits. The generation process is iterated over the least computationally involved O_c^f until four days of computation time per O_c^f is reached. This generation process results in a total of 2384 feasible generated topologies. This set is generated while applying condition set CT^f. The number of processed component combinations is shown in Figure 4.2. The total number of possible topologies generated from the component library is unknown due to the high computation time involved.

The estimated total processing time of the topology generation process based on the number of components in the topology is shown in Figure 4.3. As shown, the computation time significantly increases when introducing more components to the topology. The number of occurrences based on the computation time is presented in the histogram Figure 4.4. All computation time estimations are based on a single-core of an Intel i7 7700HQ, 32GB, Windows 10 system.

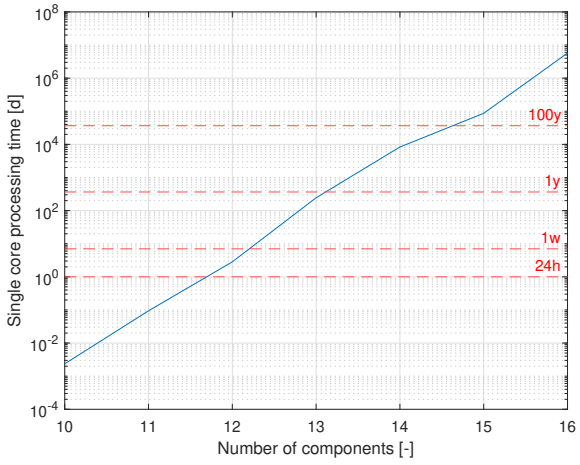

Figure 4.3: Topology generation processing time

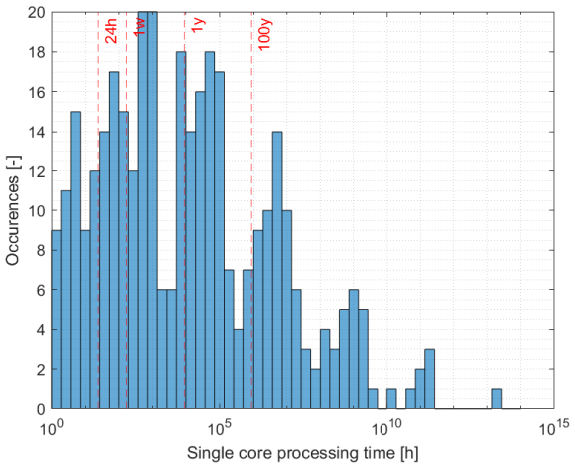

Figure 4.4: Topology generation processing time

4.4 Topology to model conversion

The next step is to convert the feasible topology connection matrixes (T_c^f) to models to be used within the optimisation framework. These models represent the torque-speed conversion between the wheels and the power sources. The first step in this process is to convert the matrix representation to an undirected graph followed by conversion to a directed graph by defining the power flow between nodes. This conversion is achieved by following the graph node chain and, where multiple directions are possible, applying a rule set ($RM\{RM_1, ..., RM_3\}$) to determine the direction of flow. To determine the downstream edge if > 2 edges are present at a node, apply the following rules:

RM_1 dismiss edges connected to a power source
RM_2 if multiple possibilities remain, dismiss edges indirectly connected to a power source
RM_3 if no possibilities remain, remove PSDs from dismissed possibilities

A model description is generated from the created directional graph by following the nodes according to the prescribed flow direction and converting its path to code. This method is repeated to trace the dependency for each power source to their respective wheel loads in speed and torque.

$$
\begin{aligned}
ICE_T &= AX4_T \cdot PSD1_b \cdot (1 - PSD1_{split}) \cdot TR5_{ratio} \\
ICE_v &= \frac{AX4_v}{PSD1_b \cdot TR5_{ratio}} \\
MG1_T &= AX2_T \cdot TR1_{ratio} \\
MG1_v &= \frac{AX2_v}{TR1_{ratio}} \\
MG2_T &= AX4_T \cdot PSD1_a \cdot PSD1_{split} \cdot TR2_{ratio} \\
MG2_v &= \frac{AX4_v}{PSD1_a \cdot TR2_{ratio}} \\
MG3_T &= AX3_T \cdot TR3_{ratio} \\
MG3_v &= \frac{AX3_v}{TR3_{ratio}} \\
MG4_T &= AX1_T \cdot TR4_{ratio} \\
MG4_v &= \frac{AX1_v}{TR4_{ratio}}
\end{aligned}
\tag{4.7}
$$

An example of a topology is presented in Table 4.3 and Equation 4.7. Table 4.3 shows the connection matrix of the topology indication connections between components with logical values $\{1, 0\}$ Equation

4.7 represents the model describing the relationship between the required torque and speed from the axles to the power sources. The model is unaltered and presented as it is generated and used within the optimisation process. Torque is indicated by the subscript $_T$, speed by the subscript $_v$, and transmission ratios are described as $TR(m)_{ratio}$ $m \in \{1, 2 \ldots 5\}$. Power split devices are described by two variables, one to accommodate torque split $PSD(k)_{split}$ $k \in \{1, 2, 3, 4\}$ and one to accommodate a transmission ratio $PSD(k)_a$ and $PSD(k)_b$.

Table 4.3: Topology component connection matrix

	ICE	MG1	MG2	MG3	MG4	PSD1	PSD2	PSD3	PSD4	TR1	TR2	TR3	TR4	TR5	DIF2v_1	DIF2v_2	DIF3v	DIF4v	AX1	AX2	AX3	AX4	GBM
ICE	0	0	0	0	0	0	0	0	0	0	0	0	0	**1**	0	0	0	0	0	0	0	0	0
MG1	0	0	0	0	0	0	0	0	0	**1**	0	0	0	0	0	0	0	0	0	0	0	0	0
MG2	0	0	0	0	0	0	0	0	0	0	**1**	0	0	0	0	0	0	0	0	0	0	0	0
MG3	0	0	0	0	0	0	0	0	0	0	0	**1**	0	0	0	0	0	0	0	0	0	0	0
MG4	0	0	0	0	0	0	0	0	0	0	0	0	**1**	0	0	0	0	0	0	0	0	0	0
PSD1	0	0	0	0	0	0	0	0	0	0	**1**	0	0	**1**	0	0	0	0	0	0	0	**1**	0
PSD2	0	0	0	0	0	0	0	0	0	0	0	0	0	0	0	0	0	0	0	0	0	0	0
PSD3	0	0	0	0	0	0	0	0	0	0	0	0	0	0	0	0	0	0	0	0	0	0	0
PSD4	0	0	0	0	0	0	0	0	0	0	0	0	0	0	0	0	0	0	0	0	0	0	0
TR1	0	**1**	0	0	0	0	0	0	0	0	0	0	0	0	0	0	0	0	0	**1**	0	0	0
TR2	0	0	**1**	0	0	**1**	0	0	0	0	0	0	0	0	0	0	0	0	0	0	0	0	0
TR3	0	0	0	**1**	0	0	0	0	0	0	0	0	0	0	0	0	0	0	0	0	**1**	0	0
TR4	0	0	0	0	**1**	0	0	0	0	0	0	0	0	0	0	0	0	0	**1**	0	0	0	0
TR5	**1**	0	0	0	0	**1**	0	0	0	0	0	0	0	0	0	0	0	0	0	0	0	0	0
DIF2v_1	0	0	0	0	0	0	0	0	0	0	0	0	0	0	0	0	0	0	0	0	0	0	0
DIF2v_2	0	0	0	0	0	0	0	0	0	0	0	0	0	0	0	0	0	0	0	0	0	0	0
DIF3v	0	0	0	0	0	0	0	0	0	0	0	0	0	0	0	0	0	0	0	0	0	0	0
DIF4v	0	0	0	0	0	0	0	0	0	0	0	0	0	0	0	0	0	0	0	0	0	0	0
AX1	0	0	0	0	0	0	0	0	0	0	0	0	**1**	0	0	0	0	0	0	0	0	0	0
AX2	0	0	0	0	0	0	0	0	0	**1**	0	0	0	0	0	0	0	0	0	0	0	0	0
AX3	0	0	0	0	0	0	0	0	0	0	0	**1**	0	0	0	0	0	0	0	0	0	0	0
AX4	0	0	0	0	0	**1**	0	0	0	0	0	0	0	0	0	0	0	0	0	0	0	0	0
GBM	0	0	0	0	0	0	0	0	0	0	0	0	0	0	0	0	0	0	0	0	0	0	0

4.5 Topology verification

The first step in the verification process is to verify the topologies' uniqueness and remove isomorphic topologies. Van Harselaar [50] suggested using the unique properties of prime numbers to determine unique power paths. Each variant of transmission components, planetary gearsets and transmissions, is replaced by a prime number. Because the transmission components are interchangeable within its variant set, they are assigned the same prime number. Assuming a fixed wheel torque at all wheels, the required torque at all power sources is calculated for all feasible models. The models producing identical required torques represent topologies with an equal overall transmission ratio and are therefore isomorphic and redundant. The redundant models are removed from the set. The generated topology set is reduced further from 2384 to 264 by eliminating these isomorphic topologies.

The specific representation of the transmission components is varied within the optimisation framework. A PSD can serve as a fixed gear set to couple two power sources to a single output shaft coupling the rotational velocities. However, the models are structured so that they can be replaced by a conventional

planetary gearset with variable rotational speeds as well. In this research, only the fixed gear sets are considered as PSDs. Additionally, the transmissions can be represented as either a single or a multi-speed transmission. Given the required high torque levels, continuously variable transmissions (CVTs) are not considered in this research.

4.6 Summary

The generation of topologies is a multi-step process. A heuristic filter design constructed by constraints is applied to the consecutive steps of the generation process. Using graph theory, the components and the connections in between are represented as nodes and edge combinations.

The first step is, based on a library, generating a set of component combinations covering all possible combinations of components and reducing them to a feasible set by applying constraints. The next step is to inventory all possible connections between components and filter the set over constraints. The connections between components are referred to as edge connections. These edge connections and the generated component combinations are integrated into topologies in the form of a logical connection matrix describing the presence and connections between components. This integration is computationally intensive, increasing exponentially with the number of components in a set. Topologies are generated from the least computationally involved set upwards. For practicality, the generation of topologies is limited to a maximum of four days per component set.

The following step is to convert the generated topologies to simplified models using graph theory; this allows them to be used for simulations in the optimisation process. Lastly, during the topology verification process, a final constraint set is applied to refine the selection, and all isomorphic topologies are removed. The resulting set of feasible topologies is used as input for the optimisation framework.

Chapter 5 Vehicle model and control

The aspects of vehicle modelling and control are addressed in this chapter. First, an overview is provided of the component models, describing the characteristic component specifications of the components used to construct the topologies. These characteristics include mass and cost calculations and are concluded by the mass and cost calculations at vehicle level. Secondly, an elaboration is provided on the transmission design and transmission gearshift control. Thirdly, the energy and power management is explained, consisting of torque split control between axles and power sources. These controllers allow for asymmetric power and torque distribution based on efficiency and torque transfer capabilities. Finally, the thermostat charge control to manage the State-of-Charge (SOC) of the battery is addressed.

5.1 Characteristic component specifications

All components directly scaled in the optimisation framework, such as the ICE or battery, are map-based models. Additionally, both the directly scaled components and the indirectly scaled components, such as a transmission or power electronics, are described by a linear relationship between maximum power $P_{j,max}$ $[kW]$, costs C_j [€] and mass m_j $[kg]$, j being the components. The costs are calculated with a fixed cost per component $C_{j,0}$ and variable power-dependent costs $C_{j,var}$. Similarly, the mass calculation is constructed by a minimal mass $m_{j,0}$ with added power rating dependent mass $m_{j,var}$. Both generalised calculation methods are presented in Equation 5.1. Each component's mass and cost plot indicate the data source and the data collection date or the estimated year of validity for the approximation. ICE and MG component parameters are scaled to 100$[kW]$ before scaling by the PSO algorithm. Battery scaling is performed by scaling the number of strings in parallel. Whereas the number of strings in parallel should be discrete, PSO only accepts continuous scaling; therefore, fractions of strings in parallel are accepted even though this is infeasible. Appendix B contains all referenced data used for mass and cost calculation of the components.

$$\begin{aligned} C_j &= C_{j,0} + P_{j,max} \cdot C_{j,var} \\ m_j &= m_{j,0} + P_{j,max} \cdot m_{j,var} \end{aligned} \tag{5.1}$$

5.1.1 Combustion engine

The ICE is represented by multiple map-based models of different size ICEs. The maximum torque vector and the efficiency map along the torque axis are scaled for different ICE sizes using scaling variable s_{ICE}. The base efficiency and maximum torque maps of these models are scaled to 100 $[kW]$ and plotted in Figure 5.1, 5.2 and 5.3. The first efficiency map ICEa in Figure 5.1, is a Audi 2.5L (88 $[kW]$) Turbo Diesel Engine[67]. The second plot, Figure 5.2, is a Cummins M11-330 (246 $[kW]$) Diesel Engine[67]. The third plot, Figure 5.3 is an empirically fitted model of an arbitrary 330 $[kW]$ diesel engine by TNO; further specifications of this engine are not disclosed due to confidentiality.

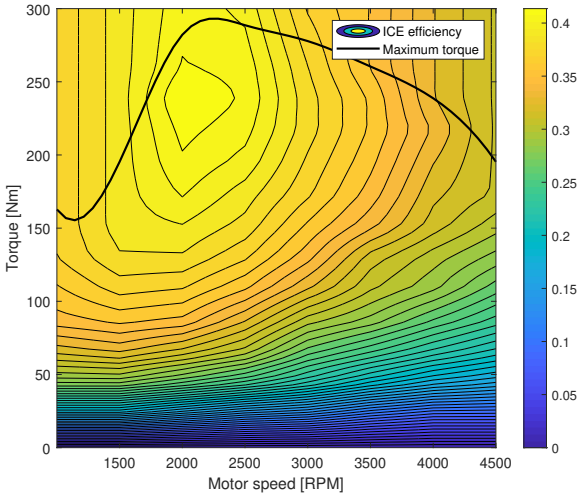

Figure 5.1: ICEa efficiency, LD

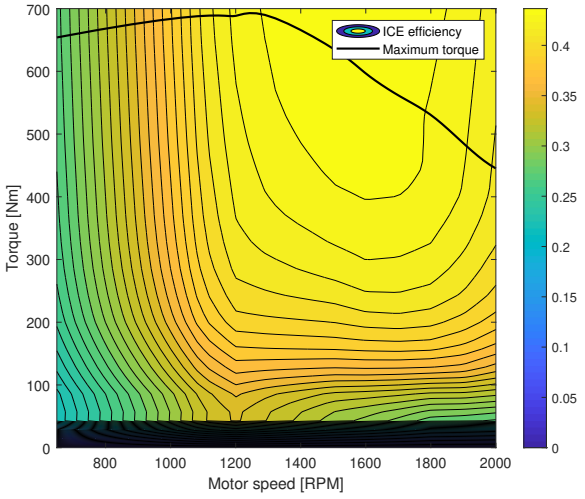

Figure 5.2: ICEb efficiency, HD

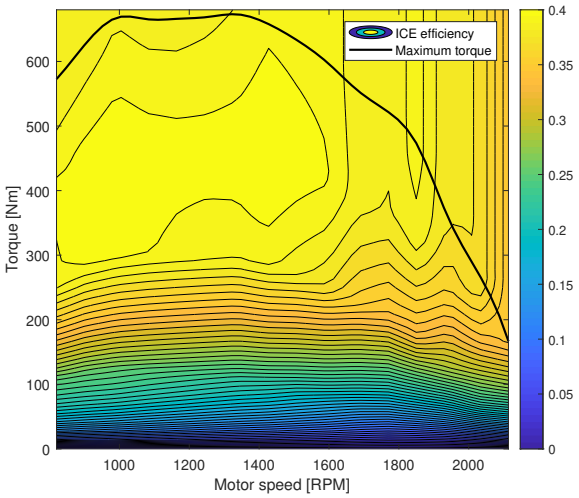

Figure 5.3: ICEc efficiency, HD

The applied scaling of the ICE models allows the use of multiple models for different size components and transitions between models depending on the scale s_{ICE}. The scaling determines the factor of each property $f_{ICE,(i)}$, $i \in \{1,2,3\}$, used of each model based on the maximum power of each ICE $P_{max,ICE(i)}$ to form the parameter set $F(s_{ICE})$. The threshold values indicating the maximum scale of the models are indicated by $s_{limit,(i)}$. A linear ratio is used to scale between the models; the relationship is shown in Equation 5.2.

$$F(s_{ICE}) = \begin{cases} s_{ICE} \cdot f_{ICE,1} & \text{for} \quad s_{ICE} \leq s_{limit,1} \\ 1 - \frac{s_{ICE} - s_{limit,1}}{s_{limit,2} - s_{limit,1}} \cdot f_{ICE,1} + \frac{s_{ICE} - s_{limit,1}}{s_{limit,2} - s_{limit,1}} \cdot f_{ICE,2} & \text{for} \quad s_{limit,1} < s_{ICE} \leq s_{limit,2} \\ 1 - \frac{s_{ICE} - s_{limit,2}}{s_{limit,3} - s_{limit,2}} \cdot f_{ICE,2} + \frac{s_{ICE} - s_{limit,2}}{s_{limit,3} - s_{limit,2}} \cdot f_{ICE,3} & \text{for} \quad s_{limit,2} < s_{ICE} \leq s_{limit,3} \\ s_{ICE} \cdot f_{ICE,3} & \text{for} \quad s_{ICE} > s_{limit,3} \end{cases} \tag{5.2}$$

$$s_{limit,(i)} = \frac{P_{max,ICE(i)}}{100} \tag{5.3}$$

The costs and mass of the ICE is described by a linear relationship to its maximum power $P_{ICE,max}$ as shown in Equation 5.1. The cost C_j [€] estimation is based on the most recent available data for HD engines for this study, assuming no fixed cost $C_{ICE,0}$ and variable costs $C_{ICE,var}$ of 56.5 [€/kW]. The TNO [68] mass approximation for ICE mass deviates significantly from the other sources; therefore, the engine's mass is estimated averaged between Kleiner [69] and ADVISOR [67] data resulting in no minimal mass $m_{ICE,0}$ and variable mass $m_{ICE,var}$ of 3.37 [kg/kW].

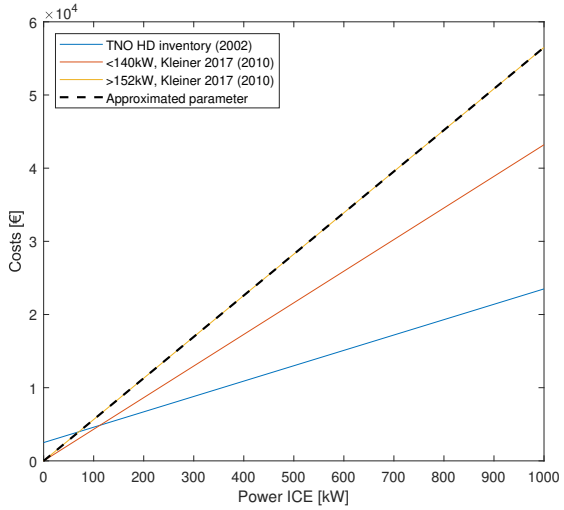

Figure 5.4: ICE costs

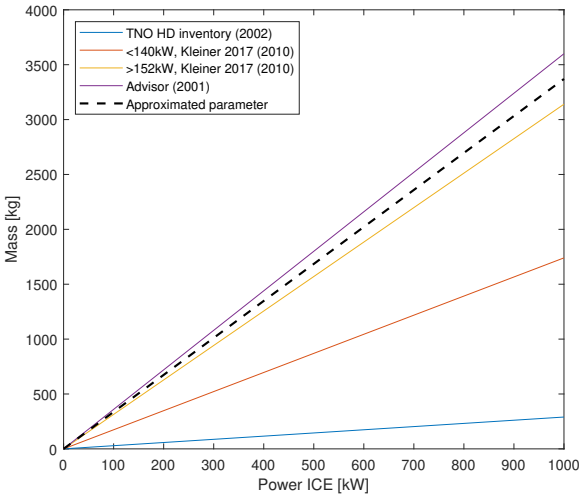

Figure 5.5: ICE mass

5.1.2 Electric motor-generator

Identical to the ICE, the maximum torque vector and the efficiency map along the torque axis are scaled for different MG sizes. A single base model is used to scale the component properties with scaling variable s_{MG} using Equation 5.4. The base model is a 140 $[kW]$ e-motor fitted to experimental data by TNO scaled to 100 $[kW]$, the efficiency η_{MG} is combined for the motor and inverter as shown in Figure 5.6. This scaling method allows for scaling of MGS greater than currently commercially available; in practice, this would be resolved by implementing multiple MGs connected in series. Simulating the efficiency for multiple motors in series would require an additional sizing optimisation and torque split controller and is therefore accepted to scale linearly.

$$f(s_{MG}) = s_{MG} \cdot f_{MG} \tag{5.4}$$

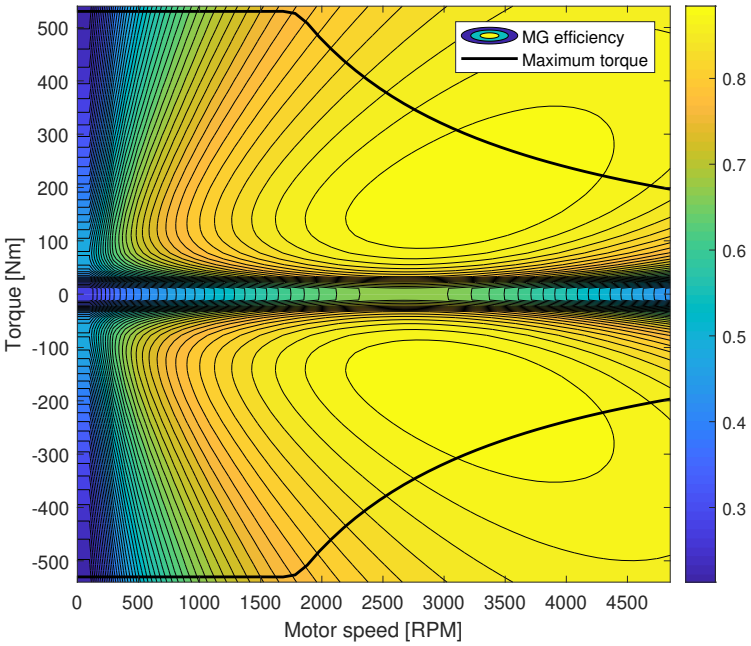

Figure 5.6: Motor-generator efficiency

The cost estimation C_{MG} [€] is based on the most recent dataset used by a respective source, the ICCT (2017) approximation with a fixed cost per component $C_{MG,0}$ of 76 [€] and variable costs $C_{MG,var}$ of 15 [€/kW]. The MG mass estimation m_{MG} [kg] is averaged halfway between Verbruggen [70] and Kleiner [69] since they both base their approximations on the most recent datasets of the investigated sources. The mass calculation uses no minimal mass $m_{MG,0}$ and a variable component $m_{MG,var}$ of 0.68 [kg/kW].

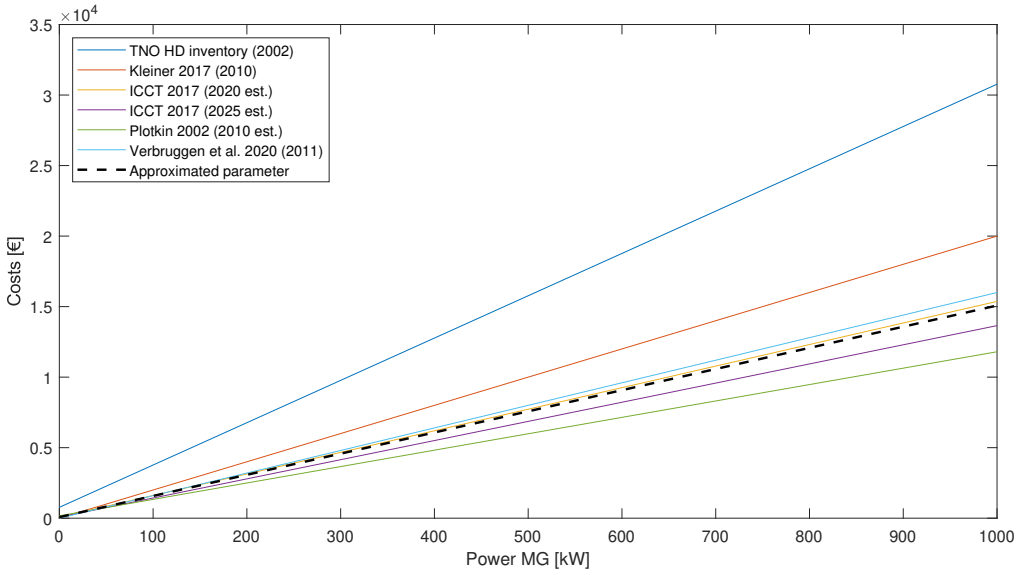

Figure 5.7: Motor-generator costs

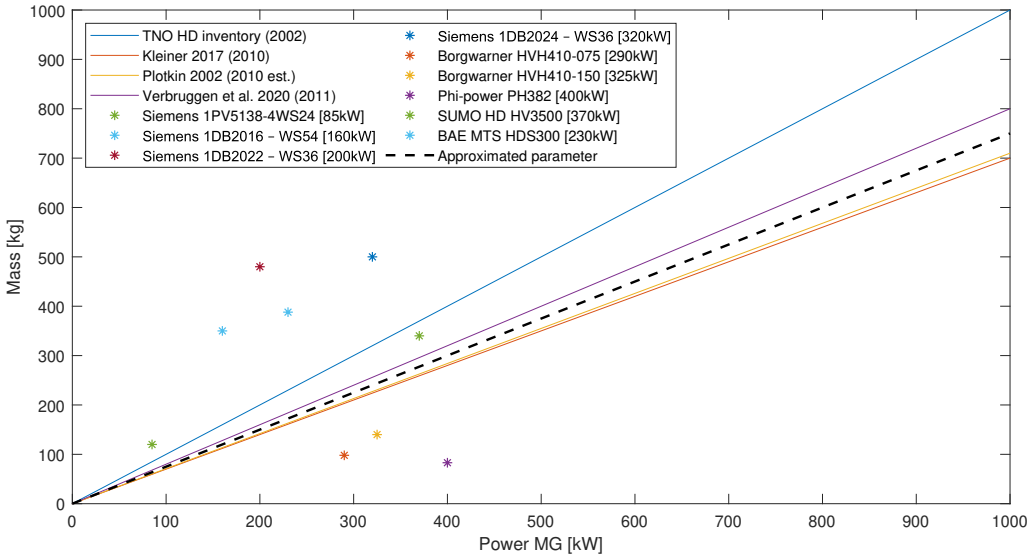

Figure 5.8: Motor-generator mass

The electric power consumption of the MG E_{MG} is calculated as,

$$E_{MG} = T_{MG} \cdot \omega_{MG} \cdot \eta_{MG}^{-sign(T_{MG})} \tag{5.5}$$

5.1.3 Generator, series topologies

The generator in series topologies is automatically scaled to operate as efficiently as possible in combination with the ICE. First, the optimal operation point, ω^*_{ICE} and T^*_{ICE}, of the ICE is determined, followed by the optimal operating point of the generator model ω^*_G and T^*_G. The second step is to calculate the transmission ratio $r_{ICE,G}$ to match ω^*_G with ω^*_{ICE} and multiply T^*_G by this ratio; this produces the torque

rating of the generator when connected to the ICE by a single-gear transmission with ratio $r_{ICE,G}$. The final step is scaling the generator torque rating to match T^*_{ICE} as shown in Equation 5.6.

$$\begin{aligned} r_{ICE,G} &= \frac{\omega^*_G}{\omega^*_{ICE}} \\ T^*_{G,scaled} &= T^*_G \cdot \frac{T^*_{ICE}}{T^*_G \cdot r_{ICE,G}} \end{aligned} \tag{5.6}$$

5.1.4 Power electronics

The cost of the power electronics C_{PE} [€] is based on the most recent available data from the International Council on Clean Transportation [55] (ICCT) for 2020. ICCT includes the cost for the complete electrical system required to operate a motor, while other sources only quote the inverters and therefore provide lower estimates. The cost estimation does not assume fixed cost $C_{PE,0}$ and variable costs $C_{PE,var}$ are 54.18 [€/kW]. Due to the low number of sources, the estimated mass m_{PE} [kg] is chosen to be centred between both most recent HD sources Kleiner [69] and Verbruggen [70], ignoring the LD estimation by Kleiner [69]. The mass calculation parameters are a zero minimal mass $m_{PE,0}$ and variable mass $m_{PE,var}$ estimated at 0.13 [kg/kW].

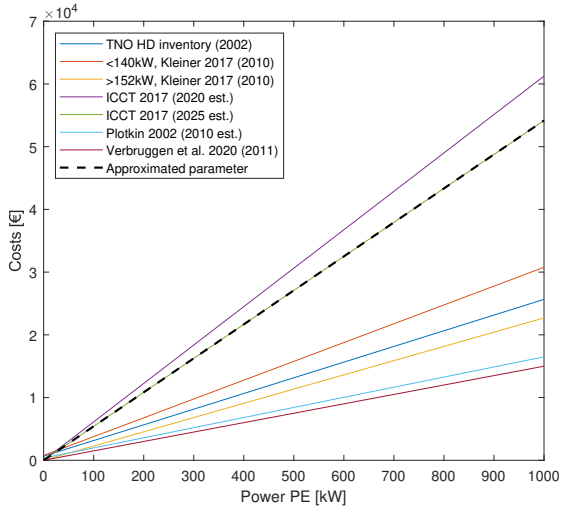

Figure 5.9: Power electronics costs

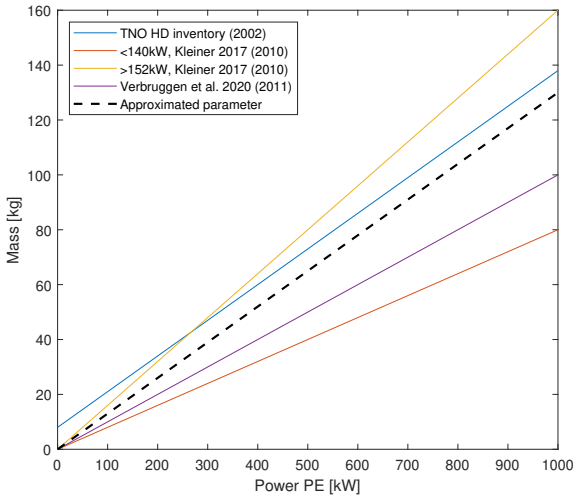

Figure 5.10: Power electronics mass

5.1.5 Battery

The battery is modelled as an equivalent circuit model. A single cell is modelled and connected in series n_{series} to achieve the desired voltage U_{OC} [V] and scaled parallel n_{par} to achieve the desired capacity Q_{bat} [kW/h]. The open circuit voltage U_{oc} is described as,

$$U_{OC} = U_{OC,cell(\xi)} \cdot n_{series} \tag{5.7}$$

where $U_{OC,cell}$ is state-of-charge ξ dependent, as shown in Figure 5.11. The battery capacity is only dependent on the number of cells in parallel; the nominal cell capacity $Q_{bat,cell}$ for the simulated battery is 20 [A] [3].The influence of coulomb efficiency on energy usage is not incorporated in the model.

$$Q_{bat} = Q_{bat,cell} \cdot n_{par} \tag{5.8}$$

The battery resistance R_{bat} is dependent on ξ, n_{series} and n_{par},

$$R_{bat} = R_{bat,cell(\xi)} \cdot \frac{n_{series}}{n_{par}} \tag{5.9}$$

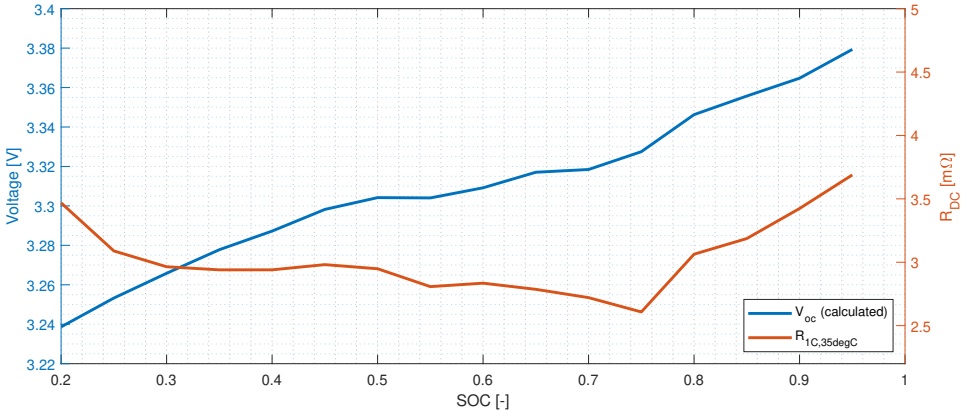

Figure 5.11: Voltage and resistance of a LiFePO4 cell [3]

The currentflow I_{bat} is calculated by,

$$I_{bat} = \frac{U_{OC} - \sqrt{U_{OC}^2 - 4 \cdot R_{bat} \cdot Pbat}}{2 \cdot R_{bat}} \tag{5.10}$$
$$P_{bat} = P_{MG} + P_{aux}$$

Where P_{aux} is auxiliary power request and MG power P_{MG} can be positive or negative, $k \in \{1, 2, 3, 4\}$.

$$P_{MG} = \sum T_{MG,k} \cdot \omega_{MG,k} \tag{5.11}$$

The maximum current through the battery $I_{bat,max}$ is limited by the maximum current over the cells $I_{bat,cell,MAX}$ and dependent on the number of cells in parallel n_{par}. Therefore, both the capacity and the current demands are a factor in scaling the battery.

$$I_{bat,max} = I_{bat,cell,MAX} \cdot n_{par} \tag{5.12}$$

A wide variety of sources is available for battery cost C_{bat} [€] and mass m_{bat} [kg] estimation. Both the mass and cost estimations are based on the only source separating HD from off-road machinery, using the 2020 values determined by Batteries Europe [71]. The mass and cost calculation is constructed by only a variable component, $C_{bat,var}$ is 350 [€/kWh] and $m_{bat,var}$ is 5 [kg/kWh].

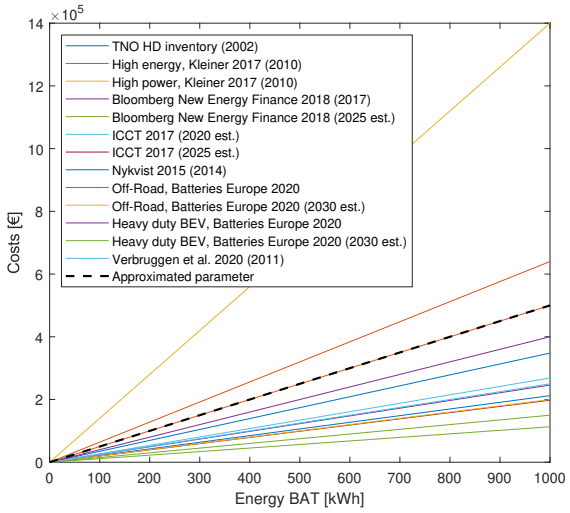

Figure 5.12: Battery costs

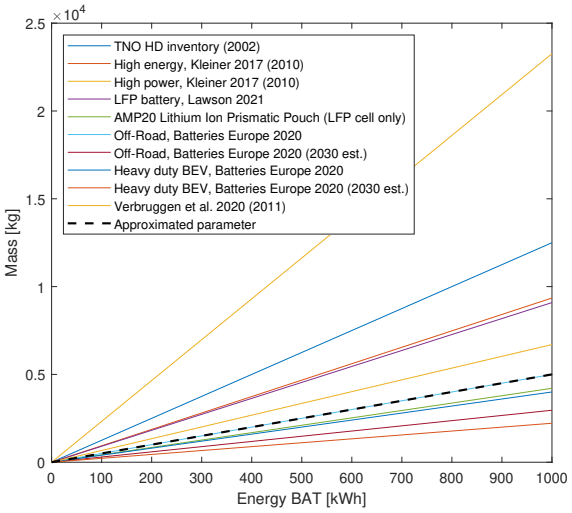

Figure 5.13: Battery mass

5.1.6 Differential

In order to include as many components as realistically possible in the approximation of the powertrain, the parameters of the differential are also included. Guidelines for this approximation are not found within the investigated sources; therefore, the calculation method for a single-stage reduction by Plotkin et al.[72] is used for mass m_{DIF} and cost C_{DIF} values of the differentials. Initial costs $C_{DIF,0}$ for any differential is estimated at 72.17 [€] with an added $C_{DIF,var}$ of 1.44 [€/kW] depending on the power of attached power sources. The mass is only dependent only power-based, and $m_{DIF,var}$ is set at 0.59 [kg/kW].

5.1.7 Transmission

For the transmission cost estimation C_{TR} [€], only one LD estimation was found by Plotkin[72], the estimated cost appears to be unrealistically low for HD application. In the absence of an alternative calculation method, the costs are scaled upwards depending on the number of gears from the reference value[72].

The mass m_{TR} [kg] is estimated between the highest and lowest source value, with a linear spread of transmissions with increasing gear numbers. Since the specifications for COTS transmissions are based on torque capabilities, the maximum power of the attached MGs is assumed to be achieved at 1500 [RPM]. This assumption allows plotting the COTS torque specifications on a power scale as used in Figure 5.15. Figure 5.14 and 5.15 show the approximated mass and costs for several transmission options ranging from three to twelve gears. Equation 5.13 and 5.14 describe a fitted approximation of the mass and cost of a transmission based on the maximum power $P_{TR,max}$ of the attached power source.

$$\begin{aligned} m_{TR} &= m_{TR,0} + m_{TR,var} \cdot P_{TR,max} \\ m_{TR,0} &= 20 + (n_{gears} - 9) \cdot 3.33 \\ m_{TR,var} &= \frac{1}{1.55} + (n_{gears} - 9) \cdot \frac{3}{160} \end{aligned} \tag{5.13}$$

$$\begin{aligned} C_{TR} &= C_{TR,0} + C_{TR,var} \cdot P_{TR,max} \\ C_{TR,0} &= 229.23 \\ C_{TR,var} &= 5 + (n_{gears} - 9) \cdot \frac{1}{7} \end{aligned} \tag{5.14}$$

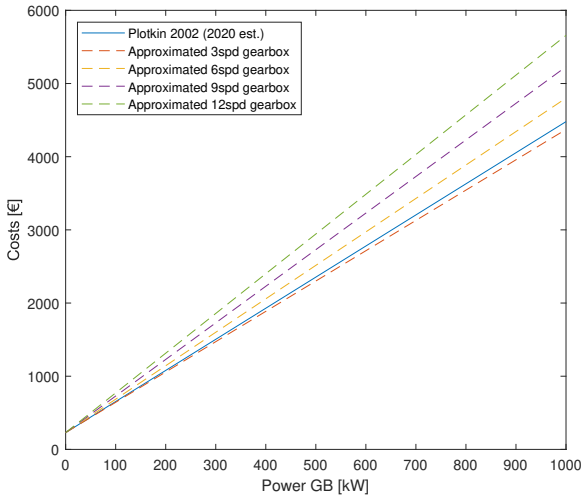

Figure 5.14: Transmission costs

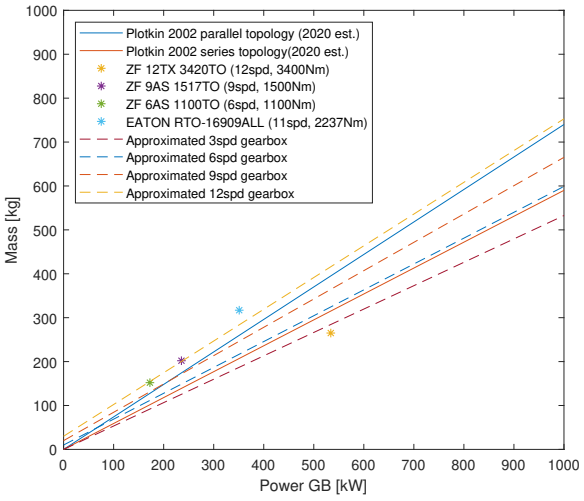

Figure 5.15: Transmission mass

Alternative calculation methods for mass m_{TR} and costs C_{TR}, Equation 5.15 , are provided in[73] and[74] respectively. These methods base their calculation on the outgoing torque capability of transmission. Since the required outgoing torque is dependent and the final drive ratio, these methods are compatible

with the used vehicle model. This calculation method would be a good alternative would the final drive ratio be known.

$$\begin{aligned} m_{TR} &= 2.382 \cdot ((T_{out}{}^{0.411}) \cdot (n_{gears}{}^{0.206})) \\ C_{TR} &= 16.73 \cdot m_{gb} \end{aligned} \tag{5.15}$$

The losses caused by gearshifts due to inertia losses of components is not included in the transmission model. Nonetheless, clutch losses $P_{clutchloss}$ due to slipping of the clutch at vehicle launch are incorporated. Clutch losses are present when the ICE speed ω_{ICE} is under the stall limit $\omega_{ICE,stall}$, these losses are calculated in Equation 5.16

$$P_{clutchloss} = \begin{cases} \frac{(\omega_{ICE,stall} - \omega_{ICE}) \cdot T_{ICE}}{\eta_{ICE}} & \text{for} \quad \omega_{ICE} < \omega_{ICE,stall} \\ 0 & \text{for} \quad \omega_{ICE} \geq \omega_{ICE,stall} \end{cases} \tag{5.16}$$

The transmission efficiency is dependent on the gear stages required to achieve the transmission ratio of the respective gear $r_{TR,m,n}$. A single gear stage is assumed to achieve a maximum ratio of four efficiently with an efficiency μ_{gs} of 98.5 [%]. The efficiency of a gear ratio μ_n is calculated in Equation 5.17.

$$\mu_n = \begin{cases} \mu_{gs} & \text{for} \quad r_{TR,m,n} \leq 4 \\ \mu_{gs}^2 & \text{for} \quad 4 < r_{TR,m,n} \leq 16 \\ \mu_{gs}^3 & \text{for} \quad r_{TR,m,n} > 16 \end{cases} \tag{5.17}$$

5.2 Transmission design

Geometric gear design [74] is the method chosen to determine the transmission gear ratio's $r_{TR,m,n}$ of the simulated AMT, m indicating the transmission and n the respective gear. The geometric design allows for a constant speed difference between gearshifts at max motor speed and continuous availability of power at all velocities as shown in Figure 5.17 and 5.19. A final drive ratio is not included in the topologies; therefore, the gear ratios are for the complete transmission between the power source and the wheels. In actual application, a component with an arbitrary final transmission ratio drive will be present. This component can be a differential, a hub gearset, spur gear, or any gear linkage between the transmission and the wheel. The gear ratio's n, $n \in \{1, 2, \ldots N\}$, are calculated according to Equation 5.18. N being the number of gears in the transmission.

$$\begin{aligned} W_{TR} &= \sqrt[N-1]{\frac{n_{low}}{n_{high}}} \\ n_i &= n_{i+1} \cdot W_{TR} \end{aligned} \tag{5.18}$$

Where n_{low} is the transmission ratio to achieve maximum gradient hill start given the current power source sizing, the ratio n_{high} depends on the connected power source type. n_{high} is scaled such that either the maximum vehicle speed is achieved at maximum MG speed $\omega_{MG,max}$ or n_{high} is scaled to allow maximum vehicle speed is at maximum ICE power. Scaling to $\omega_{MG,max}$ is possible because of the MG's continuous power curve from base speed upwards; alternatively, scaling towards the ICE maximum power operating point is done to compensate for the decreasing power at high engine speeds.

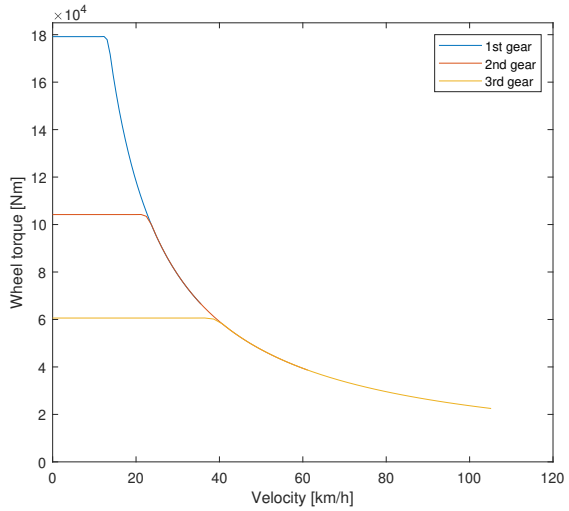

Figure 5.16: Geometric gear design, MG 3-speed

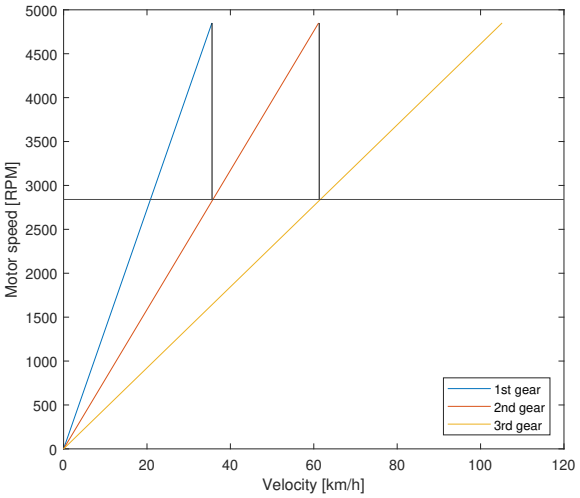

Figure 5.17: Geometric gear design, MG 3-speed

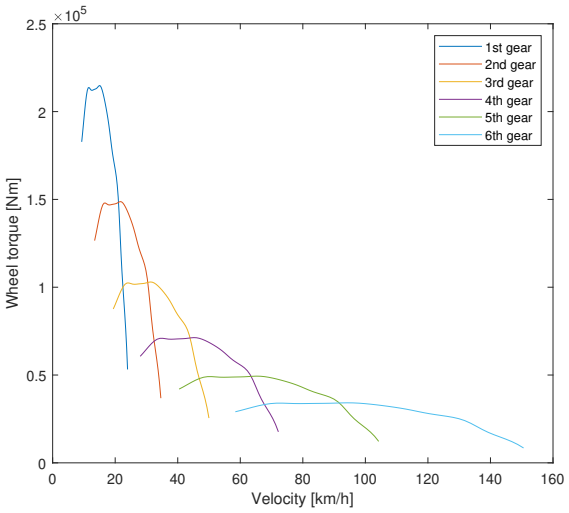

Figure 5.18: Geometric gear design, ICE 6-speed

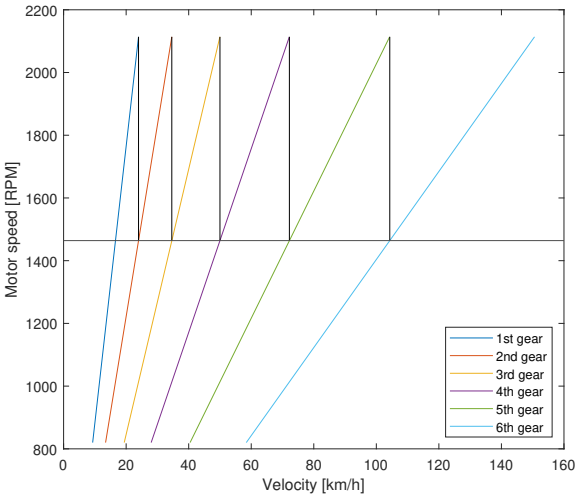

Figure 5.19: Geometric gear design, ICE 6-speed

5.3 Vehicle mass model

Separate component models are described in previous sections, and the vehicle model integrates all individual components within the topology. The vehicle mass model is a summation of all component masses. The Dutch road regulation limit the maximum vehicle mass $m_{v,max}$ by applying a maximum axle load $m_{axle,max}$. The allowable gravimetric cargo on or in the vehicle is determined by $m_{v,max}$, the mass of the empty vehicle without the powertrain $m_{v,hull}$ and the mass of the powertrain m_{pwtr}. Fuel, AdBlue or any other variable mass is excluded from the mass calculation.

$$\begin{aligned} m_{cargo} &= m_{v,max} - m_{v,hull} - m_{pwtr} \\ m_{v,max} &= 4 \cdot m_{axle,max} \\ m_{pwtr} &= m_{ICE} + m_{MG} + m_{PE} + m_{bat} + m_{TR} + m_{DIF} \\ m_{MG} &= m_{MG1} + m_{MG2} + m_{MG3} + m_{MG4} \\ m_{TR} &= m_{TR1} + m_{TR2} + m_{TR3} + m_{TR4} + m_{TR5} \\ m_{DIF} &= m_{DIF,4v} + m_{DIF,3v} + m_{DIF,2v,a} + m_{DIF,2v,b} \end{aligned} \tag{5.19}$$

5.4 Total Costs of Ownership

Only the powertrain dependent costs are considered in the cost model of the vehicle; any base vehicle costs are excluded from the calculations since these remain constant independently of the powertrain choice. The possible difference in resale value is disregarded since there is no information available on the resale value of used military HEVs. Additionally, except for foreseen battery replacements, preventive and corrective maintenance is not considered in the optimisation.

The total costs of ownership (TCO) can be divided into two categories, capital expenses (CAPEX) and operational expenses (OPEX). The CAPEX C_{CAPEX} cover the initial non-recurring cost for the vehicle; this covers the initial purchase and the development costs. The vehicle costs is a summation of all powertrain component costs. Development costs are the additional expenses required to develop a hybrid electric vehicle instead of an ICE vehicle. These costs are expressed as costs for development time per extra component $C_{develop,comp}$ compared to a central drive ICE topology. These costs are estimated as one year, one engineer for each additional component at $1e6$ [€] over an initial batch of 100 vehicles. This derivation results in $1e3$ [€] per additional component $C_{develop,comp}$.

The operational costs C_{OPEX} cover the energy costs C_{energy} and foreseen component replacement over the vehicle's lifetime C_{comp_repl}. C_{energy} is a summation of electricity costs $C_{electricity}$ and fuel costs C_{diesel}. These costs are calculated over 5000 repetitions n_{dc} of the drive cycle to simulate the expected usage over its lifetime. The latest 2020 EU prices [75] are incorporated in $C_{electricity}$ at 0.1254 [€/kWh]. As fuel costs during deployment of military vehicles can rise to 100 times the regular market price [11], an exact prediction on fuel costs during lifetime is unrealistic. Therefore, the diesel cost C_{diesel} is estimated higher than the current non-consumer costs according to [55] at 1.50 [€/l]. This value will be higher as the vehicle is used more in an operational theatre, affecting the optimisation results.

Only battery replacement is foreseen as a plannable expense. Given an estimated lifetime of 15 years before a significant midlife update for a defence vehicle, the battery pack is estimated to be replaced twice. This estimation takes the challenging environmental operating conditions of the vehicle and high C-loads on the battery into account.

$$
\begin{aligned}
C_{TCO} &= C_{CAPEX} + C_{OPEX} \\
C_{CAPEX} &= C_{ICE} + C_{MG} + C_{PE} + C_{bat} + C_{TR} + C_{PSD} + C_{DIF} + C_{develop} \\
C_{develop} &= (n_{components} - 7) \cdot C_{develop,comp} \\
C_{OPEX} &= C_{energy} + C_{comp\_repl} \\
C_{energy} &= (\frac{E_{electric}}{3.6} \cdot C_{electricity} + V_{fuel\_total} \cdot C_{diesel}) \cdot n_{dc} \\
C_{comp\_repl} &= C_{bat} \cdot n_{batt\_repl}
\end{aligned}
\tag{5.20}
$$

5.5 Energy and power management

All controllers used in this vehicle model are rule-based (RB). Due to computational expenses, the variables within these controllers are fixed. Further optimisation is possible by replacing the fixed variables with dynamic variables optimised at each time step. The vehicle control consists of the transmission gearshift control, torque-split control over the axles, torque-split control over the power sources and a thermostat charge controller.

5.5.1 Transmission gearshift control

Transmission gearshift control is rule-based, using variables to describe transition lines for up-and downshifts. The gearshift method is derived from the Vehicle Energy Consumption calculation Tool (VECTO) [76] gearshift methodology. VECTO's gearshift methodology is based on the current motor speed and requested torque. Using the normalised version of transmission speed $\omega_{TR,m}$ to represent the speed of connected motor or engine, and instead of required torque, using the normalised acceleration and normalised inclination angle to represent the load. The acceleration is normalised between zero and the maximum possible acceleration with the available power at the current vehicle speed. Added to the normalised acceleration is the normalised inclination angle, for [0...15] [%] road inclination. All factors are normalised to a range of [0...1].

A schematic representation of the shift lines and the controlling variables are included in Figure 5.20. The downshift action is controlled by two variables, $D1$ indicating the minimum downshift speed and $D2$

describing the angle of the downshift threshold. Upshifting is controlled by four variables, $U1$ indicating the minimum upshift motor speed, $U2$ is the normalised acceleration+gradient value to start dynamic upshifts, $U3$ is the angle of the dynamic upshift section, and $U4$ describes the maximum upshift engine/-motor speed. In this optimisation, the variables are fixed, although they can be added as additional variables to the PSO optimisation algorithm. Due to computational expenses, these variables are fixed during this research.

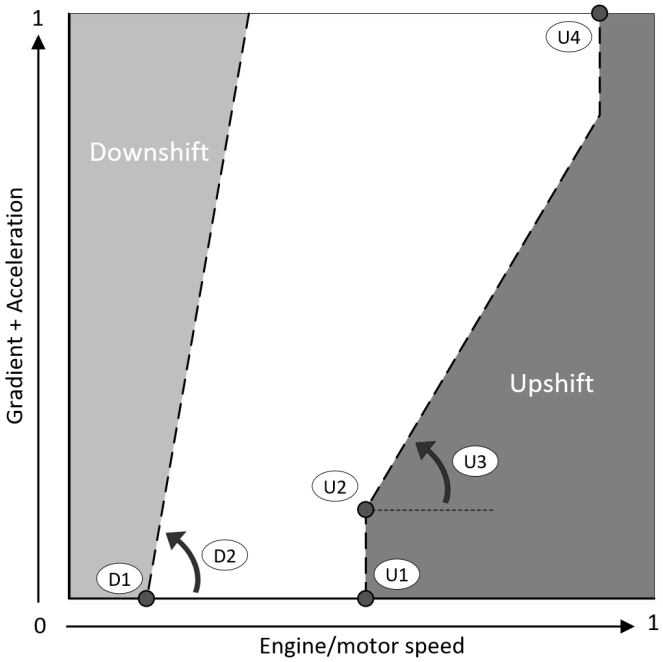

Figure 5.20: Schematic representation of shift control

5.5.2 Torque-split control over axles

The axle torque-split control is a rule-based controller considering maximum transmittable torque of the axles and maximum torque capabilities of the power sources connected to the axles. The controller does not incorporate the most efficient torque split between axles. The efficiency-based torque-split control between power sources connected to a single axle is described in Section 5.5.3.

For the torque transfer capability calculation of the axles, the Centre-of-Gravity (COG) is assumed to be in the centre of the vehicle. The calculation is performed in two stages, first separating the front and rear of the vehicle, secondly dividing the force between the axles. Equations 5.21 and 5.22 describe the forces in the z-direction $[N]$ in the centre between the front set and rear set of axles. The same method is applied in the second stage using Fz_{front} instead of $M_{truck} \cdot g$ as input for the front two axles and Fz_{rear} as input for the rear two axles.

$$Fz_{front} = M_{truck} \cdot g \cdot \frac{cos(\alpha) \cdot B_{COG-rear} - sin(\alpha) \cdot h_{COG}}{cos(\alpha) \cdot A_{COG-front} + cos((\alpha) \cdot B_{COG-rear}} \tag{5.21}$$

$$Fz_{rear} = M_{truck} \cdot g \cdot \frac{cos(\alpha) \cdot A_{COG-front} + sin(\alpha) \cdot h_{COG}}{cos(\alpha) \cdot A_{COG-front} + cos((\alpha) \cdot B_{COG-rear}} \tag{5.22}$$

The maximum transmittable torque depends on the surface friction coefficient μ of the road and the force in the Z direction of the vehicle; dependent on the inclination angle. Equation 5.23 shows the maximum transmittable torque of an axle.

$$\begin{aligned} Fn_{axle} &= Fz_{axle} \cdot cos(\alpha) \\ T_{max\_axle} &= Fn_{axle} \cdot \mu \cdot R_{tire} \end{aligned} \tag{5.23}$$

As a basis, the required torque to propel the vehicle is split equally over the axles; if an axle cannot transfer the required torque to the road, the residual torque is transferred to the next rearwards axle.

This process continues until the rear axle is reached. An alternative approach would be to distribute the torque over all axles using a spread ratio based on the inclination angle, inherently staying within the traction limits.

A similar control action is performed between the power sources to distribute the required torque. If a power source cannot provide the required torque, residual torque capabilities of the other power sources are used, limited by the torque transfer capability of the connected axle. The redistribution of torque over power sources allows for an asymmetric power distribution over the axles.

5.5.3 Torque-split control over power sources

The power source torque-split controller is efficiency and sizing dependent and is limited to torque-split between power sources connected to the same axle. Two distinct situations can be separated, one for parallel topologies and one for the case where only MGs are connected to an axle.

In the case of multiple motor-generators connected to an axle without an ICE mechanically connected, the required tractive torque is split between the connected MGs to operate the combined set as efficiently as possible. In series topologies, the ICE is operated by the thermostat charge controller and is not influenced by the required tractive torque. Section 5.5.4 provides an explanation on the workings of this charge controller.

For parallel topologies, multiple operating modes are possible, MG-only, ICE-only, hybrid traction or hybrid charging. If the SOC is sufficient and therefore charging process is inactive, ICE only mode is only engaged if the requested torque is within the optimal efficiency region of the ICE; otherwise, the torque is provided by motor-generators in the MG-only mode.

The ICE and MG-only modes are limited by the capabilities of the connected components. If the connected components cannot provide the required torque, hybrid mode is engaged to bridge the gap. When hybrid traction mode is activated and the motor operates at its most efficient operating point at its current speed, motor-generators provide the residual torque. If the maximum torque of the motor-generators is exceeded in hybrid traction mode, the provided torque by the ICE is increased to match the required torque.

5.5.4 Thermostat charge control

The charge controller is a SOC dependent thermostat and is integrated into the vehicle models power source torque-split controller. The controller uses two variables, a lower threshold to activate the charging process and an upper threshold that deactivates the charging. Simultaneously, the motors-generators are used to regenerate energy while decelerating. The mechanical brakes are only activated if the SOC is above a specific limit or the required brake torque exceeds the motor-generators capabilities.

In a series topology powertrain, the controller uses the thermostat as described to activate the charging mode and operates both the ICE and the generator at their optimal operating point, as shown in Figure 5.22. The hysteresis introduced by the upper and lower threshold results in a sawtooth movement of the SOC.

In a parallel topology, the charging process is initiated by the upper and lower thresholds and can also be activated on a torque and efficiency dependent base. Identical to the series topology, If the SOC is below the threshold value and the vehicle is stationary, charging mode will be activated, the axles will be disengaged, and the ICE will be operated at the optimal operating point to charge the battery. When the vehicle is in motion, the SOC combined with the requested torque and the efficiency regions of the ICE determine whether the ICE is engaged and to what extent to facilitate the hybrid charging mode. If the charging process is activated due to low SOC, the ICE is engaged at maximum torque level within its optimal efficiency region; all excessive torque generated by the ICE not required for propulsion is directed to the motor-generators to charge the battery. A simplified version of the decision flowchart describing this process is included in Figure 5.21. The complete decision flowchart for torque-split and charge control is Appendix C.

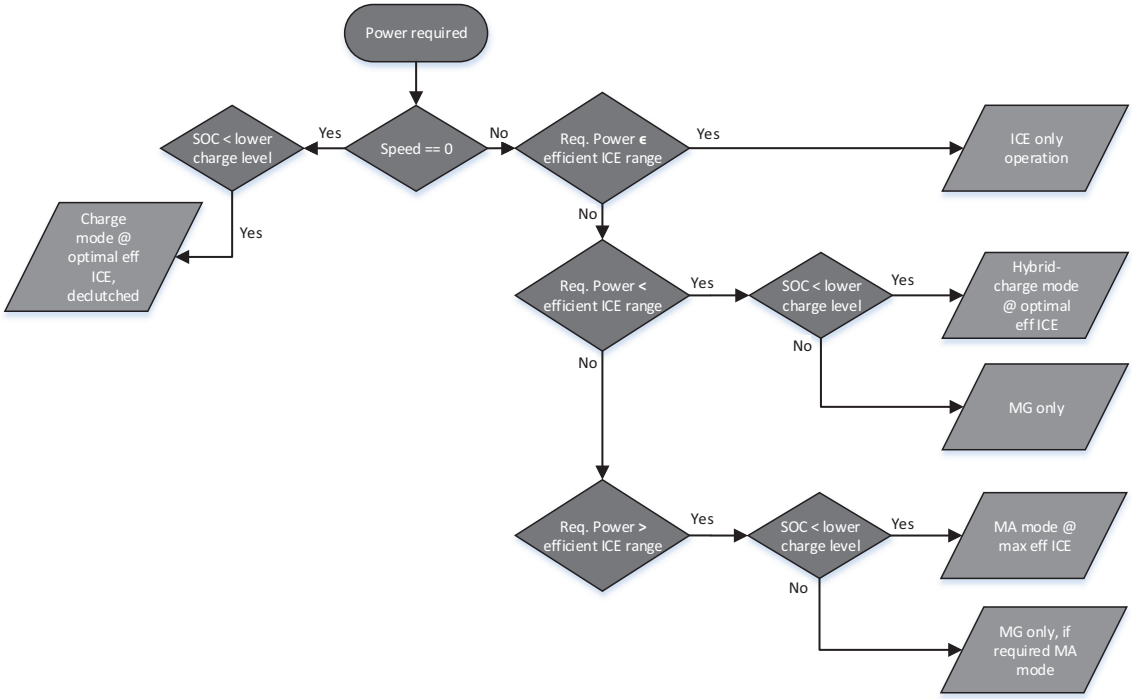

Figure 5.21: Thermostat charge control of parallel topologies

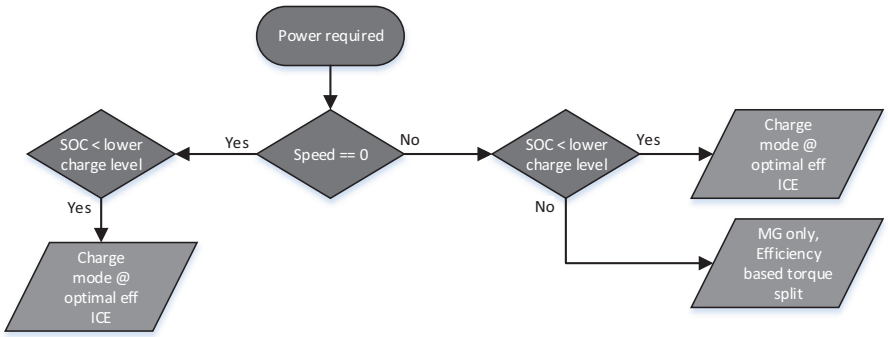

Figure 5.22: Thermostat charge control of series topologies

5.6 Summary

Vehicle model and control covers all component models and control within the vehicle. An overview is provided of the component models, describing the characteristic specifications of the components used to construct the topologies. These characteristics include linear mass and cost calculations and are concluded by the mass and cost calculations at vehicle level. Whereas a single model characterises the MG, multiple models are used to characterise the ICE. The scaling factor determines which ICE model or combination of models is used. The linear single model scaling method allows for scaling MGs larger than currently commercially available; in practice, this would be resolved by implementing multiple MGs connected in series. Simulating the efficiency for multiple motors in series would require an additional sizing optimisation and torque split controller. These additional layers would require additional computational effort; therefore, the linear scaling solution is accepted.

A power-dependent cost and mass model of a transmission is altered to produce values based on both power and the number of gears. Additionally, the transmission efficiency is constructed to be dependent on the individual gear ratios. These gear ratios are calculated by the geometric gear design method, allowing for a constant speed difference between gears.

The vehicle's TCO calculation covers both CAPEX and OPEX. Maintenance and resale values are not considered in the optimisation. The CAPEX covers development and powertrain costs, while the base

vehicle costs are excluded from the research as they are the same independent of the powertrain.

The control layers of the vehicle model are energy and power management. All controllers are rule-based to reduce the computational resources required for the optimisation process. The power management consists of torque split control between axles, between power sources and transmission gearshift control.

Torque split over axles prevents torque levels from exceeding the traction limits of the axles given the road gradient. Furthermore, the power source torque split control is efficiency-based and integrated with the charge controller to balance the torque delivery for propulsion and battery charging. The combination of these controllers allows for asymmetric power and torque distribution based on efficiency and torque transfer capabilities.

The transmission gearshift controller is a derivation of VECTO's gearshift method, which uses normalised speed and torque as an input. The derived method uses a combined approximation of the required acceleration and road gradient to estimate the required torque. Although this method is sub-optimal, it is sufficient for connected MGs with a broad powerband. On the other hand, the ICE is more sensitive to sub-optimal control, as will be shown in Section 6.3.1.

Finally, the thermostat charge control to manage the State-of-Charge (SOC) of the battery is addressed. The charge controller engages charging mode depending on either preset SOC thresholds, or in the case of parallel topologies, by harnessing residual power produced by the ICE to operate the ICE as efficient as possible.

Chapter 6 Optimisation analysis

The implemented optimisation method consists of a multi-layer nested approach framework. The framework consists of three layers to conduct the topology selection, component sizing and optimise the transmission gear numbers. In this chapter, the optimisation algorithms are elaborated upon as they are integrated into the framework. The second part of the approach are the optimisation objectives and corresponding calculation methods, followed by an extensive analysis of the results.

6.1 Optimisation framework

The optimisation framework uses a multi-layer nested approach to select and optimise topologies. Optimising the design space as a whole in a single layer would be inefficient and impractical, as each problem within the optimisation requires a unique approach. A multi-layer nested approach is considered to be the most computationally efficient, wherein large sections of the design space with low merit potential can be quickly disregarded. Different algorithms were selected which were considered most suitable to the nature of the problem in each layer. Since the objective functions are highly nonlinear with multiple local minima over a broad design space, including discrete numbers of gears and a whole topology design space, derivative-free heuristic methods are selected. Simulated Annealing (SA), GA and PSO are considered as appropriate methods. A comparison between these algorithms by Jia et al.[77] concluded that PSO and GA are best suited for large scale optimisation due to the relative high runtime required by SA compared to its competitors, and therefore it was decided to discard SA as a candidate algorithm.

GA is selected as the outer optimisation layer to select the topologies since it can deal with the optimisation of elements with discrete variables. The middle layer uses exhaustive search iterating over different numbers of gears within the transmissions and PSO for continuous component sizing. An alternative method such as Convex Optimisation (CO) was not selected since many of the problems could not be expressed in convex terms. Dynamic Programming (DP) would be suitable, although it was quickly ruled out due to the high computational burden for the problems considered. The inner layer consists of a rule-based transmission design, a rule-based gearshift controller, and a vehicle model with integrated torque-split control over the axles, torque-split between powersources a SOC depending thermostat charging controller. All controllers are rule-based to reduce computational resources required for the optimisation process. A visual representation of the framework is included in Figure 6.1.

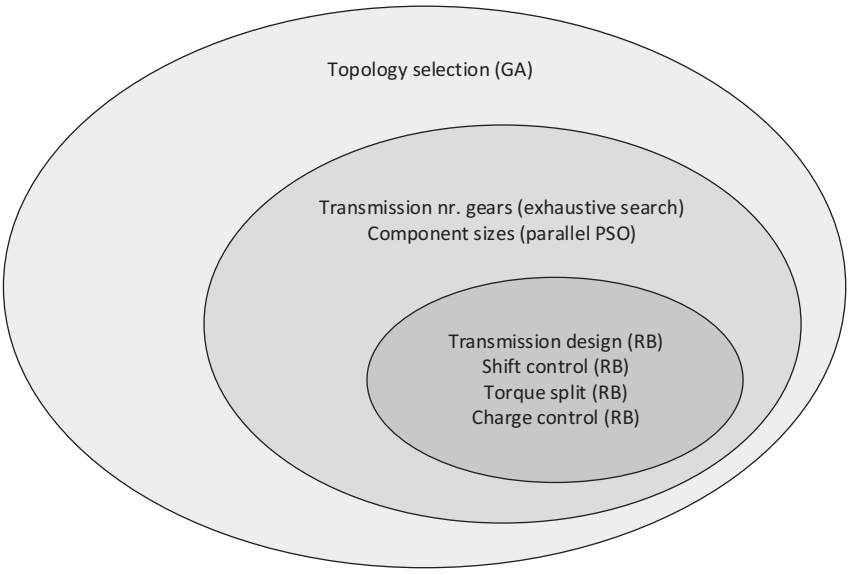

Figure 6.1: Optimisation framework layers

6.1.1 Genetic Algorithm; topology selection

Genetic Algorithm (GA) is a nonlinear optimisation method for continuous and discrete variables to find optimal solutions for a highly nonlinear optimisation problem. GA is an evolutionary method that uses a population simulating the selection of the fittest, each member representing a set of variables. After

each iteration, the best performing members are kept, a new set is created based on a cross-over of the best performing members, and a third set are random mutations.

The topologies are distinguished by a set of characteristics D_{top} identifying smaller subsets. These subsets are used as input for the GA for optimisation. The set consists of 48 unique combinations describing all investigated topologies; if chosen to exclude BEV and ICE-only topologies, 34 unique topology identifiers remain.

$D_{top,1}$ Topology type, BEV, Series, Parallel, series-parallel or ICE.
$D_{top,2}$ Number of axles connected to a single differential.
$D_{top,3}$ Number of power-split devices present in the topology.
$D_{top,4}$ Number of motor-generators present in the topology.
$D_{top,5}$ Total number of components present in the topology.
$D_{top,6}$ Number of additional axles connected together with axle four to a powersource at the same differential (if a differential is present).

The topology type is selected with $D_{top,1}$, $D_{top,4}$ and $D_{top,5}$ count the number of motor-generators and the total number of components present in the topology. $D_{top,2}$ indicates to what degree the topology uses a centralised or distributed drive system by the number of axles connected to a single differential. The more axles connected to a differential, the more centralised the topology is. $D_{top,3}$ lists the number of power-split devices present in the topology as a characteristic that describes flexibility for torque-split between powersources.

The last selection criteria $D_{top,6}$ is introduced to differentiate between topologies that are identical in the first identifiers but differentiate in the distribution of axles over differential(s). For example, a topology consisting of two MGs, one MG connected to a single axle, the other MG to the remaining three through a differential. The last criteria will single out one topology with a single MG connected to axle four from all topologies that fulfil that description.

Due to its random nature and the nonlinear approach, the results cannot be guaranteed global minima. The probability of finding the global minimum can be improved by tuning the algorithm. Tuning of the GA optimisation is done conservatively within this particular research. A large population size is chosen to maximise the probability of finding the global minimum. Further optimisation of the algorithm is possible to find the balance between global minima probability and physical computation time. The chosen conservative approach is computationally more intensive than an optimal tuned GA optimisation process.

6.1.2 Particle Swarm Optimisation; component sizing

Particle Swarm Optimisation (PSO) is a continuous optimisation method for nonlinear optimisation problems. This evolutionary method mimics the swarm-like behaviour of birds as all particles swarm towards a minimum function value. Each particle represents a set of variables and is each iteration adjusted towards its historically best-found function value and the swarm's best-found function value. Similar to GA, PSO cannot guarantee to find the global minima; nevertheless, tuning the algorithm can increase the probability.

Several parameters are available to be altered to tune the PSO algorithm. However, variations of the tuning parameters away from the standard settings [78] do not produce better or faster results of this particular objective function. The only parameter significantly improving the results is the number of particles, the swarm size.

The physical computational time to run the PSO function on a single transmission variant scales almost linearly with the number of particles. A minimal overhead is present for each PSO run; individual runs of the objective function consume the majority of the time. Therefore, the difference in physical computational time between multiple iterations using smaller swarm sizes compared to a single large swarm computation is minimal. However, the difference in results is significant; the probability of finding the global optimum using a single large swarm computation is higher than multiple small swarm computations. A large swarm size provides better coverage of the design space.

With the knowledge of two local minima's within a specific test-topology objective function, one is the global minima; multiple experiments indicated the necessity for a large particle swarm. Adjustments to

the particle spread by tuning the particles' inertia W, swarm confidence factor $y1$, and self-confidence factor $y2$ could not prevent the PSO algorithm from converging to local minima. An increase in particle swarm size increases the probability of finding global minima. Within PSO, the values of the respective variables are represented as particle locations. The particle's velocity is calculated at each iteration to determine its new location by [78],

$$v_{i+1} = W \cdot v_i + y1 \cdot u1 \cdot (p - x_i) + y2 \cdot u2 \cdot (g - x_i). \tag{6.1}$$

where $u1$ and $u2$ are randomised vectors $u1, u2 \in \{0 \dots 1\}$ with the length of the number of variables. x is the particle's current location, p the personal best position of the particle, and g the global best position of all particles. Increasing $y1$ or $y2$ will direct the particle's velocity more towards its personal best or global best position, respectively. Increasing W decreases the tendency to move away from its current position.

6.1.3 Exhaustive search number of gears

An exhaustive search of a selection of the possible transmissions determines the optimal number of discrete gears. A distinction is made between two use-cases, whether an ICE is incorporated in the power flow or not.

If an ICE is present in the power flow, the selection of gear numbers is limited to six and twelve. Less than six gears lead to a significant increase of the ICE size; additionally, the investigated commercially available transmissions capable of handling the torque levels involved start at six-speed. The second option for topologies with an ICE, twelve gears, is introduced to analyse the influence of higher gear numbers on the optimisation objectives.

An electric motor's high torque and broad powerband allow for fewer gears when no ICE is present in the power flow. Single-speed transmissions are infeasible due to high torque demands at low speed combined with the top speed requirements. Two-speed transmissions require unrealistically sized motors to provide the required torque over a wide speed range; therefore, the first feasible number of gears is three. A transmission option with four gears is added to identify the influence of more gears.

6.1.4 Vehicle simulation

The vehicle simulation includes the torque-split control over the axles and powersources and the thermostat charge control. The torque-split control over the axles allows for asymmetric power distribution between axles, distributing torque based on the adhesion limitations of the axles. The power delivery is allowed to be asymmetric between axles since adhesion is less of a limiting factor at low inclination angles. High power demanding situations are all in a forward direction: driving at top speed, high speed through terrain or high speed at low inclination angles. The torque requirements at low speed at the axles are symmetric due to the forward and reverse hill-start capability.

Since the availability of external charging is unknown and currently unlikely during deployment of the subject vehicle, a charge sustaining strategy is chosen for energy management. Instead of opting for the R101 method [79] to compensate the SOC difference $\Delta\xi$ between start and end of the drive cycle, which would involve multiple simulations per component size iteration, a less computationally involved method is selected. In the case of a series topology, the combined efficiency of the engine-generator combination is used. For parallel topologies, the instances where the engine is engaged are selected; subsequently, the average efficiency of the engine and the present motor-generators are combined, resulting in a single efficiency factor as described in Equation 6.2. Fuel volume $V_{fuel,\Delta\xi}$ to compensate for $\Delta\xi$ is calculated by,

$$\begin{aligned} V_{fuel,\Delta\xi} &= \frac{\Delta\xi}{LHV_d} \cdot \frac{1}{\eta_{\Delta\xi}} \cdot \rho_d \\ \Delta\xi &= \xi_{t0} - \xi_{t,end} \\ \eta_{\Delta\xi,series} &= \eta_{max,MG} \cdot \eta_{max,ICE} \\ \eta_{\Delta\xi,parallel} &= \{\overline{\eta}_{MG(t)} \cdot \overline{\eta}_{ICE(t)} \mid T_{ICE(t)>0}\} \end{aligned} \tag{6.2}$$

were ρ_d is the density of diesel fuel in $[kg/dm^3]$, LHV_d the lower heating value in $[J/kg]$.

6.2 Optimisation objectives

Multiple optimisation objectives are identified, integration of these objectives into a single result is highly subjective. The weighing factors of these objectives is a subjective matter, and thus, is left for interpretation of the reader. All objectives analysed to determine the influence of a change in objective. The analysed objectives are:

1. The average fuel consumption per km, $\overline{V}_{fuel,km}$ $[L/km]$

$$\overline{V}_{fuel,km} = \frac{V_{fuel,\Delta\xi} + \int_{t_0}^{t_{end}} \dot{m}_{fuel}(t) \cdot \rho_d}{l_{dc}} \tag{6.3}$$

2. The average energy consumption per km, $\overline{E}_{km}$ $[kWh/km]$

$$\overline{E}_{km} = \frac{E_{total}}{l_{dc}} \tag{6.4}$$

3. The average energy consumption per tonne cargo per km, $\overline{E}_{t/km}$ $[kWh/t/km]$

$$\overline{E}_{t/km} = \frac{E_{total}}{l_{dc} \cdot m_{cargo}} \tag{6.5}$$

4. The average costs per km, covering both CAPEX and OPEX, $\overline{C}_{km}$ $[€/km]$

$$\overline{C}_{km} = \frac{C_{TCO}}{l_{dc}} \cdot n_{dc} \tag{6.6}$$

5. The average costs per tonne cargo per km, covering both CAPEX and OPEX, $\overline{C}_{t/km}$ $[€/t/km]$

$$\overline{C}_{t/km} = \frac{C_{TCO}}{l_{dc} \cdot n_{dc} \cdot m_{cargo}} \tag{6.7}$$

$V_{fuel,\Delta\xi}$ is calculated according to Equation 6.2 and the cargo mass m_{cargo} according to Equation 5.19. The remaining parameters to be calculated are the total energy consumption E_{total},

$$E_{total} = E_{\Delta\xi} + \int_{t_0}^{t_{end}} P_{total}(t) \tag{6.8}$$

the total power flow during the drivecycle $P_{total}(t)$ in $[kW]$,

$$P_{total}(t) = P_{MG}(t) + P_{ICE}(t) \tag{6.9}$$

and the total length of the drive cycle l_{dc} in $[km]$,

$$l_{dc} = \int_{t_0}^{t_{end}} v_{veh}(t) \cdot 3.6 \tag{6.10}$$

and finally, the number of repetitions of the drive cycle over the lifetime of the vehicle n_{dc}.

6.3 Optimisation analyses

The implemented optimisation methods do not guarantee the global optimum per topology or the global optimal topology overall; therefore, the presented results can not be guaranteed to represent the optimal solutions. Each optimisation process for the individual objectives is performed separately; due to the partially random nature of the GA algorithm responsible for selecting topologies, the topology set processed for each objective is unique. The plotted Pareto fronts in Figure 6.7 to 6.6 are the result of these unique topology sets per objective. Table 6.1 lists the number of unique topologies and transmission combinations optimised per objective.

This section starts with comparing the base calculations and the optimised specifications of a central drive BEV and ICE-only topology. This is followed by an interpretation of the results for each optimisation objective and concluded with a comparison and sensitivity analyses of all objectives with respect to vehicle characteristics. The analyses conclude with an overview of each objective's function values for each objective separated per topology category, series or parallel.

Table 6.1: Optimised topologies per objective

Objective	Unique topologies	Transmission combinations
$\overline{E}_{km}$	152	986
$\overline{E}_{t/km}$	157	1008
$\overline{C}_{km}$	151	954
$\overline{C}_{t/km}$	177	1105
$\overline{V}_{fuel,km}$	173	1154

6.3.1 Base calculation comparison

As shown in Table 6.2, the minimum motor size to fulfil the requirements $P_{min,vehicle}$ does not correspond with the calculated minimum motor P_{BEV} and engine P_{ICE} sizing. Both BEV and ICE topologies are single powersource, central drive powertrains connected to a single transmission. The transmissions are a 3-speed discrete gearbox for the BEV and a 12-speed gearbox for the ICE-only topology.

Table 6.2: Vehicle power requirement compared to BEV and ICE-only topologies

Symbol	Value	Unit
$P_{min,vehicle}$	800.3	$[kW]$
P_{BEV}	869.5	$[kW]$
P_{ICE}	1251.3	$[kW]$

The 8.6 $[\%]$ difference between the $P_{min,vehicle}$ and the calculated optimised value for the BEV powertrain P_{BEV} can be explained by the use of a discrete gearbox, sub-optimal gearshift strategy and transmission losses. The RB shift controller uses an approximation of the required torque derived from the acceleration and gradient information and does not precisely determine the required torque; therefore, the gearshifts can be sub-optimal. Where the broad powerband of an MG is more forgiving for sub-optimal gearshift control, the power delivery of the ICE is not. The ICE will be scaled to compensate when not effectively using the peak power and torque of an ICE due to sub-optimal gearshift control. Therefore, the discrete gearbox combined with an RB shift control explains most of the difference between the P_{ICE} and $P_{min,vehicle}$, with a minor contribution from the efficiency losses within the transmission.

Table 6.3 and 6.4 provide a full lists of the optimisation results for the BEV and the ICE-only topology. The battery size E_{BAT} is calculated for a single drive cycle length l_{dc} of 226 $[km]$ and has to be multiplied by a factor $\frac{600}{226}$ to find the required battery size to fulfil the mission capabilities. This would result in an approximate 24 $[tonne]$ battery mass to achieve 600 $[km]$ range. Given the current technology, efficiency gains by topology optimisation can not reduce the battery to an acceptable size; therefore, BEV topologies are excluded from the optimisation.

Table 6.3: BEV, single MG, central drive, 3-speed optimisation results

Parameter	Value	Unit
$\overline{V}_{fuel,km}$	0	$[L/km]$
$\overline{E}_{km}$	7.5514	$[kWh/km]$
$\overline{E}_{t/km}$	0.3639	$[kWh/t/km]$
$\overline{C}_{km}$	3.1664	$[€/km]$
$\overline{C}_{t/km}$	0.1526	$[€/t/km]$
m_{ptr}	10246.1	$[kg]$
E_{BAT}	1802.8	$[kWh]$

Table 6.4: ICE-only, single ICE, central drive, 12-speed optimisation results

Parameter	Value	Unit
$\overline{V}_{fuel,km}$	1.0067	$[L/km]$
$\overline{E}_{km}$	14.2647	$[kWh/km]$
$\overline{E}_{t/km}$	0.4622	$[kWh/t/km]$
$\overline{C}_{km}$	1.5793	$[€/km]$
$\overline{C}_{t/km}$	0.0512	$[€/t/km]$
m_{ptr}	5138.25	$[kg]$
E_{BAT}	0	$[kWh]$

6.3.2 Sensitivity analysis of the topology category

The generated topologies are categorised as BEV, series, parallel or ICE-only. Since the BEV variant and the ICE-only variants are excluded, only the series and parallel topologies are optimised. Figure 6.2 to 6.5 show scatter plots of the function values optimised towards their respective objective. For the majority of the objectives, the series topologies outperformed the parallel, with one exception.

Figure 6.2 shows a small set of topologies with a relatively large offset to the rest of the results. These topologies do not differ significantly from the rest of the set; however, they produce a lower fuel consumption. The optimisation of these topologies resulted in a sizing combination where the vehicle practically operates as a BEV. The battery size is increased to such an extent that it needs minimal recharge during the drive cycle. This optimisation result only benefits $\overline{V}_{fuel,km}$, and has adverse effects on the other objectives. When optimising towards other objectives, these topologies perform poorly.

The most noteworthy observation in all figures in this section are the two series topologies substantially outperforming the other topologies. These points represent a central drive, two motors and a generator, series topology with a power split device in two transmission variants.

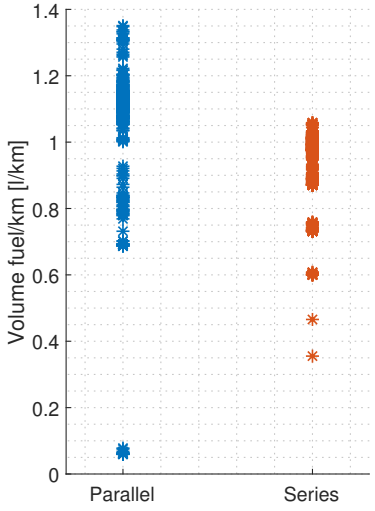

Figure 6.2: Minimum $\overline{V}_{fuel,km}$ $[L/km]$ - Topology category

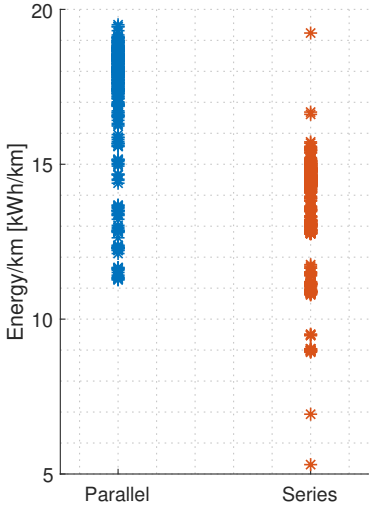

Figure 6.3: Minimum $\overline{E}_{km}$ $[kWh/km]$ - Topology category

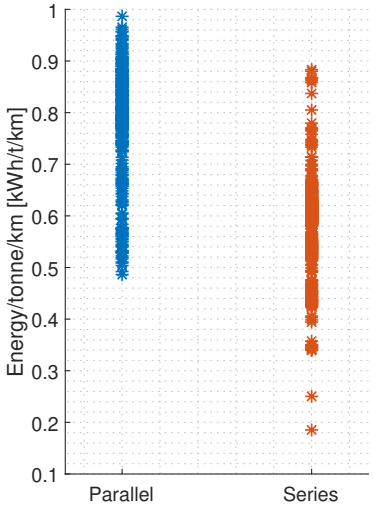

Figure 6.4: Minimum $\overline{E}_{t/km}$ $[kWh/t/km]$ - Topology category

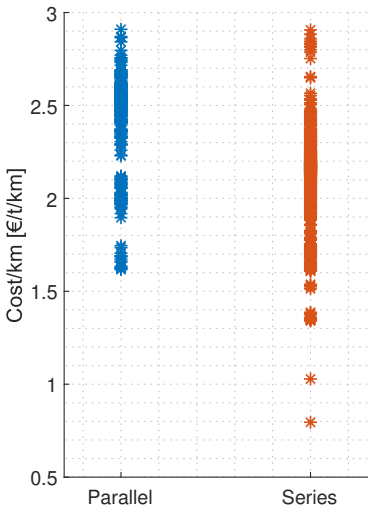

Figure 6.5:
Minimum $\overline{C}_{km}$ [€/km] - Topology category

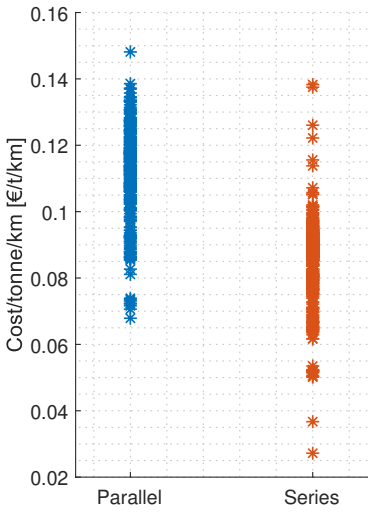

Figure 6.6:
Minimum $\overline{C}_{t/km}$ [€/t/km] - Topology category

6.3.3 Sensitivity analysis of the number of motor-generators

Figures 6.7 to 6.11 show the relationships between optimisation objectives and number of MGs present in the topology. Each plot shows multiple lines; each separate line is a linear interpolation of the Pareto front of the function values optimised toward its respective objective.

For the majority of the optimisation objectives, increasing the number of motor generators has an adverse effect on the function values. The only exception is when optimising towards $\overline{V}_{fuel,km}$, for this objective, reducing the number too low has negative consequences.

A comparison between Figure 6.7 and 6.8 shows an increase in powertrain mass when optimising towards $\overline{V}_{fuel,km}$ and therefore a higher $\overline{E}_{t/km}$. A rather remarkable result is the difference in $\overline{V}_{fuel,km}$ for different optimisation objectives in Figure 6.11. The low function values for the $\overline{V}_{fuel,km}$ line in this Figure are caused by the two previously described topologies in Section 6.3.2 behaving as BEVs.

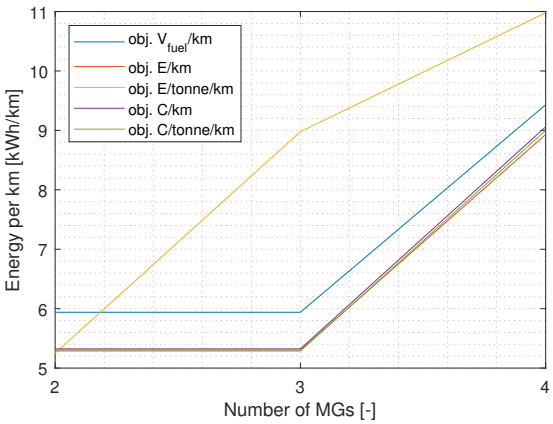

Figure 6.7: Minimum $\overline{E}_{km}$ [kWh/km] - number of MGs

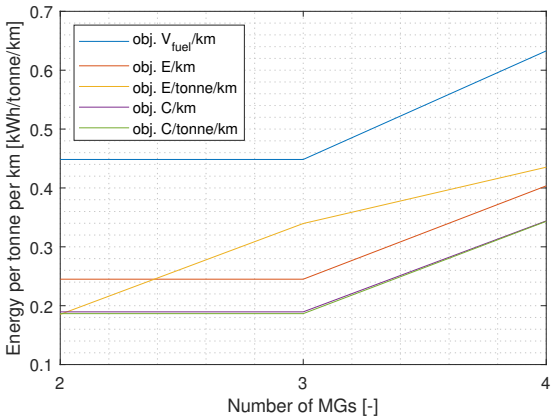

Figure 6.8: Minimum $\overline{E}_{t/km}$ [$kWh/t/km$] - number of MGs

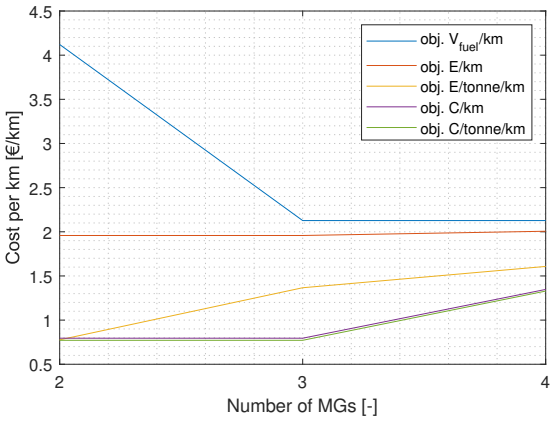

Figure 6.9: Minimum $\overline{C}_{km}$ $[€/km]$ - number of MGs

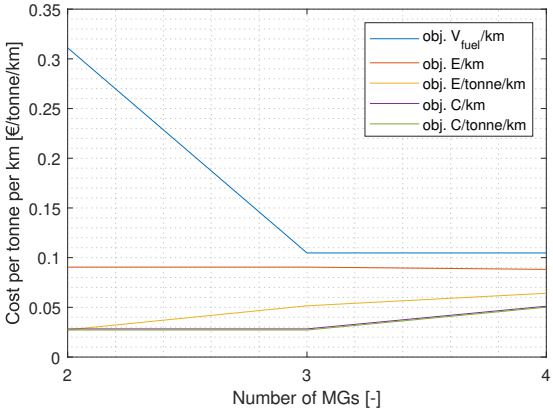

Figure 6.10: Minimum $\overline{C}_{t/km}$ $[€/t/km]$ - number of MGs

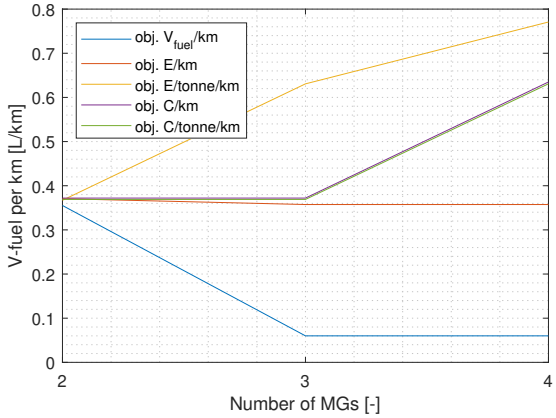

Figure 6.11: Minimum $\overline{V}_{fuel,km}$ $[L/km]$ - number of MGs

6.3.4 Sensitivity analysis of the number of components

The objective functions generally show an upward trend for more components, with some exceptions as shown in Figures 6.12 to 6.16. Optimising towards lower fuel consumption $\overline{V}_{fuel,km}$ results in a rather erratic behaviour for all objective values except $\overline{E}_{km}$. Similar to Figure 6.9 and 6.10, the significant increase in cost for lower number of components in Figure 6.14 and 6.15 is caused by the topologies using an oversized battery. Overall, topologies constructed of fewer components produce the best results, independent of the objective.

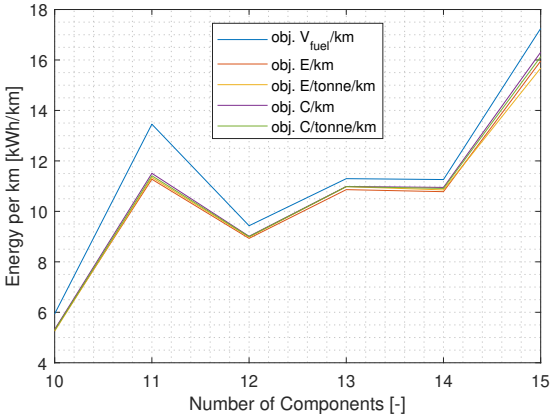

Figure 6.12: Minimum $\overline{E}_{km}$ $[kWh/km]$ - number of Components

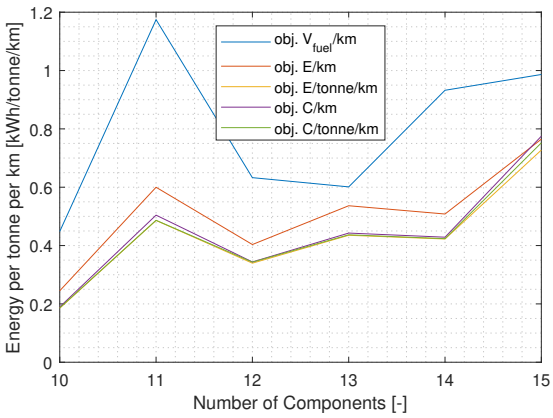

Figure 6.13: Minimum $\overline{E}_{t/km}$ $[kWh/t/km]$ - number of Components

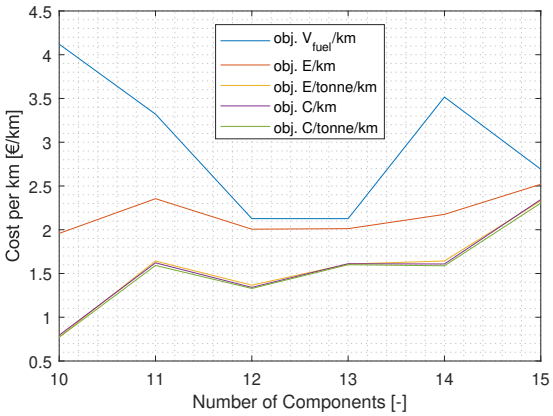

Figure 6.14: Minimum $\overline{C}_{km}$ $[€/km]$ - number of Components

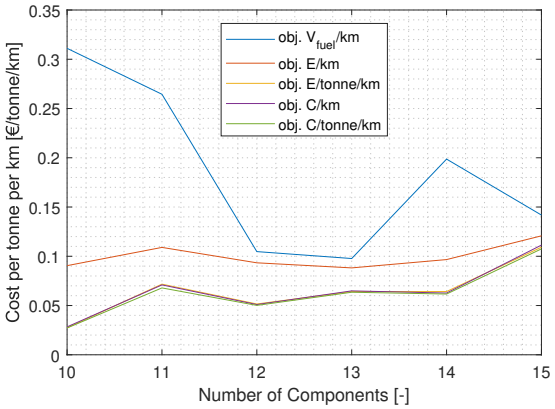

Figure 6.15: Minimum $\overline{C}_{t/km}$ $[€/t/km]$ - number of Components

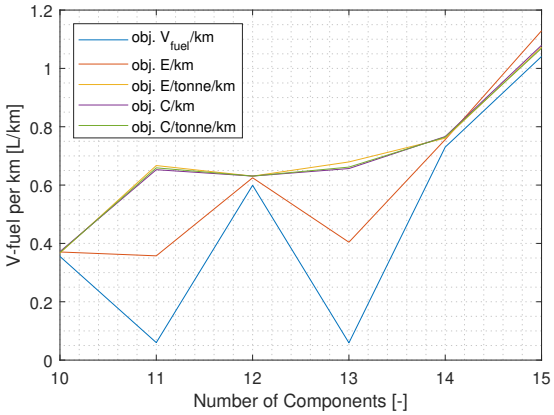

Figure 6.16: Minimum $\overline{V}_{fuel,km}$ $[L/km]$ - number of Components

6.3.5 Sensitivity analysis of the number of discrete gears

Independent of the optimisation objective, the function values show the same trends. In each plot, Figure 6.17 to 6.21, the number of gears in the range {3,4} are connected to a MG and the gears in range {6,12} are connected to an ICE. For transmissions connected to an MG, the overall trend is the more gears result in a lower function value. In contrast to the MG, function values of transmissions connected to an ICE increase for a higher number of gears. A possible explanation for this phenomenon is the RB gearshift control. The controller is not optimised for use in combination with an ICE, and therefore not using the powersources at their full potential. This results in an inability to counteract the increased mass and cost of the larger transmission when more gears are added.

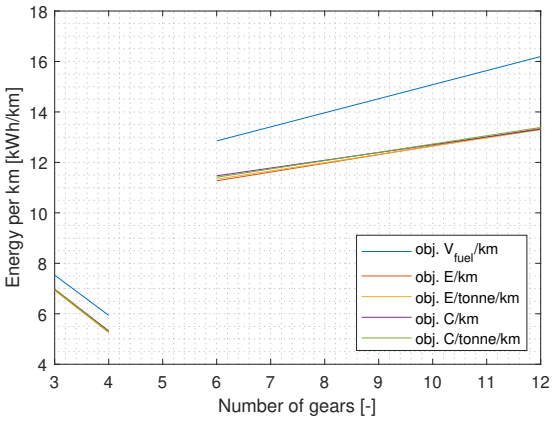

Figure 6.17: Minimum $\overline{E}_{km}$ $[kWh/km]$ - number of discrete gears

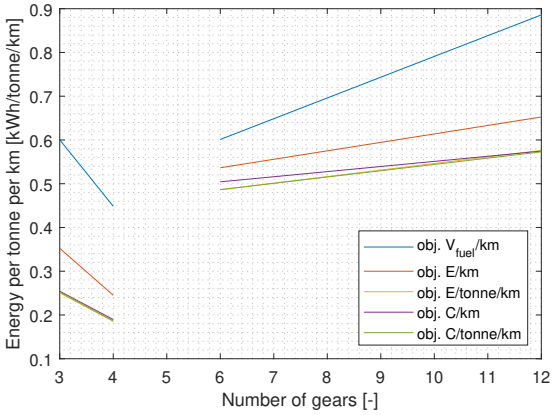

Figure 6.18: Minimum $\overline{E}_{t/km}$ $[kWh/t/km]$ - number of discrete gears

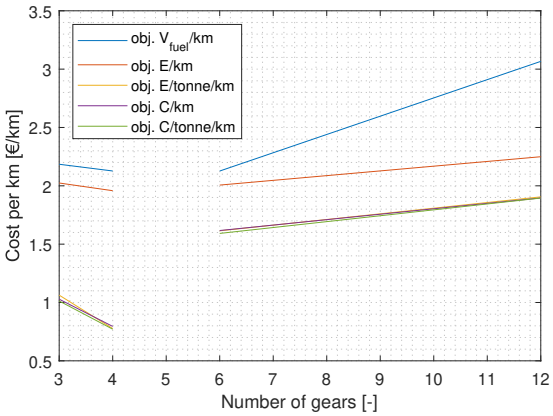

Figure 6.19: Minimum $\overline{C}_{km}$ $[€/km]$ - number of discrete gears

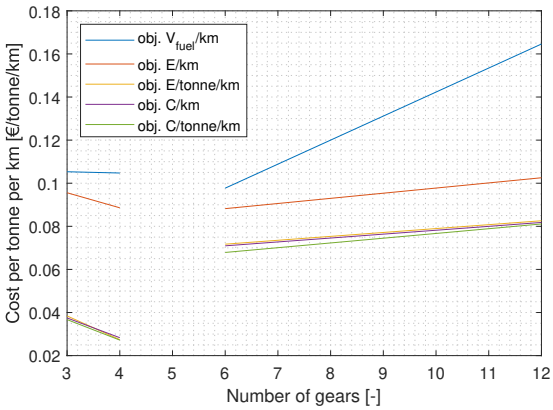

Figure 6.20: Minimum $\overline{C}_{t/km}$ $[€/t/km]$ - number of discrete gears

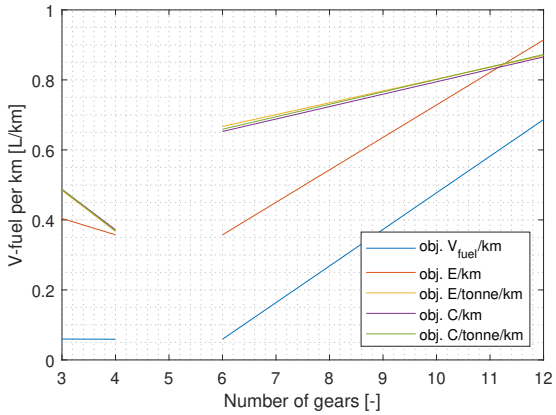

Figure 6.21: Minimum $\overline{V}_{fuel,km}$ $[L/km]$ - number of discrete gears

6.3.6 Best performing topology characteristics

The objective $\overline{C}_{t/km}$ includes most factors, including the cost of components, and thereby its sizing, the energy costs and thus rewarding more efficient topologies, and the mass of the powertrain by dividing over the available cargo mass. A more extensive analysis of $\overline{C}_{t/km}$ is performed to find the unique specifications of best-performing topologies.

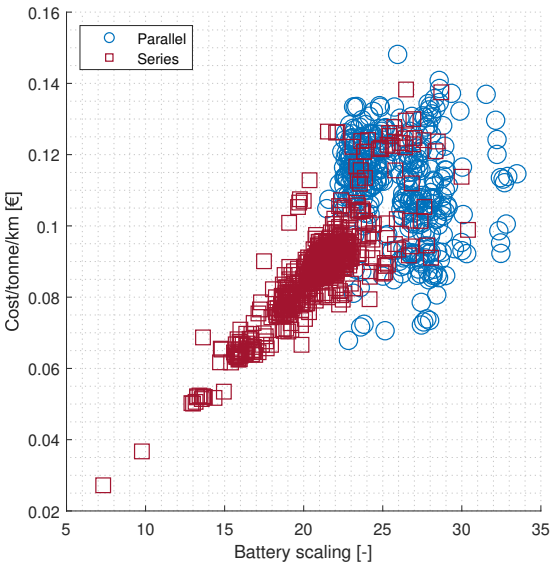

Figure 6.22: $\overline{C}_{t/km}$ [€/t/km] - Battery scaling [-], incl. category

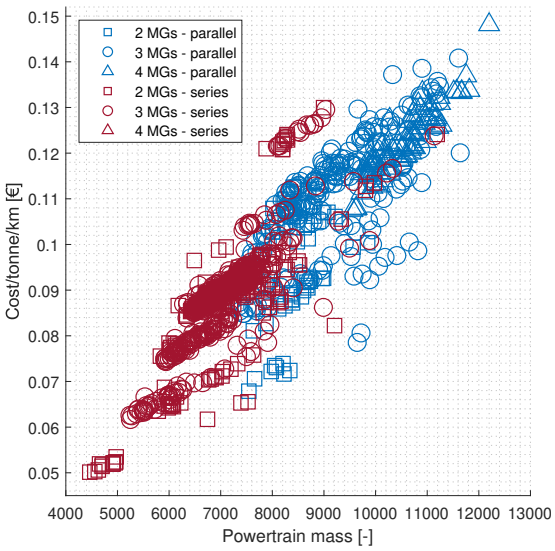

Figure 6.23: $\overline{C}_{t/km}$ [€/t/km] - Powertrain mass [kg], incl. category and number of MGs

The relationship between the battery sizing and the $\overline{C}_{t/km}$ is plotted in Figure 6.22. In general, series topologies tend to favour smaller sized batteries and show a fairly linear relation between battery size and $\overline{C}_{t/km}$. In contrast, the parallel topologies present a widely scattered range of data points and generally larger sized battery. Figure 6.23 shows the relation between powertrain mass in [kg] and the $\overline{C}_{t/km}$. The battery contributes heavily to the powertrain mass and thus, the series outperform the parallel topologies.

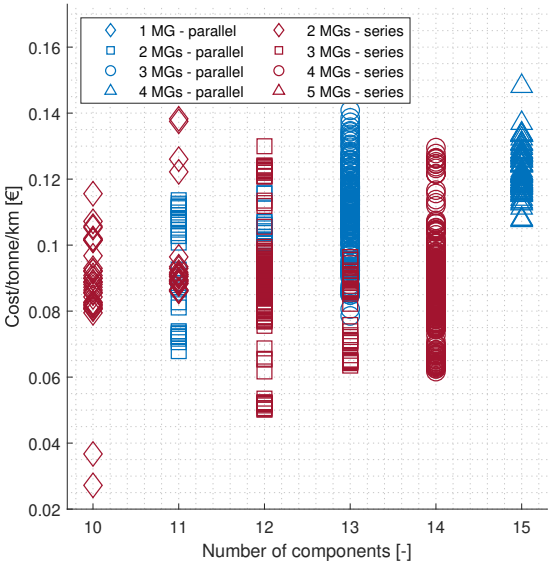

Figure 6.24: $\overline{C}_{t/km}$ [€/t/km] - number of components, incl. category and number of MGs

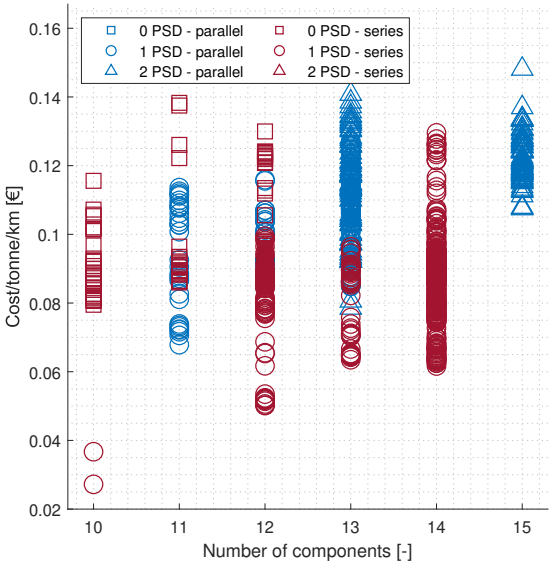

Figure 6.25: $\overline{C}_{t/km}$ [€/t/km] - number of components, incl. category and number of PSDs

Figure 6.24 and 6.25 provide more detailed information of the optimised topologies. As previously explained, the best performing topology identified consists of 10 components, has all four axles connected through a DIF to a TR and a PSD, the PSD is connected to two MGs. Separately an ICE is connected to a generator to charge the battery as shown in Figure 6.26. Only the mechanical connections are drawn in the figures, the electrical connections and the battery are not depicted. The optimised component sizes are include in Table 6.5. The next best-performing topologies are also a subset of the series topologies and are constructed by 12 components. These topologies have one axle separately connected to a TR followed by an MG as visualised in Figure 6.27. The other three axles are connected to a differential, a TR, a PSD, followed by two MGs. For battery charging, an ICE is connected to a generator.

Table 6.5: Dual-motor, central-drive, series topology, component sizes optimised for minimal $\overline{C}_{t/km}$

Component	Value	Unit
Diesel engine	253	$[kW]$
Motor-Generator 1	91	$[kW]$
Motor-Generator 2	526	$[kW]$
Generator	408	$[kW]$
Battery	110	$[kWh]$

These results can be explained by the dynamical nature of the drivecycle, where the series topologies have an advantage in regeneration and mechanical independence of the ICE. This independence also provides the greatest potential for optimisation of the ICE operation combined with the generator. The component sizing suggests a relatively small battery that can provide sufficient energy for short term electric-only operation while keeping the weight as low as possible. Furthermore, two significantly different sizes of MGs allow for the most efficient power delivery, dependent on the situation.

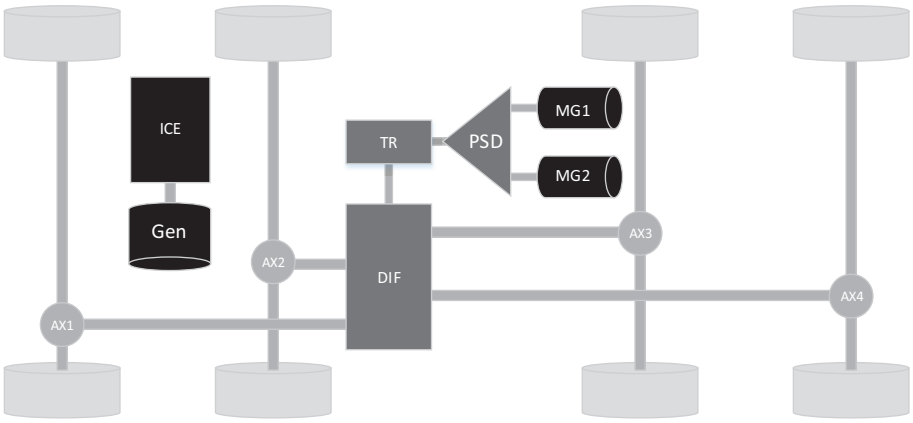

Figure 6.26: Dual-motor, central-drive, series topology, optimised for minimal $\overline{C}_{t/km}$

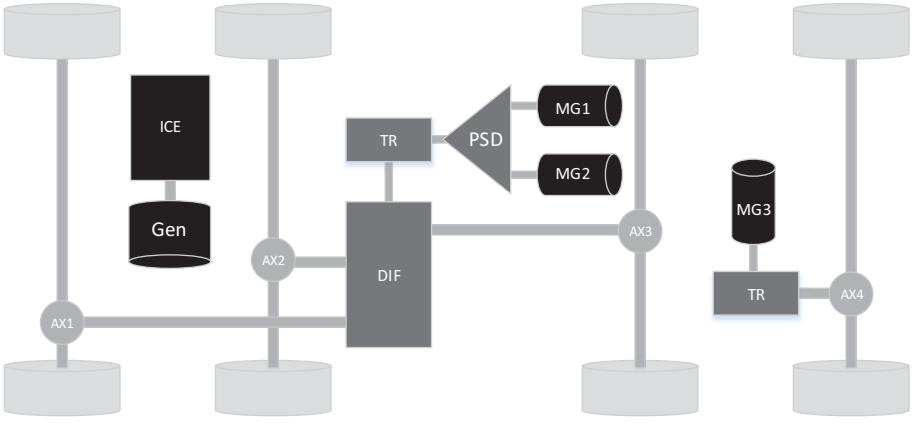

Figure 6.27: Triple-motor, partial central-drive, series topology, optimised for minimal $\overline{C}_{t/km}$

6.3.7 Objectives reflection

Two final objectives for reflection are the resilience and complexity of the powertrain. Resilience is interpreted as the ability for the vehicle to remain mobile when individual components are disabled. This mobility can be achieved by ensuring multiple independent power-to-wheel flows. Factors contributing to resilience are a decentralised topology layout, multiple powersources and a mechanical connection

between the ICE and the wheels as present in parallel topologies. The complexity of the topology influences, among others, the maintainability, logistical footprint and development costs of a vehicle. An indication of powertrain complexity can be obtained from the number of components or power-split devices. An additional constraint reducing complexity that can be introduced is to share the same size components within the powertrain. This enhances the interchangeability of components and reduces the logistical footprint.

The trade-off between all optimisation objectives will depend on the intended use case.

6.4 Summary

The optimisation framework uses a multi-layer nested approach consisting of three layers. The outer layer is a Genetic Algorithm (GA) optimisation layer to select the topologies using discrete variables. These variables distinguish smaller subsets by a set of topology characteristics. The middle layer uses exhaustive search iterating over different numbers of gears within the transmissions and Particle Swarm Optimisation (PSO) for continuous component sizing. The inner layer consists of rule-based (RB) energy and power management controllers.

Due to the random nature and the nonlinear approach of GA and PSO, the results cannot be guaranteed global minima. Several parameters can be altered to tune the GA and PSO algorithms to increase the probability of finding the global minimum. The only parameter significantly improving the results in this particular use case is the number of particles.

The exhaustive search in the middle layer determines the optimal number of discrete gears. A distinction is made between two use-cases, whether an ICE is incorporated in the power flow or not; this determines which two transmission types are used, $\{3, 4\}$ or $\{6, 12\}$ respectively.

Since the availability of external charging is unknown and currently unlikely during deployment of the subject vehicle, a charge sustaining strategy is chosen for energy management. After an optimisation iteration, the fuel required to compensate for State-of-Charge (SOC) difference between start and end has to be calculated. In the case of a series topology, the combined efficiency of the engine-generator combination is used. For parallel topologies, the instances where the engine is engaged are selected; subsequently, the average efficiency of the engine and the present motor-generators are combined, resulting in a single efficiency factor.

The optimisation analysis starts with a base calculation comparison; this compares the calculated minimum topology requirements with optimised single powersource central drive BEV and ICE-only topologies. BEV topology optimisation results in unrealistically large battery requirements and are therefore excluded from optimisation. The ICE-only topology oversized the ICE significantly; this is most likely caused by the gearshift controller not utilising the ICE peak power and torque and compensating with sizing.

In general, all optimisation objectives show similar trends except optimisation for minimal average fuel consumption per km $[L/km]$ $\overline{V}_{fuel,km}$. The other optimisation objectives are: average energy consumption per km $[kWh/km]$ $\overline{E}_{km}$, average energy consumption per tonne cargo per km $[kWh/t/km]$ $\overline{E}_{t/km}$, average costs per km $[€/km]$ $\overline{C}_{km}$ and the average costs per tonne cargo per km $[€/t/km]$ $\overline{C}_{t/km}$.

When optimising for minimal energy or costs, fewer MGs result in better function values as a rule. Analog to the MGs, fewer components generally provide better results for optimising towards these objectives. The topology category, series or parallel, also influences the results significantly. Series topologies outperform parallel in $\overline{C}_{t/km}$ and, in most cases, result in lighter powertrains. Although the sub-optimal scaling of ICE almost certainly negatively influences the overall optimisation results of parallel topologies.

An analysis of the influence of the number of discrete gears at the optimisation results concludes the following. For transmissions connected to MGs, more gears reduce the objectives function values. Additional computations are required to determine the limitations of increasing the number of gears. The results for transmissions connected to an ICE are the opposite of the MGs' results; the function values increase with the number of gears. This unexpected outcome is most likely caused by sub-optimal gearshift control, consequently oversizing the ICE to compensate.

Optimisation towards a minimal $\overline{C}_{t/km}$ is the most comprehensive as it integrates energy, component and development costs with the cargo capability of the vehicle. The best performing topology characteristics,

when optimising for minimal $\overline{C}_{t/km}$, are found in a central-drive dual-motor series topology and a central-drive triple-motor topology with one separate driven axle.

Two final objectives for reflection are the resilience and complexity of the powertrain. Resilience is interpreted as the ability of the vehicle to remain mobile when individual components are disabled. This mobility can be achieved by ensuring multiple independent power-to-wheel flows. The complexity of the topology influences, among others, the maintainability, logistical footprint and development costs of a vehicle. An indication of powertrain complexity can be obtained from the number of components or power-split devices. As can be seen, these objectives can be conflicting with each other and the other optimisation objectives. The selected trade-off between all optimisation objectives will depend on the intended use case.

Chapter 7 Conclusion

7.1 Conclusion

This study set out to develop an *Optimisation approach of a hybrid multi-axle heavy-duty military vehicle.* This optimisation approach is achieved by a four-step method: vehicle use profile identification, topology generation, vehicle modelling and control, and topology selection and optimisation.

A limited set of topologies is investigated due to computational time constraints; all topologies constructed by less than twelve components, and a part of the topologies up to eighteen components are processed. However, current results indicate that more components in a topology negatively influence the optimised objective values; therefore, the probability of finding better performing topologies with more components is low.

Fewer components, fewer Motor-Generators (MGs), and thus less complex topologies, generally produce better results when optimised for minimal energy consumption or costs, per km or tonne cargo per km. Series topologies outperform parallel topologies when optimising for minimal cost per tonne cargo per km, although the oversized ICEs might partially influence this. These significantly oversized ICEs appear to be the result of sub-optimal gearshift control. The best performing topology identified, independent of the optimisation objective, is a dual-motor central-drive series topology. The following best performing topology is a triple-motor partial central-drive series topology with one separately driven axle.

Vehicle use profile

The general use profile is determined as a basis for the creating of a drive cycle. Part of the use profile are the requirements describing the vehicle's performance, mission capabilities, and additional vehicle constraints. The requirements are combined with the reference vehicle properties and converted into topology constraints. The minimal topology performance requirements are a combined torque at the wheels of 179 $[kNm]$ for the 60 $[\%]$ incline static hill-start, a minimum power of 800.3 $[kW]$ to achieve 32 [km/h] on a 10 $[\%]$ incline and the minimum required wheel speed is 43.26 $[rad/s]$ to realise top speed.

Topology generation

The generation of topologies is a multi-step process since this was considered to be the most computationally efficient for defining a candidate group. A heuristic filter design constructed by constraints is applied to the consecutive steps of the generation process. Using graph theory, the components and the connections in between are represented as nodes and edge combinations.

A set of $8.4 \cdot 10^6$ possible component combinations is generated and reduced to a feasible set of 523 combinations by applying constraints. This step is followed by generating all possible edge combinations and reducing them from $7.7 \cdot 10^{57}$ to $3.1 \cdot 10^{27}$ feasible possibilities. This integration of the component sets with the edge combinations is computationally intensive, increasing exponentially with the number of components in a set. Topologies were generated from the least computationally involved set upwards. For practicality, the generation of topologies was limited to a maximum of four days per component set. In the final step of the topology generation process, the isomorphic models are removed from the set. The generated topology set is reduced from 2384 to 264 by eliminating these topologies.

Vehicle model and control

The vehicle model and control cover all component models and control within the vehicle. All components are linearly scaled based on a single parameter set per component except for the ICE. Multiple models are used to characterise the ICE, each for different size engines. The scaling factor determines which ICE model or combination of models is used.

The linear single model scaling method for the MG allows for scaling MGs larger than currently commercially available; in practice, this would be resolved by implementing multiple MGs connected in series. Simulating the efficiency for multiple motors in series would require an additional sizing optimisation and torque split controller. These additional layers require additional computational effort; therefore, the linear scaling solution and a sub-optimal approximation of efficiency is accepted.

The control layers of the vehicle model are energy and power management. All controllers are rule-based to reduce the computational resources required for the optimisation process. The combination of these controllers allows for asymmetric power and torque distribution based on MG/ICE efficiency and torque transfer capabilities of the axles.

The transmission gearshift controller is a derivation of VECTO's gearshift method, which uses normalised speed and torque as an input. The derived method uses a combined approximation of the required acceleration and road gradient to estimate the required torque. Although this method is sub-optimal, it is sufficiently capable for the connected MGs with a broad powerband. On the other hand, the ICE is more sensitive to sub-optimal control resulting in oversized scaling of the ICE.

Optimisation analysis An 8x8 vehicle presents a uniquely large design space, which is considerably larger than those commonly addressed in the literature. Optimising this design space as a whole in a single layer would be inefficient and impractical, as each problem within the optimisation requires a unique approach. A multi-layer nested approach is considered to be the most computationally efficient, wherein large sections of the design space with low merit potential can be quickly disregarded. Different algorithms were selected which were considered most suitable to the nature of the problem in each layer. The outer layer is a Genetic Algorithm (GA) optimisation layer to select the topologies using discrete variables. The middle layer uses exhaustive search iterating over different numbers of gears within the transmissions and Particle Swarm Optimisation (PSO) for continuous component sizing. The inner layer consists of rule-based (RB) energy and power management controllers.

Due to the random nature and the nonlinear approach of GA and PSO, the results cannot be guaranteed global minima. Tuning of algorithm parameters can increase the probability of finding the global minimum. The only parameter significantly improving the results in this particular use case is the number of particles for both GA and PSO.

The optimisation analyses start with a base calculation comparison; this compares the calculated minimum topology requirements with optimised single power source, central drive BEV and ICE-only topologies. BEV topology optimisation results in unrealistically large battery requirements and are therefore excluded. The ICE-only topology optimisation oversized the ICE significantly; this is most likely caused by the gearshift controller not utilising the ICE peak power and torque and compensating with sizing.

In general, all optimisation objectives show similar trends except optimisation for minimal average fuel consumption per km $[L/km]$. The other objectives are: the average energy consumption per km $[kWh/km]$, the average energy consumption per tonne cargo per km $[kWh/t/km]$, the average costs per km $[€/km]$ and the average costs per tonne cargo per km $[€/t/km]$.

When optimising for minimal energy or costs, fewer MGs result in better function values as a rule. Analog to the MGs, fewer components generally provide better results for optimising towards these objectives. The topology category, series or parallel, also influences the results significantly. Series topologies outperform parallel in costs per tonne cargo per km and, in most cases, result in lighter powertrains. The sub-optimal scaling of ICE almost certainly negatively influences the overall optimisation results of parallel topologies.

For transmissions connected to MGs, a higher number of gears reduces the objective function values. Additional computations are required to determine the limitations of increasing the number of gears. The transmissions connected to an ICE are the opposite of the MGs' results; the function values increase with the number of gears. This unexpected result is most likely caused by sub-optimal gearshift control, resulting in oversizing the ICE and the inability to compensate for the heavier, more expensive transmission.

Optimisation towards minimal costs per tonne cargo per km is the most comprehensive objective as it integrates energy, component and development costs with the cargo capability of the vehicle. The best performing topology characteristics are found in a central-drive dual-motor series topology and a central-drive triple-motor topology with one separate driven axle when optimising for this objective. These results can be explained by the dynamical nature of the drivecycle, where the series topologies have an advantage in regeneration and mechanical independence of the ICE. This independence also provides the greatest potential for optimisation of the ICE operation combined with the generator. The component sizing suggests a reasonably small battery that can provide sufficient energy for short term electric-only operation while keeping the weight as low as possible. Furthermore, two significantly different sizes of MGs allow for the most efficient power delivery, dependent on the situation.

Two final objectives for reflection are the resilience and complexity of the powertrain. These objectives can be conflicting with each other and the other optimisation objectives. The selected trade-off between all optimisation objectives will depend on the intended use case.

7.2 Research questions

The research revolved around two main research quests; answering these questions is the basis for the developed optimisation approach.

How should the system level multi-objective function be defined to adequately represent the optimisation criteria applicable to military usage using weighing factors?'

Literature research did not provide conclusive results regarding the weighing of objectives for military application. Conversations with MOD personnel indicated that these weighing factors for optimisation objectives are highly subjective. This report shows the results for all objectives separately and marks the similarities and differences.

'How to integrate the topology, technology/sizing and control optimisation within the optimisation framework?'

A multi-layer topology optimisation framework is constructed integrating GA, PSO, exhaustive search and RB methods in a nested approach. Set theory and conditions based filtering is implemented to reduce the generated topology set to a feasible subset. All feasible topologies are converted from logical matrices to usable topology models by graph theory. Control is optimisation limited to RB control to reduce computational burden due to the scale of the design space.

7.3 Discussion

During the preparation of this research, two main risks were identified; the achievability of automated topology generation and subsequent integration into an optimisation framework and the acquisition of sufficient data to generate representative results.

The automatisation and integration of topologies are achieved, although the number of generated topologies is limited due to the required physical computation time. All topologies requiring less than four days to render are generated and used in this research. The optimisations' results using the rendered topologies indicate that topologies comprised of fewer components tend to produce better results. Increasing component numbers generally has an adverse effect on the results; therefore, generating topologies comprised of more components appears redundant.

The second risk regarding data acquisitions impacted drive cycle generation, component characterisation and the creation of a multi-objective optimisation function. Synthesising a realistic drivecycle was achieved by combining the limited available data with practical experience and data filtering using existing requirements. A representative weighted multi-objective optimisation function is partially achieved. Multiple analyses are performed on different objectives to present the differences between objectives and their individual results and sensitivities. Acquiring input data regarding the mass and costs of components proved to be a more significant challenge. Component masses are usually included in their respective datasheets; the costs, however, are kept confidential. Multiple sources providing estimated guidelines were consulted and their information combined into new mass and cost approximations.

7.4 Recommendations

Considering the results of this research, further research can be directed towards the following topics:

- Integrating active torque split control between axles to operate the power sources within their most efficient operating regions would further enhance optimisation potential. The currently applied torque split control between axles is limited to dividing torque based on transfer limitations of the wheels.
- Further optimisation is possible by integrating DP for transmission control and an ECMS energy management strategy into the optimisation framework. Additionally, planetary gearsets can be introduced as power split devices to optimise the power split between components further. These additions increase the computational load significantly and are, therefore, most realistic when applied to a reduced topology set.
- Investigate the influence of a hybrid energy storage system combining batteries and ultracapacitors instead of a regular lithium-based battery pack. The ultracapacitors would provide the peak power demands, and the battery would provide the large scale energy demand. This could reduce the battery size because the maximum current limit would be omitted in scaling the battery size. Additionally, this could increase the battery life due to reduced cycling and current fluctuations.

- Adapt the optimisation approach to support two and three-axle topologies to make the approach flexible for other vehicle configurations.
- Integrate more component models for different scaling ranges of components. Utilising different models for different scaling ranges results in more realistic representations of components.
- Investigate the possibilities to extend vehicles capabilities by adding modular components to the vehicle depending on its role. These modular components could be batteries or a range extender, depending on the intended result.

Although the results indicate reasonably clear trends, a number of limitations need to be noted regarding the present study. The results might have been affected by: the limited input dataset, the limited number of topologies processed, the limited transmission types, the limited number of components, the applied parameter approximation, the use of a synthesised drive cycle, and the sub-optimal RB control.

This study has shown that fewer components, fewer motor-generators, and thus less complex topologies, generally produce better results. Furthermore, series topologies appear to outperform parallel; however, the control design should be optimised to achieve better representative results for parallel topologies.

Bibliography

[1] Defesanet, "DefesaNet - Land - RENAULT TRUCKS Defense: pioneer of parallel hybrid drive for Defense," 2016. [Online]. Available: https://www.defesanet.com.br/en/land/noticia/22568/RENAULT-TRUCKS-Defense--pioneer-of-parallel-hybrid-drive-for-Defense/

[2] Drawingdatabase.com, "Boxer armoured fighting vehicle Blueprint," 2018. [Online]. Available: https://drawingdatabase.com/boxer-armoured-fighting-vehicle/

[3] A123 Systems, "Battery Pack Design , Validation , and Assembly Guide using A123 Systems," Tech. Rep., 2014. [Online]. Available: https://www.buya123products.com/uploads/vipcase/b24d4f5b63934c59d43e93b3bb4db60a.pdf

[4] E. W. R. Belt van den, "Design analysis study of military (hybrid) electric vehicles," p. 34, 2020.

[5] M. van Defensie, "Operationele energie strategie defensie," Tech. Rep., 2015. [Online]. Available: https://www.rijksoverheid.nl/documenten/rapporten/2016/02/15/operationele-energie-strategie

[6] A. Bijleveld-Schouten and B. Visser, "Kamerbrief: Defensie Energie en Omgeving Strategie 2019-2022," 2019.

[7] J. Stoltenberg, "NATO - Opinion: Opening remarks by NATO Secretary General Jens Stoltenberg on NATO 2030 and the importance of strengthening the transatlantic bond in the next decade and beyond, 04-Feb.-2021," feb 2021. [Online]. Available: https://www.nato.int/cps/en/natohq/opinions_181208.htm

[8] C. Young, "NATO May Be Planning to Build Solar Panel-Powered Tanks — IE," apr 2021. [Online]. Available: https://interestingengineering.com/nato-may-be-planning-to-build-solar-panel-powered-tanks?utm_source=IGStory&utm_medium=Article&utm_campaign=organic&utm_content=Apr15

[9] G. Khalil, "Challenges of hybrid electric vehicles for military applications," in *2009 IEEE Vehicle Power and Propulsion Conference*, 2009, pp. 1–3.

[10] L. Raslavičius, A. Keršys, and R. Makaras, "Management of hybrid powertrain dynamics and energy consumption for 2WD, 4WD, and HMMWV vehicles," *Renewable and Sustainable Energy Reviews*, vol. 68, pp. 380–396, 2017. [Online]. Available: http://www.sciencedirect.com/science/article/pii/S1364032116306037

[11] D. Rizzo, "MILITARY VEHICLE OPTIMIZATION AND CONTROL," *Dissertation, Michigan Technological University*, p. 132, 2014. [Online]. Available: http://digitalcommons.mtu.edu/etds/863

[12] J. Keller, "Army asks BAE Systems and General Dynamics to recycle GCV vetronics for Future Fighting Vehicle," aug 2014. [Online]. Available: https://www.militaryaerospace.com/power/article/16718673/army-asks-bae-systems-and-general-dynamics-to-recycle-gcv-vetronics-for-future-fighting-vehicle

[13] S. Fish and T. B. Savoie, "Simulation-based optimal sizing of hybrid electric vehicle components for specific combat missions," *IEEE Transactions on Magnetics*, vol. 37, no. 1, pp. 485–488, jan 2001.

[14] G. Sheftick, "The next-generation combat vehicle could have lasers, run on hybrid power," nov 2016. [Online]. Available: https://www.army.mil/article/177734/the_next_generation_combat_vehicle_could_have_lasers_run_on_hybrid_power

[15] European Defence Agency, "CapTech Ground Systems," 2017. [Online]. Available: https://www.eda.europa.eu/what-we-do/activities/activities-search/captech-ground-systems

[16] R. O. Lindström, "Project SEP," 2016. [Online]. Available: http://www.ointres.se/projekt_sep.htm

[17] Military-Today, "SEP 8x8 Armored Personnel Carrier — Military-Today.com," 2010. [Online]. Available: http://www.military-today.com/apc/sep_8x8.htm

[18] Army Recognition, "BAE Systems may upgrade CV90 armoured infantry fighting vehicle with hybrid-electric propulsion 1008 — August 2013 defense industry military army news UK — Military army defense industry news year 2013," 2013. [Online]. Available: https://www.armyrecognition.com/august_2013_defense_industry_military_army_news_uk/bae_systems_may_upgrade_cv90_armoured_infantry_fighting_vehicle_with_hybrid-electric_propulsion_1008.html

[19] BAE Systems Hägglunds, "BAE Systems Hägglunds AB — LinkedIn," 2020. [Online]. Available: https://www.linkedin.com/company/bae-systems-h-gglunds

[20] Defesanet, "DefesaNet - Land - The hybrid drive pioneer puts on a show for the MEDEF," 2017. [Online]. Available: https://www.defesanet.com.br/en/land/noticia/26898/The-hybrid-drive-pioneer-puts-on-a-show-for-the-MEDEF/

[21] P. Valpolini, "Arquus: managing the vehicles' energy budget to reduce fuel consumption - EDR Magazine," 2020. [Online]. Available: https://www.edrmagazine.eu/arquus-managing-the-vehicles-energy-budget-to-reduce-fuel-consumption

[22] Arquus-Defence, "Innovation is at the core of our DNA — Arquus," 2020. [Online]. Available: https://www.arquus-defense.com/innovations/vehicules

[23] P. Valpolini, "IDEF 19: Otokar's Akrep IIe, an electric-driven recce platform - EDR Magazine," 2019. [Online]. Available: https://www.edrmagazine.eu/idef-19-otokars-akrep-iie-an-electric-driven-recce-platform

[24] European Defense Review, "UK: Armoured vehicles to test electric technology - EDR Magazine," 2020. [Online]. Available: https://www.edrmagazine.eu/uk-armoured-vehicles-to-test-electric-technology

[25] General Dynamics, "GDELS — PIRANHA," 2020. [Online]. Available: https://www.gdels.com/piranha.php

[26] Government of Canada, "LAV III - Light Armoured Vehicle — Canadian Army," 2017. [Online]. Available: http://www.army-armee.forces.gc.ca/en/vehicles/light-armoured-vehicle.page

[27] Ministerie van Defensie, "Boxer-pantserwielvoertuig — Materieel — Defensie.nl." [Online]. Available: https://www.defensie.nl/onderwerpen/materieel/voertuigen/boxer

[28] M. Annati, "Military Technology, Wheels of Fortune: Armoured Vehicle Evolution," *MT 6/2020*, 2020. [Online]. Available: https://www.monch.com/mpg/ebooks/military-technology/2020/06tdc3qkm/8/

[29] M. Kaanders and J. van der Burgt, "Ontwikkelingen in de electriciteitsvoorziening van miliraire voertuigen," TNO-DV 2006 A449, Tech. Rep., 2007.

[30] C. Tol, "Energy supply during silent watch," TNO-RPT-DTS-2011-01413, Tech. Rep., 2012.

[31] ——, "Fuel cells for vehicle APU applications and consequences of their implementation," TNO-DV 2009 A581, Tech. Rep., 2009.

[32] NATO, *All Electric Combat Vehicles (AECV) for Future Applications.* RTO-TR-AVT-047, 2004.

[33] ——, "Technical Report Hybrid Vehicle Rating Criteria RTO-TR-AVT-106," Tech. Rep., 2009. [Online]. Available: https://www.sto.nato.int/publications/STO Technical Reports/Forms/Technical Report Document Set/docsethomepage.aspx?ID=2143&FolderCTID=0x0120D5200078F9E87043356C409A0D30823AFA16F6010066D541ED10A62C40B2AB0FEBE9841A61&List=92d5819c-e6ec-4241-aa4e-57bf918681

[34] ——, "Evaluation Criteria for Military Hybrid Electric Vehicles RTO-TR-AVT-166," Tech. Rep., 2012. [Online]. Available: https://www.sto.nato.int/publications/STO Technical Reports/Forms/Technical Report Document Set/docsethomepage.aspx?ID=2117&FolderCTID=0x0120D5200078F9E87043356C409A0D30823AFA16F6010066D541ED10A62C40B2AB0FEBE9841A61&List=92d5819c-e6ec-4241-aa4e-57bf918681

[35] QinetiQ, "E-X-Drive TM Transmission," Tech. Rep., 2005. [Online]. Available: www.QinetiQ.com http://www.offroadvehicle.ru/AZBUCAR/QinetiQ/HED transmission.pdf

[36] ——, "Vehicle Drive Technology Systems & Solutions from QinetiQ." [Online]. Available: https://www.qinetiq.com/expertise/power-sources-energy-storage-and-distribution/vehicle-drive-technology

[37] UK Ministry of Defence, "The Future Rapid Effect System (FRES) Programme Takes Another Step Forward," 2005. [Online]. Available: https://www.defense-aerospace.com/article-view/release/62131/uk-mod-awards-fres-contract-(aug-25).html

[38] Army Technology, "Future Rapid Effects System (FRES) - Army Technology." [Online]. Available: https://www.army-technology.com/projects/fres/

[39] T. C. Lopez, "First FCS Manned Vehicle to Make Public Debut," 2008. [Online]. Available: https://www.army.mil/article/9539/first_fcs_manned_vehicle_to_make_public_debut

[40] P. Koogh van der, N. Arts, and A. Hauzer, "Technische haalbaarheidsstudie universeel voertuigplatform," TNO, DMKL/MVA-3, A84/KL/084, Tech. Rep., 1985.

[41] F. Verbruggen, A. Hoekstra, and T. Hofman, "Evaluation of the state-of-the-art of full-electric medium and heavy-duty trucks," no. June 2019, 2018.

[42] D. Smith, B. Ozpineci, R. L. Graves, P. T. Jones, J. Lustbader, and ..., "Medium-and Heavy-Duty Vehicle Electrification: An Assessment of Technology and Knowledge Gaps," no. December 2019, 2020. [Online]. Available: https://www.osti.gov/servlets/purl/1615213

[43] F. J. Verbruggen, E. Silvas, and T. Hofman, "Electric powertrain topology analysis and design for heavy-duty trucks," *Energies*, vol. 13, no. 10, 2020.

[44] D. S. Han, N. W. Choi, S. L. Cho, J. S. Yang, K. S. Kim, W. S. Yoo, and C. H. Jeon, "Characterization of driving patterns and development of a driving cycle in a military area," *Transportation Research Part D: Transport and Environment*, vol. 17, no. 7, pp. 519–524, 2012. [Online]. Available: http://www.sciencedirect.com/science/article/pii/S1361920912000600

[45] K. Sebeck, J. Mange, J. Maclennan, and D. Rizzo, "CHARACTERIZATION OF ARMY GROUND VEHICLE DRIVE CYCLES," 2017.

[46] J. Kern, N. Clark, and R. Nine, "Factoring terrain effects into vehicle emissions modeling and inventory," in *Proceedings of the 10th Annual Coordinating Research Council On-Road Vehicle Emissions Workshop, San Diego, CA, USA*, vol. 2729, 2000.

[47] A. D. T.-A.-A. U. S. A. A. T. Center, "Test Operations Procedure (TOP) 01-1-011A Vehicle Test Facilities at Aberdeen Test Center and Yuma Test Center," US Army Test and Evaluation Command, Tech. Rep., 2012. [Online]. Available: https://apps.dtic.mil/dtic/tr/fulltext/u2/a557002.pdf

[48] M. P. O'Keefe, A. Simpson, K. J. Kelly, and D. S. Pedersen, "Duty Cycle Characterization and Evaluation Towards Heavy Hybrid Vehicle Applications," in *SAE Technical Paper*. SAE International, 2007. [Online]. Available: https://doi.org/10.4271/2007-01-0302

[49] E. Silvas, "Integrated optimal design for hybrid electric vehicles," Ph.D. dissertation, 2015.

[50] V. Harselaar, "(Thesis) Automated dynamic modeling of arbitrary hybrid drivetrain topologies," 2017.

[51] V. Rangarajan, "Powertrain Topology Design Analysis for Battery Electric Heavy Duty Trucks," Master Thesis, Technische Universiteit Eindhoven, 2018.

[52] H. L. Bartlett, B. E. Lawson, and M. Goldfarb, "On the design of power gear trains: Insight regarding number of stages and their respective ratios," *PLOS ONE*, vol. 13, no. 6, p. e0198048, jun 2018. [Online]. Available: https://dx.plos.org/10.1371/journal.pone.0198048

[53] Y. Li, B. Zhu, N. Zhang, H. Peng, and Y. Chen, "Parameters optimization of two-speed powertrain of electric vehicle based on genetic algorithm," *Advances in Mechanical Engineering*, vol. 12, no. 1, pp. 1–16, 2020.

[54] D. D. Tran, M. Vafaeipour, M. El Baghdadi, R. Barrero, J. Van Mierlo, and O. Hegazy, "Thorough state-of-the-art analysis of electric and hybrid vehicle powertrains: Topologies and integrated energy management strategies," *Renewable and Sustainable Energy Reviews*, vol. 119, 2020.

[55] ICCT, M. Moultak, N. Lutsey, and D. Hall, "Transitioning to zero-emission heavy-duty freight vehicles," *The International Council on Clean Transportation*, no. September, p. 53, 2017. [Online]. Available: www.theicct.org

[56] Bloomberg New Energy Finance, "Electric Buses in Cities: Driving Towards Cleaner Air and Lower CO2," p. 63, 2018. [Online]. Available: https://c40-production-images.s3.amazonaws.com/other_uploads/images/1726_BNEF_C40_Electric_buses_in_cities_FINAL_APPROVED_%282%29.original.pdf?1523363881

[57] Battery University, "BU-216: Summary Table of Lithium-based Batteries – Battery University," 2019. [Online]. Available: https://batteryuniversity.com/learn/article/bu_216_summary_table_of_lithium_based_batteries

[58] B. Lawson, "Lithium Secondary - Rechargeable - Cells." [Online]. Available: https://mpoweruk.com/lithiumS.htm

[59] M. A. Hannan, M. M. Hoque, A. Hussain, Y. Yusof, and P. J. Ker, "State-of-the-Art and Energy Management System of Lithium-Ion Batteries in Electric Vehicle Applications: Issues and Recommendations," *IEEE Access*, vol. 6, pp. 19 362–19 378, 2018.

[60] Army Technology, "Boxer Cargo Vehicle - Army Technology." [Online]. Available: https://www.army-technology.com/projects/boxer-cargo-vehicle/

[61] R. voor wegverkeer, "Overzicht maten en gewichten in Nederland," p. 10, 2012. [Online]. Available: https://www.rdw.nl/-/media/rdw/rdw/pdf/sitecollectiondocuments/ontheffingen-tet/themasite-ontheffingen/handleidingen/2-b-1097b-overzicht-maten-en-gewichten.pdf

[62] Ministerie van Verkeer en Waterstaat, "wetten.nl - Regeling - Regeling voertuigen - BWBR0025798," 2021. [Online]. Available: https://wetten.overheid.nl/BWBR0025798/2021-01-21

[63] IHS Janes, *GTK/MRAV/PWV (Boxer) Wheeled Armoured Vehicle Programme*, F. F. Christopher, Ed. IHS Jane's, oct 2016. [Online]. Available: https://janes.ihs.com/Janes/Display/1501156

[64] F. Hausdorff, *Set theory*. American Mathematical Society (RI), 1991.

[65] R. Diestel, *Graph Theory, 5th edition 2017*, 2017.

[66] D. R. Mazur, *Combinatorics: A Guided Tour*. The Mathematical Association of America, 2010.

[67] National Renewable Energy Laboratory, "ADVISOR Advanced Vehicle Simulator," oct 2003. [Online]. Available: http://adv-vehicle-sim.sourceforge.net/

[68] TNO, "Eindrapportage DEVE, Fase 1," Codema overeenkomst nr. CO/DGPM/DWOO C01/02, Tech. Rep., 2003.

[69] F. Kleiner and H. E. Friedrich, "Development of a Transport Application based Cost Model for the assessment of future commercial vehicle concepts," *European Battery, Hybrid and Fuel Cell Electric Vehicle Congress Geneva*, no. March, pp. 1–20, 2017.

[70] F. J. R. Verbruggen, E. Silvas, and T. Hofman, "Electric Powertrain Topology Analysis and Design for Heavy-Duty Trucks," *Energies*, vol. 13, no. 10, 2020. [Online]. Available: https://www.mdpi.com/1996-1073/13/10/2434

[71] European Technology and Innovation Platform on Batteries, "Strategic Research Agenda for batteries 2020," 2020. [Online]. Available: https://ec.europa.eu/energy/sites/ener/files/documents/batteries_europe_strategic_research_agenda_december_2020__1.pdf

[72] S. Plotkin, D. Santini, A. Vyas, J. Anderson, M. Wang, D. Bharathan, and J. He, "Hybrid electric vehicle technology assessment : methodology, analytical issues, and interim results." *Other Information: PBD: 13 Mar 2002*, 2002. [Online]. Available: http://worldwidescience.org/wws/desktop/en/ostiblue/service/link/track?redirectUrl=http%3A%2F%2Fwww.etde.org%2Fetdeweb%2Fdetails.jsp%3Fquery_id%3D1%26page%3D0%26osti_id%3D807353&collectionCode=ETDEWEB-EN&searchId=4cef205b-355b-48ba-a4e2-a5eca8c5537d&type=

[73] H. Naunheimer, B. Bertsche, J. Ryborz, W. Novak, and P. Fietkau, *Fahrzeuggetriebe Grundlagen, Auswahl, Auslegung und Konstruktion*, 2019.

[74] H. Naunheimer, B. Bertsche, R. Joachim, and N. Wolfgang, *Automotive Transmision*, 2011.

[75] Eurostat, "Electricity price statistics - Statistics Explained," nov 2020. [Online]. Available: https://ec.europa.eu/eurostat/statistics-explained/index.php?title=Electricity_price_statistics#Electricity_prices_for_non-household_consumers

[76] European Commission, "Vehicle Energy Consumption calculation TOol - VECTO — Climate Action," 2019. [Online]. Available: https://ec.europa.eu/clima/policies/transport/vehicles/vecto_en#tab-0-1

[77] F. Jia and D. Lichti, "A COMPARISON OF SIMULATED ANNEALING, GENETIC ALGORITHM AND PARTICLE SWARM OPTIMIZATION IN OPTIMAL FIRST-ORDER DESIGN OF INDOOR TLS NETWORKS," 2017. [Online]. Available: https://doi.org/10.5194/isprs-annals-IV-2-W4-75-2017

[78] Mathworks, "Particle Swarm - MATLAB & Simulink - MathWorks Benelux," 2021. [Online]. Available: https://nl.mathworks.com/help/gads/particle-swarm.html

[79] United Nations, "AE/ECE/TRANS/505/Rev.2/Add.100/Rev.3 Uniform provisions concerning the approval of passenger cars powered by an internal combustion engine only, or powered by a hybrid electric power train with regard to the measurement of the emission of carbon dioxide a," *Usa Gov*, no. April, p. 100, 2013. [Online]. Available: http://www.unece.org/fileadmin/DAM/trans/main/wp29/wp29regs/updates/R101r3e.pdf

[80] Siemens, "ELFA Components Data Sheets," 2011. [Online]. Available: https://www.industry.usa.siemens.com/drives/us/en/electric-drives/hybrid-drives/automotive/Documents/elfa-components-data-sheets.pdf

[81] BorgWarner, "HVH410-075 Electric Motor," 2016. [Online]. Available: https://cdn.borgwarner.com/docs/default-source/default-document-library/remy-pds---hvh410-075-sheet-euro-pr-3-16.pdf?sfvrsn=a742cd3c_13

[82] ——, "HVH410-150 Electric Motor," 2016. [Online]. Available: https://cdn.borgwarner.com/docs/default-source/default-document-library/remy-pds---hvh410-150-sheet-euro-pr-3-16.pdf?sfvrsn=a642cd3c_11

[83] M. Lampérth, "PH38χ Series Typical Performance (PH.382)," Tech. Rep., 2018. [Online]. Available: www.phi-power.com

[84] Dana TM4, "SUMO HD HV3500-9P." [Online]. Available: https://www.danatm4.com/products/direct-drive-electric-powertrain/sumo-hd/

[85] B. systems, "MODULAR TRACTION System (MTS)," 2013. [Online]. Available: http://www.hybridrive.com/pdfs/HybriDrive-MTS.pdf

[86] B. Nykvist and M. Nilsson, "Rapidly falling costs of battery packs for electric vehicles," *Nature Climate Change*, vol. 5, no. 4, pp. 329–332, 2015. [Online]. Available: https://doi.org/10.1038/nclimate2564

[87] ZF Friedrichshafen AG, "Product Overview, Truck & Van Driveline Technology," 2020. [Online]. Available: https://www.zf.com/master/media/corporate/m_zf_com/company/download_center/products/trucks/2020_3/TT_Product_Overview_202009_DE_EN_LowRes.pdf

[88] E. vehicle group, "High Reduction Transmissions for Special-Purpose Low-Speed Applications, Fuller 11-Speed Transmissions," 2015.

Appendix A Mission Profile

This appendix presents a visual representation of the mission profile in Figure A.1. The total length of the drive cycle is 226 $[km]$.

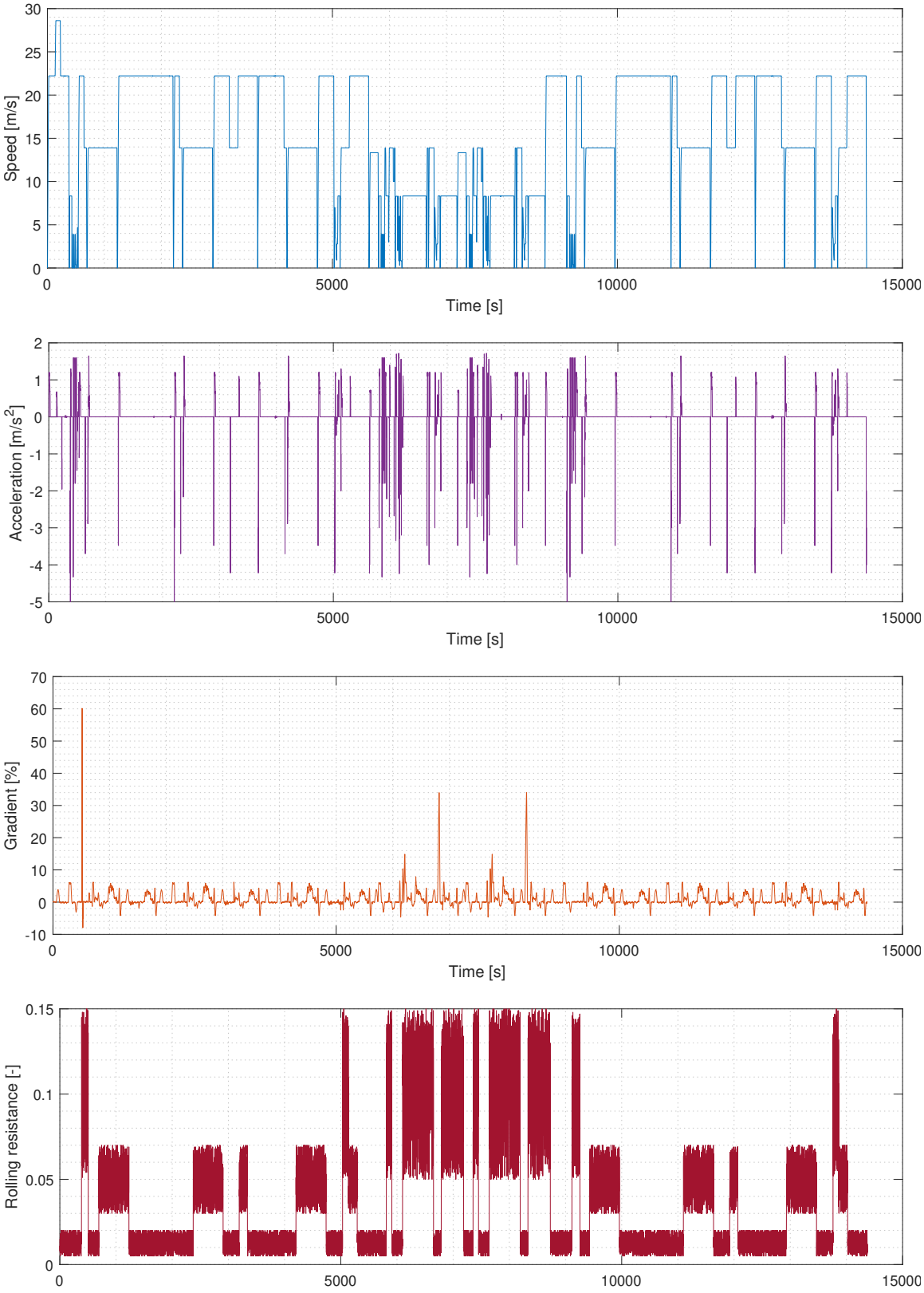

Figure A.1: Drivecycle

Appendix B Component parameters

An overview of the considered component mass and cost approximations are included in Table B.1. The variable P represents the power rating of the components.

Table B.1: Component parameters

Component	Mass	unit	year	Costs	unit	year	Source	Additional information
ICE (diesel)	0.29	$[kg/kW]$	2002	2500 + 21 · P	[€]	2002	[68]	HD
ICE (diesel)	1.74	$[kg/kW]$	2010	43.20	$[€/kW]$	2010	[69]	77-140 $[kW]$
ICE (diesel)	3.14	$[kg/kW]$	2010	56.50	$[€/kW]$	2010	[69]	152-375 $[kW]$
ICE (diesel)	3.60	$[kg/kW]$					[67]	advisor CI246 model & CI88 model
ICE (diesel)	3.37	$[kg/kW]$	2020 est.	56.50	$[€/kW]$	2020 est.		Used approximation
e-motor	1.00	$[kg/kW]$	2002	770 + 30 · P	[€]	2002	[68]	Costs incl. inverter and reduction
e-motor	0.70	$[kg/kW]$	2010	20.00	$[€/kW]$	2010	[69]	ass. low production (<10k)
e-motor				79.80 + 15.29 · P	[€]	2020 est.	[55]	Converted to EUR
e-motor				72.17 + 13.58 · P	[€]	2025 est.	[55]	Converted to EUR
e-motor	0.71	$[kg/kW]$	2020 est.	169.80 + 11.63 · P	[€]	2010 est.	[72]	Converted to EUR
e-motor	0.80	$[kg/kW]$	2011	16 · P	[€]	2011	[70]	
e-motor	500.00	$[kg]$	2020				[80]	Siemens PEM 1DB2024–WS36 320 $[kW]$
e-motor	480.00	$[kg]$	2020				[80]	Siemens PEM 1DB2022–WS36 200 $[kW]$
e-motor	350.00	$[kg]$	2020				[80]	Siemens PEM 1DB2016–WS54 160 $[kW]$
e-motor	120.00	$[kg]$	2020				[80]	Siemens DM 1PV5138-4WS24 85 $[kW]$
e-motor	98.00	$[kg]$	2020				[81]	Borgwarner HVH410-075 290 $[kW]$
e-motor	140.00	$[kg]$	2020				[82]	Borgwarner HVH410-150 325 $[kW]$
e-motor	83.00	$[kg]$	2020				[83]	Phi-power PH382 400 $[kW]$
e-motor	340.00	$[kg]$	2020				[84]	SUMO HD HV3500 370 $[kW]$
e-motor	388.00	$[kg]$	2020				[85]	BAE MTS HDS300 230 $[kW]$
e-motor	0.75	$[kg/kW]$	2020 est.	76 + 15 · P	[€]	2020 est.		Used approximation
Power electronics	8 + 0.13 · P	$[kg]$	2002	650 + 25 · P	[€]	2002	[68]	
Power electronics	0.08	$[kg/kW]$	2010	770 + 30 · P	[€]	2010	[69]	low production (<10k)
Power electronics	0.16	$[kg/kW]$	2010	22.70	$[€/kW]$	2010	[69]	low production (<10k)
Power electronics				61.25	$[€/kW]$	2020 est.	[55]	cpl. elec system, converted to EUR
Power electronics				54.18	$[€/kW]$	2025 est.	[55]	cpl. elec system, converted to EUR
Power electronics				360.83 + 16.13 · P	[€]	2010 est.	[72]	Converted to EUR
Power electronics	0.10	$[kg/kW]$	2011	15 · P	[€]	2011	[70]	
Power electronics	0.13	$[kg/kW]$	2020 est.	54.18	$[€/kW]$	2020 est.		Used approximation
Battery	12.50	$[kg/kW]$	2002	212.25	$[€/kWh]$	2002	[68]	
Battery	9.35	$[kg/kW]$	2010	640.00	$[€/kWh]$	2010	[69]	high energy, low production (<10k)
Battery	23.26	$[kg/kW]$	2010	1400.00	$[€/kWh]$	2010	[69]	high power low production (<10k)
Battery				246.17	$[€/kWh]$	2017	[56]	Converted to EUR
Battery				113.07	$[€/kWh]$	2025 est.	[56]	Converted to EUR
Battery				268.55	$[€/kWh]$	2020 est.	[55]	Converted to EUR
Battery				197.88	$[€/kWh]$	2025 est.	[55]	Converted to EUR
Battery				348.09	$[€/kWh]$	2014	[86]	
Battery	9.09	$[kg/kW]$					[58]	Iron Phosphate (LFP)
Battery	4.21	$[kg/kW]$				2014	[3]	AMP20 Lithium Ion Prismatic Pouch
Battery	5.00	$[kg/kW]$		500.00	$[€/kWh]$	2020	[71]	Off-Road Mobile Machinery 2020
Battery	2.96	$[kg/kW]$		200.00	$[€/kWh]$	2030 est.	[71]	Off-Road Mobile Machinery 2020
Battery	4.00	$[kg/kW]$		400.00	$[€/kWh]$	2020	[71]	Heavy duty BEV 2020
Battery	2.22	$[kg/kW]$		150.00	$[€/kWh]$	2030 est.	[71]	Heavy duty BEV 2020
Battery	6.70	$[kg/kW]$	2011	250.00	$[€/kWh]$	2011	[70]	
Battery	5.00	$[kg/kW]$	2020 est.	350.00	$[€/kWh]$	2020 est.		Used approximation
Transmission				18.50	[€/kg]	2010	[69]	AMT
Transmission	0.74	$[kg/kW]$	2020 est.				[72]	AMT for parallel topologies
Transmission	0.59	$[kg/kW]$	2020 est.				[72]	AMT for series topologies
Transmission				229.23 + 4.25 · P	[€]	2010 est.	[72]	AMT LD, converted to EUR
Transmission	265.00	$[kg]$	2020				[87]	ZF 12 TX 3420 TO (12spd, 3400Nm T_{max})
Transmission	202.00	$[kg]$	2020				[87]	ZF 9 AS 1517 TO (9spd, 1500Nm T_{max})
Transmission	152.00	$[kg]$	2020				[87]	ZF 6 AS 1100 TO (6spd, 1100Nm T_{max})
Transmission	317.00	$[kg]$	2020				[88]	EATON Fuller RTO-16909ALL (11spd, 2237Nm T_{max})
Transmission	20 + (n_{gears}-9) · 3.33 + P/1.55 + (n_{gears}-9) · (3/160) · P	$[kg]$	2020 est.	229.23 + P · 5 + (n_{gears}-9) · (1/7) · P	[€]	2020 est.		Used approximation
Reduction (Differential)	0.59	$[kg/kW]$	2020 est.	72.17 + 1.44 · P	[€]	2010 est.	[72]	Converted to EUR

Appendix C Torque split flowcharts

Figure C.1 and C.2 contain the flowcharts for torque split control between powersources. The controller uses a fixed 'forced charge limit' at 0.2 SOC and a variable 'lower charge limit' $\in \{0.4, 0.6\}$. This lower charge limit varies depending on the state variable of the ICE. Without hysteresis, the controller would switch continuously, provided the temperature is within the setpoint value range.

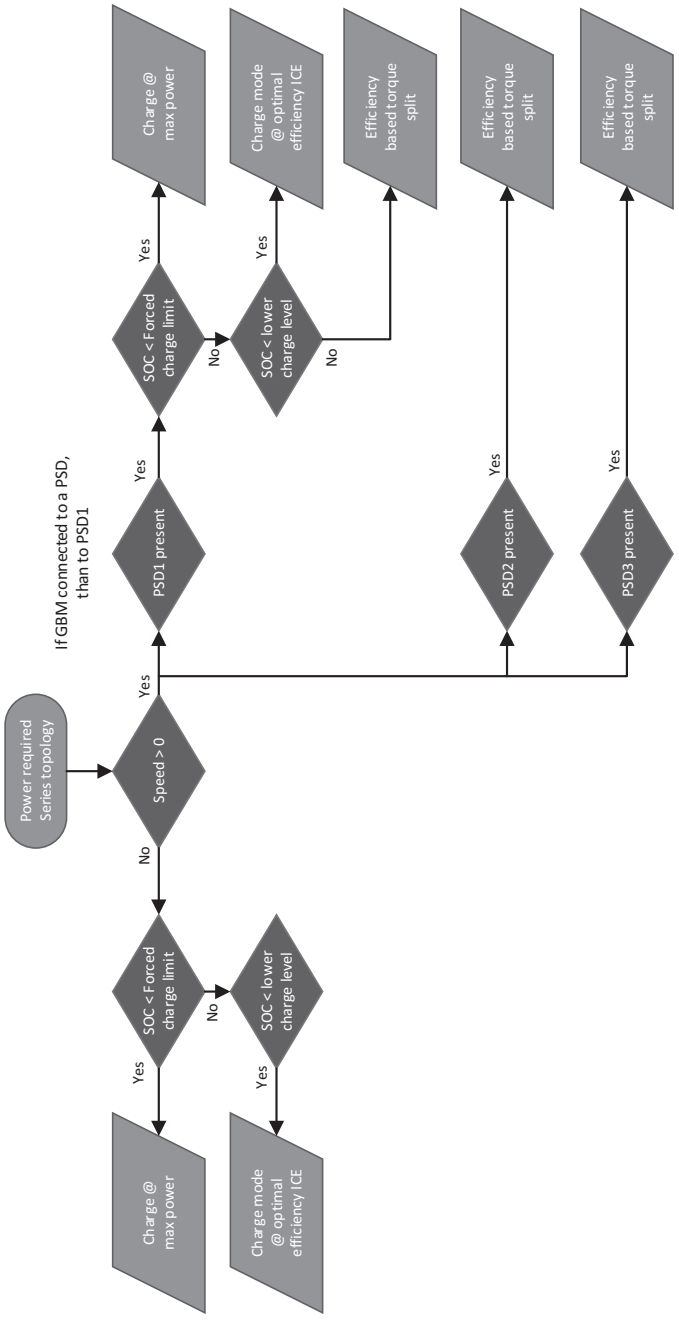

Figure C.1: Torque split control for series topologies

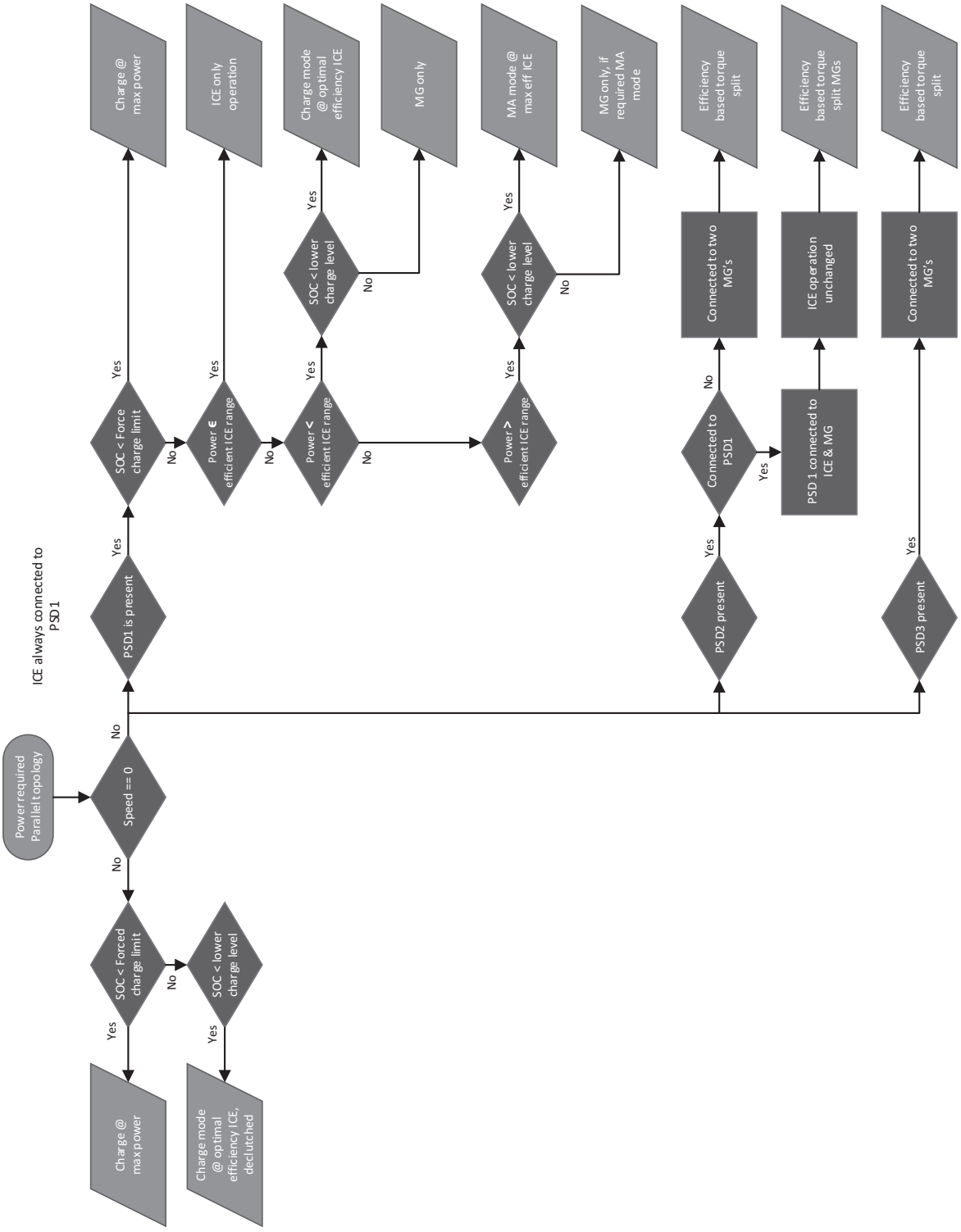

Figure C.2: Torque split control for parallel topologies